

ATTENTION REPRO:

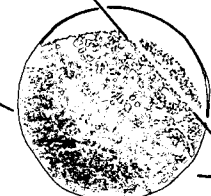
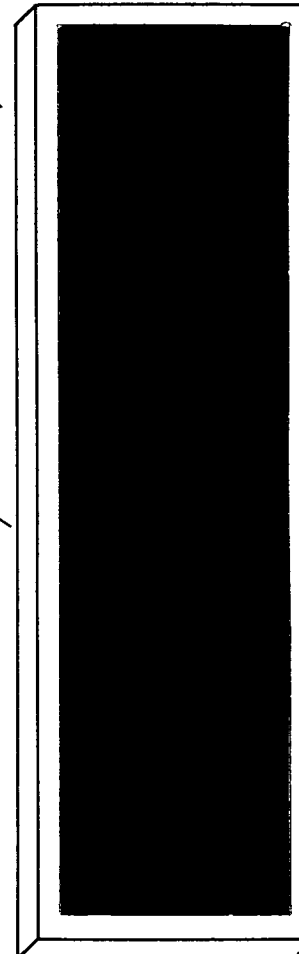
BEFORE PRINTING, CONTACT INPUT FOR PAGINATION

PROCESSOR D. Bush

(NASA-CR-134010) ANALYSIS OF A
TWO-DIMENSIONAL TYPE 6 SHOCK-INTERFERENCE
PATTERN USING A PERFECT-GAS CODE AND A
REAL-GAS CODE (Texas Univ.) 138 p HC
\$9.00 140 CSCL 20D G3/12 13253

N73-30242

Unclas
13253



CR-134010

ANALYSIS OF A TWO-DIMENSIONAL
TYPE VI SHOCK-INTERFERENCE PATTERN
USING A PERFECT-GAS CODE AND A REAL-GAS CODE*

by John J. Bertin and Bruce W. Graumann

Aerospace Engineering Report 73003

*This effort was supported in
part by the Johnson Space Center
through NASA Contract NAS 9-10976

Department of Aerospace Engineering and
Engineering Mechanics

The University of Texas at Austin
August 1973

TABLE OF CONTENTS

	Page
INTRODUCTION	1
NOMENCLATURE	3
THEORETICAL ANALYSIS	5
Perfect-gas code	6
Real-gas code	7
DISCUSSION OF RESULTS	9
CONCLUDING REMARKS	19
REFERENCES	21
FIGURES	23
APPENDIX A: - GENERAL DESCRIPTION OF PERFECT GAS CODE	A-1
Flow-Field Conditions in Regions 2, 3, and 6.	A-1
Wing Leading-Edge Heat-Transfer-Rate Calculations	A-5
Calculation of the Stagnation Conditions Behind a Normal Shock and of the Reference Heating	A-5
Calculation of the Shock-Wave Angles and the Inter- section Points of the Shock Wave with the Expansion Fan.. . .	A-6
Input Codes	
Listing of Codes	
Description of Output	
Sample Output	
APPENDIX B: - GENERAL DESCRIPTION OF REAL-GAS CODE	B-1
Calculation of Flow-Field Conditions.	B-1
Calculation of Stagnation Conditions.	B-2
Calculation of Expansion Fan Flow	B-2
Wing Leading Edge Heat-Transfer Rate Calculations	B-4
Calculation of the Shock-Wave Angles and the Intersection Points of the Shock Wave with the Expansion Fan.. . . .	B-5
Input Cards	
Listing of Code	
Description of Output	
Sample Output	
APPENDIX C: - SOLUTIONS FOR A SINGLE WEDGE CONFIGURATION	C-1

INTRODUCTION

To determine the complete convective heat-transfer distribution for configurations flying at hypersonic speeds, one must consider the viscous:inviscid interactions associated with the complex three-dimensional flow fields. Because of the complexity of the viscous: inviscid interaction phenomena, many investigators have studied the locally perturbed flow fields using models consisting of basic elemental combinations. By varying the relative position of shock-generating elements, Edney¹ observed that there are six basic shock-interference patterns. Hains and Keyes² have categorized shock-interference patterns obtained for a variety of space-shuttle configurations in terms of the models by Edney.

Bertin, et al.³, examined surface-pressure and heat-transfer-rate data for a variety of shuttle-orbiter configurations over an angle-of-attack range from 0° to 60° . It was found that the "type" of shock-interference pattern was dominated by the leading-edge effective sweep angle. For the relatively low sweep angles of the straight-wing orbiters, the interaction between the bow-generated shock-wave and the wing-generated shock-wave was a "Type V" shock-interference pattern. For the delta-wing orbiters, the shock:shock interaction exhibited the characteristics of a "Type VI" pattern for all alphas.

Theoretical calculations^{4,5} of the inviscid shock-interaction flow-field, coupled with empirically derived surface-pressure:heat-transfer correlations of the viscous interaction phenomena, indicate that the local increases in heat transfer and in surface pressure associated with the Type IV and with the Type V interactions become markedly more severe as γ decreases. Since the current shuttle entry-configurations have highly swept wings, the present investigation was undertaken to determine the effect of the gas-property model on the Type VI shock-interference pattern.

Numerical codes were developed to calculate the two-dimensional flow field which results when supersonic flow encounters double wedge configurations whose angles are such that a Type VI pattern occurs. The flow-field model included the shock-interaction phenomena observed in ref. 3 for a delta-wing orbiter. Two numerical codes were developed: one which used the perfect gas relations and a second which incorporated a Mollier table to define equilibrium air properties. The two codes were used to generate theoretical surface-pressure and heat-transfer distributions for velocities from 1167 m/sec (3821 ft/sec), i.e., a wind-tunnel condition, to 7610 m/sec (25,000 ft/sec), i.e., an entry condition.

NOMENCLATURE

a	- speed of sound
C_p	- pressure coefficient
$\frac{dP}{dn}$	- pressure gradient normal to surface
f''	- velocity gradient function
g'	- stagnation enthalpy gradient function
h	- static enthalpy
H	- stagnation enthalpy
M	- Mach number
n	- transformed η -coordinate
P	- pressure
Pr	- Prandtl number
\dot{q}	- heat-transfer rate
$\dot{q}_{t,ref}$	- heat-transfer rate to reference sphere
r	- radius of cross-section for a body of revolution
R	- radius of reference sphere
Re_x	- Reynolds number based on local properties and wetted length
R_{gas}	- gas constant
S	- wetted distance along wing leading-edge, also entropy
T	- static temperature
T_r	- recovery temperature
U	- streamwise velocity (capital letter denotes free-stream velocity)
X	- axial coordinate
α	- transformation parameter
γ	- ratio of specific heats
δ	- initial turning angle
η	- transformed y -coordinate

θ	- shock angle
Λ	- sweep angle (see Fig. 1)
Λ_s	- complement of sweep angle (see Fig. 1)
μ	- viscosity
ν	- Prandtl-Meyer angle
ϵ	- pressure ratio across a shock wave
ρ	- density

Subscript

e	- parameter evaluated at the boundary layer edge
ex	- parameter evaluated in the expansion fan
∞	- parameter evaluated in the free-stream region
n	- parameter normal to shock wave
t	- indicates stagnation condition
t2	- indicates stagnation condition in region 2
w	- parameter evaluated at the wall

THEORETICAL ANALYSIS

The complex flow field, which is established when a high-speed flow encounters a double-wedge configuration, is dominated by a shock-interaction region which imposes a highly non-uniform flow field adjacent to the wedge boundary layer. If the two wedge angles are not too large, the shock waves associated with the flow deflection are attached. The shock-interference pattern which results for this case has been designated by Edney as a Type VI pattern. For the computer code developed in the present study, it was assumed that the Type VI shock-interference pattern for a double wedge configuration (as shown in Fig. 1) includes:

- 1) the undisturbed free-stream flow,
- 2) the flow turned through the angle δ by a single shock wave,
- 3) the flow turned through the angle Λ_s by two shock waves,
- 4) the flow processed by the right-running waves of the expansion fan which are centered at the intersection of the two shock waves,
- 5) the flow which passes through the left-running waves produced by the reflection of the waves of the expansion fan, and
- 6) the flow turned through the angle Λ_s by a single shock wave.

The flow near the juncture of the two wedges, i.e., in region 3, has passed through two shock waves. Further outboard on the downstream wedge, i.e., in region 6, the flow has passed through a single shock wave and is, therefore, at a lower pressure than that in region 3. Thus, although the flow directions are the same, the gas must

undergo an expansion from the root region to equalize the pressure. The flow accelerates isentropically through the expansion regions so that the pressure and the flow direction in region 5E are identical to the values for region 6. The current study is concerned with the shock-interaction flow-field phenomena, which directly influence the wedge surface flow properties (i.e., pressure, shear, and heat transfer). Therefore, the flow-field properties along the wall were calculated including the interactions between the right-running and left-running waves in the numerical code. However, no attempt was made to model the shear layer which develops between the shock wave and the expanding flow, since this shear layer does not interact with the wedge surface for the two-dimensional Type VI interaction.

Perfect-gas code. - The first steps were the calculation of the flow conditions downstream of an oblique shock for a given flow-deflection angle and for a given gamma, i.e., in regions 2, 3, and 6. The flow conditions in region 5E could then be calculated, since the static pressure in region 5E is equal to the static pressure in region 6 and, under the isentropic-expansion assumption, the stagnation pressure in region 5E is equal to the stagnation pressure in region 3. The expansion process by which the gas accelerates from region 3 to region 5E was divided into ten equal steps. To satisfy the physical boundary condition that the flow in region 5E be parallel to the wall, the total change in the Prandtl-Meyer angle was divided into ten equal parts: the five right-running waves of region 4 and the five reflected waves constituting region 5. The governing equations for these calculations are summarized in ref. 6. Having defined the

inviscid flow-field and, hence, the conditions at the edge of the boundary layer, the heat-transfer distribution along the downstream wedge was calculated using the Eckert-reference-temperature technique⁷. For the wind-tunnel flow-condition, where the perfect gas relations accurately describe the gas behavior, the Eckert-reference-temperature heating rates compared favorably with the values obtained using the nonsimilar boundary-layer code described below. Due to the simplicity of the Eckert method, it was used with the perfect-gas calculations. The boundary-layer of the downstream wedge was assumed to originate at the intersection of the two wedges (point 0 in Fig. 1).

One way of approximating the high-temperature, or real-gas, properties of air is to use lower values of gamma in the perfect-gas relations. Therefore, the equations for the perfect-gas code have been written so that one can input one value of gamma for regions 1 and 2, another gamma for regions 3 through 5E, and a third value for region 6. Thus, one can "account for" the varying shock strengths. The perfect-gas code was used to generate three "different" types of solution. For the present paper, these types of solution are referred to as:

- (a) "perfect-gas" solution for which $\gamma = 1.400$ throughout the flow field,
- (b) "constant-gamma" solution for which $\gamma = 1.200$ throughout the flow field,
- (c) "variable-gamma" solution for which different values of gamma were assigned to the three input gamma parameters. (The required values were obtained from the real-gas solutions.)

To be consistent in the perfect-gas assumption, the specific heat of air was held constant both for the constant-gamma and the variable-gamma solution. Sutherland's relation⁶ was used to calculate the viscosity.

Assuming the Prandtl number to be 0.7 uniquely determined the thermal conductivity.

Real-gas code. - Philosophically, the calculation procedure for the shock-interaction pattern using the real-gas code was similar to that described for the perfect-gas code. However, to account for the high-temperature, or "real-gas", effects all thermodynamic properties are evaluated using numerical charts for air in chemical equilibrium⁸.

Reference 9 was used to define the temperature dependence of the transport properties of equilibrium air, i.e., viscosity, thermal conductivity, and specific heat. Once the oblique shock relations have been used to define the static pressure and the entropy for the two end regions, the expansion from region 3 to region 5E is divided into ten equal steps. The flow conditions in the intermediate regions of the isentropic expansion are calculated using the relations of ref. 10. The relations require the static enthalpy and the local speed of sound for the intermediate regions, which are evaluated using the tables for the equilibrium air⁸.

The heat-transfer distribution along the downstream wedge is calculated using a nonsimilar boundary-layer code¹¹, which was modified so that the thermodynamic properties for the viscous flow would also be calculated using ref. 8. In addition to accounting for the "real-gas" effects, the effect of the acceleration of the inviscid flow is included in the nonsimilar code. As before, the boundary layer is assumed to originate at the junction of the two wedges.

DISCUSSION OF RESULTS

The objective of the current analytical investigation was to determine how to apply the shock-interference data obtained in the wind tunnel³ to the reentry of a shuttle orbiter. For simplicity, the numerical code was restricted to a two-dimensional flow model with the second, or downstream, wedge representing the wing leading edge. The initial deflection angle δ was 5° for all solutions. This value was chosen, because the shock standoff distance in the vicinity of the wing leading-edge correlated reasonably well with the bow-wave trace observed in wind tunnel tests. The deflection angle Λ_s of the downstream wedge was varied from 25° to 63° , which corresponds to leading-edge sweep angles from 65° to 27° . The dimensions of the 0.009 scale orbiter tested in Tunnel B of AEDC³ were used to define the characteristic lengths of the wedges.

For this study, numerical solutions were generated to determine the effect of gas properties on the flow field and of the wall temperature on the heat transfer in the region where the Type VI shock-interaction influenced the "wing leading-edge". Flow-field solutions were generated for three free-stream conditions.

- 1) a wind tunnel condition where

$$U_\infty = 1167 \text{ m/sec}, P_\infty = 2.98 \text{ mmHg}, T_\infty = 53^\circ\text{K}$$

$$(U_\infty = 3821 \text{ ft/sec}, P_\infty = 0.057 \text{ psia}, T_\infty = 95^\circ\text{R})$$

- 2) an orbiter entry condition where

$$U_\infty = 4330 \text{ m/sec}, P_\infty = 0.333 \text{ mmHg}, T_\infty = 273^\circ\text{K}$$

$$(U_\infty = 14,200 \text{ ft/sec}, P_\infty = 0.0064 \text{ psia}, T_\infty = 491^\circ\text{R})$$

3) an orbiter entry condition where

$$U_{\infty} = 7610 \text{ m/sec}, P_{\infty} = 0.0268 \text{ mmHg}, T_{\infty} = 195^{\circ}\text{K}$$

$$(U_{\infty} = 25,000 \text{ ft/sec}, P_{\infty} = 0.00052 \text{ psia}, T_{\infty} = 352^{\circ}\text{R}).$$

Solutions were obtained using both the perfect-gas code and the real-gas code at all flow conditions. In addition, the variable-gamma option was used to generate solutions for flow conditions 2 and 3. Heat-transfer distributions along the downstream wedge were obtained for all three free-stream conditions for a wall temperature T_w of 394°K (710°R) and for the two entry conditions for a T_w of 1640°K (2960°R).

The effect of the gas properties on the calculated geometry of the Type VI shock-interference pattern is illustrated in Fig. 2. The output from the real-gas solutions was used to define the gamma distribution for input for the variable-gamma solution. Thus, $\gamma_1 = \gamma_2 = 1.400$, $\gamma_3 = \gamma_4 = \gamma_5 = 1.214$, while $\gamma_6 = 1.163$. The geometry for the variable-gamma solution compares favorably with the real-gas geometry. The region where the leading edge is influenced by the shock interaction is essentially the same for these two solutions. The shock layer is thicker for the real-gas solution. For these deflection angles, the location and the extent of the surface affected by the expansion fan differs little between the perfect-gas solution and the real-gas solution. This similarity exists even though, in region 3, γ is 1.214 for the real-gas solution and is, of course, 1.4000 for the perfect-gas solution. However, because the density ratio across a shock wave is higher when the real-gas properties are accounted for, the shock layer along the wing leading-edge is markedly thinner for the real-gas solution.

The pressure distributions along the leading edge of a 60° sweep "wing" are presented in Fig. 3 for the entry velocity of 4330 m/sec. So that the pressure variations could be seen more clearly, the scale

has been greatly expanded for the region where the expansion fan impinges on the "wing leading-edge". The vertical marks in Fig. 3 indicate the various regions of the field, using the same legend as the theoretical distributions.

As noted in Fig. 2, the interaction-perturbed region for the perfect-gas solution is inboard relative to the real-gas solution, although the locations differ only slightly. However, for a given region, the perfect-gas surface-pressure correlates quite well with the real-gas value (Fig. 3a), with the perfect-gas solution yielding a slightly higher pressure. Over the range of the free-stream conditions of the present study, the perfect-gas surface-pressure in a given region of the flow field was within 10% of the real-gas value. As noted in Fig. 2, the locations of the interaction-perturbed regions for the real-gas solution and for the variable-gamma solution are in close agreement. However, the pressures for the variable-gamma solution are significantly lower than the real-gas solution. The discrepancy between the real-gas and the variable-gamma values of surface pressure in a given region typically varied from 15% to 25%.

The heat-transfer distributions along the wing leading-edge are presented in Fig. 4 for the entry velocity of 4330 m/sec. The local heat-transfer rate has been divided by the stagnation-point heating rate¹² for a reference sphere, whose radius was chosen to be 0.0027m and which is at the same temperature as the wedge surface. The dimensionless heat-transfer parameter $\dot{q}/\dot{q}_{t,ref}$ (or, since the wall temperatures are equal, the equivalent ratio of heat-transfer coefficients) is commonly used in shuttle application. Heat-transfer distributions were calculated for wall temperatures of 394°K and of 1640°K.

The dimensionless heat-transfer distributions computed using the real-gas code are compared with the perfect-gas solutions and the variable-gamma solutions in Figs. 4a and 4b, respectively. The wall-temperature variation had little effect on the heat transfer. The heat-transfer distributions for the variable-gamma solution correlate closely with the real-gas heat-transfer distributions. The difference in the location of the interaction-perturbed region contributes to the only significant difference between the perfect-gas heat-transfer and the real-gas heating (and the difference is magnified by the expanded scale). However, for engineering applications, both the perfect-gas distribution and the variable gamma distribution are in satisfactory agreement with the real-gas distribution. Similar correlations were found for the highest velocity solution. However, near the wing root, the difference between the perfect-gas heat-transfer and the real-gas heating was slightly greater at the highest velocity (i.e., condition 3 in Fig. 9).

The local increases in the real-gas heat-transfer distributions which are evident at the beginning of each flow region are due to the local acceleration of the inviscid flow. The waves of the expansion fan produce a step-function decrease in pressure and a corresponding step-increase in the local velocity at the edge of the boundary layer. Thus, the nonsimilar boundary-layer solutions yield local increases in heating due to the local velocity gradient. There are no locally severe heating rates, which could cause design problems, indicated either in the real-gas solutions or in the perfect-gas solutions. However, the flow model for the calculations does not include imbedded shock waves or other three-dimensional flow phenomena, which might occur near the wing-root fairing. Such flow phenomena caused local increases in heating to delta-wing orbiter configurations³.

The location and the extent of the interaction-perturbed region of the "wing leading-edge" for the real-gas solutions are presented in Fig. 5 as a function of leading-edge sweep. The limits of the band represent the intersections of the limits of the centered expansion fan, i.e., region 4 of Fig. 1, with the leading edge. The locations are presented as the distance from the junction of the two wedges (S) divided by the radius of a reference sphere (R , which is equal to 0.0027m). Calculated locations from the real-gas solutions are presented for sweep angles from 60° down to the minimum sweep angle for which a Type VI pattern exists. The minimum sweep angle decreases as the free-stream velocity increases. For the higher velocity entry-condition, the Type VI pattern is possible for sweep angles as low as 27° . The perturbed region moves inboard toward the wedge junction as the velocity increases.

The effect of the free-stream velocity on the nondimensionalized heat-transfer rate is indicated in Fig. 6. Calculations are presented for region 3 (upstream of the expansion fan) and for region 5E (downstream of the expansion fan). Since the interaction-perturbed region moves inboard as the velocity increases, the point in region 3 is near the inboard edge of the interaction region for the highest velocity. Correspondingly, the point of region 5E is near the outboard edge for the lowest velocity. For both the perfect-gas solutions and the real-gas solutions and for both wall temperatures, the nondimensionalized heat-transfer rate increases significantly with velocity. The dimensionless heating for the higher entry velocity is roughly twice that for the wind-tunnel condition for region 3, somewhat less for region 5E. This implies that one should not extrapolate wind-tunnel data directly to flight conditions. Instead the wind-tunnel data should be used to construct a viable model of the flow field. The flow-field model can then be used to generate the required aerothermodynamic environment at the conditions of interest.

The shock-interaction geometry, the surface-pressure distributions, and the heat-transfer distributions are presented in Figs. 7, 8, and 9, respectively, for the highest velocity condition (i.e., condition 3) with a sweep angle of 60° . The correlations between the perfect-gas solution, the variable-gamma solution, and the real-gas solution are similar to those observed in the previous figures for the middle velocity condition.

As can be seen in Fig. 7, the interaction-perturbed regions are virtually the same for the variable-gamma solution and for the real-gas solution. The location for the perfect-gas solution is only slightly inboard. The shock layer for the real-gas solution is slightly thinner than that for the variable-gamma solution and markedly thinner than that for the perfect-gas solution.

The relations between the various solutions for the leading-edge pressure-distributions obtained at the highest velocity correspond to those noted for the middle velocity solutions. For a given region of the expansion fan, the perfect-gas pressure is in reasonable agreement with the real-gas value. The difference between the perfect-gas distribution and the real-gas distribution is accentuated by the expanded scale of Fig. 8. Even though the real-gas solution was used to specify the input values of gamma for the variable-gamma solution, the variable-gamma pressures do not match the real-gas values as well as the perfect-gas pressures.

As can be seen in Fig. 9, the wall-temperature variation has no significant effect on the theoretical heat-transfer distributions. The variable-gamma distribution closely follows the real-gas distribution. The differences between the perfect-gas heat-transfer and the real-gas heating are greatest in regions 3 and 4AW, i.e., near the junction of the two wedges. Downstream, the correlation between the real-gas solution and the other two solutions is similar.

Theoretical solutions have been obtained for a variety of sweep angles.

The solutions of the Type VI shock-interaction for flow condition 2 are presented in Figs. 10 through 12 with a sweep angle of 40° . These solutions exhibit several interesting characteristics. For this flow condition, the shock-interference pattern undergoes critical changes as the sweep angle varies. No perfect-gas solution is presented. This is because, for this wedge geometry, the perfect-gas relations require a Type V pattern. Even at hypersonic speeds, perfect air can not turn through a single, linear shock wave parallel to a 50° wedge⁶. Also note that the curved shock region near the reflected waves is not presented in Fig. 10a. This is because the numerical scheme used in the present real-gas code does not yield the continuously curved shock required to turn the flow from the free-stream direction parallel to the flow in region 4E. However, a solution still exists for region 6 and, therefore, region 5E. Therefore, the shock-interference pattern is still basically a Type VI pattern. The curved shock would, of course, be produced in the actual flow. But since the velocity gradients and the pressure gradients of curved streamlines are not modeled numerically in the current code, the code outputs for this situation: "curved shock not modeled". It has been noted that the geometry for the variable-gamma solution is only slightly different than the real-gas geometry. However, because of the difference, the complete variable-gamma geometry (within the assumptions of the numerical code) is generated (Fig. 10b).

As was noted at the larger sweep angles, the variable-gamma pressure do not correlate exceptionally well with the real-gas values (Fig. 11), but the heat-transfer rates do correlate well (Fig. 12).

To simulate the large density changes which exist across a shock wave in hypersonic flight, experimental investigators often make use of wind tunnels for which the test gas has a relatively low value of gamma, e.g., ref. 13. Using tetrafluoromethane (CF_4) as the test gas, the free-stream

specific-heat ratio for the Langley facility varies from 1.17 to 1.31 at Mach 6 (ref. 14). Therefore, theoretical solutions of the Type VI shock-interference pattern for the double-wedge configuration with $\Lambda = 60^\circ$ have been computed for a perfect gas with $\gamma = 1.2$ throughout the flow-field. These solutions are designated "constant-gamma" solutions.

The location of the interaction-perturbed region is presented in Fig. 13 as a function of the free-stream velocity. Reviewing the legend:

- (a) "perfect-gas" uses the perfect-gas relations with $\gamma = 1.400$ throughout the flow field,
- (b) "constant-gamma" uses the perfect-gas relations with $\gamma = 1.200$ throughout the flow field,
- (c) "variable-gamma" uses the perfect-gas relations with γ_1 , γ_3 , and γ_6 specified from the real-gas solution ($\gamma_1 = \gamma_2$ and $\gamma_3 = \gamma_4 = \gamma_5$), and
- (d) "real-gas" uses the equilibrium air properties to describe the gas behavior.

Since γ for air is, in fact, essentially 1.4 throughout the flow field for the lowest velocity considered, no variable-gamma solution was obtained for this condition (i.e., condition 1). With the exception of the constant-gamma solution, the various solutions provide similar locations of the interaction-perturbed region over the velocity range considered. At the higher velocities, the interaction-perturbed region is relatively inboard for the constant-gamma solution. For a given geometry of the double-wedge configuration, the location of the interaction-perturbed region is a function of the bow shock-wave angle (generated by the initial deflection), of the leading-edge shock-wave angle (generated by the second deflection), and of the Mach numbers in regions 3 and 4 (which determine the expansion waves). The shock angle for $\gamma = 1.2$ is nearer the surface than is the shock angle for

$\gamma = 1.4$. Thus, since the actual γ is essentially unchanged for the first deflection angle, the bow shock-wave for the constant-gamma solution intersects the leading-edge shock nearer the root than is the case for the real-gas solution or for the perfect-gas solution (which yield essentially identical results). The low-velocity, constant-gamma solution for the interaction region correlates with the other solutions because both the bow shock angle and the leading-edge shock angle are relatively small causing the shock: shock intersection to be relatively outboard.

The pressure distributions along the wing leading-edge are compared in Fig. 14. For the wind-tunnel condition, i.e., condition 1, the perfect-gas solution ($\gamma = 1.400$ everywhere) yields flow conditions in regions 3 and 6 which are identical to the corresponding flow conditions computed using the real-gas code. Differences occurred in the perfect-gas solution and the real-gas solution for the local pressures and the interaction locations of the expansion fan. Because regions 3 and 6 are identical and because the differences between the two solutions are attributed to the difficulty in using the Mollier charts at these low temperatures, the perfect-gas solution with $\gamma = 1.400$ (Fig. 14a) represents the actual flow. The constant-gamma solution yields pressures which are significantly lower than the other two solutions. As noted previously, the angles both for the bow shock and the leading-edge shock are relatively small for $\gamma = 1.200$ and, therefore, the interaction region matches that for the other two solutions.

For the middle velocity condition (Fig. 14b), the shock-interaction region for the constant-gamma solution is relatively inboard. It has been established that the difference is due to the fact that the initial shock wave is weak and, therefore, does not significantly alter gamma from its actual free-stream value of 1.400. When comparing the pressure from a

given region, the constant-gamma value is lower than the real-gas value by approximately the same amount that the perfect-gas value is higher than the real-gas value.

For condition 3 (Fig. 14c), the constant-gamma pressure in a given region is in very good agreement with the perfect-gas pressure for that region. For a given region, the real-gas solution yields pressures somewhat lower than the two other solutions. Again, however, because the bow shock-wave generated by the initial turning of the flow is much closer to the body when $\gamma = 1.200$ than it is for the real-gas solution or for the perfect-gas solution, the constant-gamma interaction region is markedly inboard.

The heat-transfer distributions for the leading-edge of a wing with 60° sweep are presented in Fig. 15. The constant-gamma solution is compared with the perfect-gas and the real-gas solutions. Because the free-stream values of temperature and of pressure were used to define the flow condition, negative heat transfer, or cooling, existed when $\gamma = 1.200$ for the wind-tunnel flow condition. Thus, heat-transfer distributions are not presented for the wind-tunnel condition. Heat-transfer distributions are presented for conditions 2 and 3 in Figs. 15a and 15b, respectively. The comparisons between the various theoretical solutions are similar for both flow conditions. The differences in the heat-transfer distributions are due principally to the differences in the locations of the interaction-perturbed regions. These differences are greatest at the higher velocity. The perfect-gas solutions ($\gamma = 1.400$ throughout) compare more favorably with the real-gas heat-transfer distributions than do the constant-gamma solutions ($\gamma = 1.200$ throughout).

CONCLUDING REMARKS

Using a two-dimensional flow model of the Type VI shock-interaction pattern, the aerothermodynamic environment has been calculated for a "simulated" wing leading-edge of a delta-wing orbiter. Calculations have been made for velocities from 1167 m/sec to 7610 m/sec for perfect-gas properties, for constant-gamma gas properties, for variable-gamma gas properties, and for real-gas properties. Based on the calculations of the present study, the following conclusions are made.

1. Free-stream flight conditions were found to produce Type VI interaction patterns for effective wing leading-edge sweep angles as low as 27° , when the real-gas effects were considered.
2. Perfect-gas solutions for the flow geometry and the pressure distribution were in good agreement with the real-gas solutions. The use of effective gammas did not adequately represent real-gas effects in the surface-pressure distribution.
3. The correlation between the perfect-gas solution and the real-gas solution for the heat-transfer distribution was essentially independent of the wall temperature, but depended on the free-stream velocity. The heat-transfer distributions for the variable-gamma solution correlated closely with the real-gas heat-transfer distributions. No locally severe heating rates, which would cause design problems, were found.
4. When the local heat-transfer rates were nondimensionalized using a current shuttle design parameter, the dimensionless heat transfer increased significantly with velocity. The increase occurred both for the perfect gas solutions and for the real-gas solutions and for both wall temperatures. Thus, one

should not extrapolate wind-tunnel data directly to flight conditions. Instead the wind-tunnel data should be used to construct a realistic model for the flow-field, which can be used to generate the required aerothermodynamic environment.

5. The shock-intersection geometry and its effect on the local flow-field was found to be a complex function of γ . The interaction-perturbed region depends on the "bow" shock-wave angle, the "leading-edge" shock-wave angle, and the expansion wave angles (or, equivalently, the local Mach numbers). Although γ often had a significant effect on the locations of the interaction-perturbed region, for a given flow condition, the location differences were never severe. This consistent correlation occurred because the shock angle discrepancies tended to be compensating in many cases and because the interaction occurred relatively near the wing root so that significant differences in angle resulted in relatively minor differences in length.

REFERENCES

1. Edney, B.: "Anomalous Heat Transfer and Pressure Distributions on Blunt Bodies at Hypersonic Speeds in the Presence of an Impinging Shock", Report 115, 1968, Flygtekniska Försöksanstalten (The Aeronautical Research Institute of Sweden).
2. Hains, F. D., and Keyes, J. W.: "Shock Interference Heating in Hypersonic Flows", AIAA Journal, November 1972, Vol. 10, No. 11, pp. 1441-1447 (also AIAA Paper 72-78).
3. Bertin, J. J., Graumann, B. W., and Goodrich, W. D.: "Aerothermodynamic Aspects of Shock-Interference Patterns for Shuttle Configurations During Entry", AIAA Paper No. 73-238, 11th Aerospace Sciences, Washington, D. C., January, 1973.
4. Edney, B. E., Bramlette, T. T., Ives, J., Hains, F. D., and Keyes, J. W.: "Theoretical and Experimental Studies of Shock Interference Heating", Report No. 9500-920-195, October 1970, Bell Aerospace Company.
5. Keyes, J. W., and Hains, F. D.: "Analytical and Experimental Studies of Shock Interference Heating in Hypersonic Flows", TND-7139, May 1973, NASA.
6. Ames Research Staff: "Equations, Tables, and Charts for Compressible Flow", Report 1135, 1953, NACA.
7. Eckert, E. R. G.: "Engineering Relations for Friction and Heat Transfer to Surfaces in High Velocity Flow", Journal of the Aeronautical Sciences, Vol. 22, No. 8, August 1955, pp. 585-587.
8. Moeckel, W. E., and Weston, K. C.: "Composition and Thermodynamic Properties of Air in Chemical Equilibrium", TN 4265, April 1958, NACA.

9. Hansen, C. F.: "Approximations for the Thermodynamic and Transport Properties of High Temperature Air", TR R-50, 1959, NASA.
10. Hayes, W. D., and Probstein, R. F.: Hypersonic Flow Theory, Volume I - Inviscid Flows, Chapter 7, Academic Press, 1966, New York.
11. Bertin, J. J., and Byrd, O. E., Jr.: "The Analysis of a Nonsimilar Boundary Layer - A Computer Code (NONSIMBL)" Aerospace Engineering Report 70002, August 1970, The University of Texas at Austin.
12. Fay, J. A., and Riddell, F. R.: "Theory of Stagnation Point Heat Transfer in Dissociated Air", Journal of the Aeronautical Sciences, Vol. 25, No. 2, February 1959, pp. 73-85, 121.
13. Hunt, J. L., and Creel, T. R., Jr.: "Shock Interference Heating and Density-Ratio Effects, Part II - Hypersonic Density-Ratio Effects", section in TMX-2272, April 1971, NASA.
14. Jones, R. A., and Hunt, J. L.: "Use of Tetrafluoromethane to Simulate Real-Gas Effects on the Hypersonic Aerodynamics of Blunt Vehicles", TR R-312, June 1969, NASA.
15. Bertin, J. J., "Boundary Layer Analysis with Similar Transpiration - A Computer Code", Aerospace Engineering Report 70001, February 1970, The University of Texas at Austin.

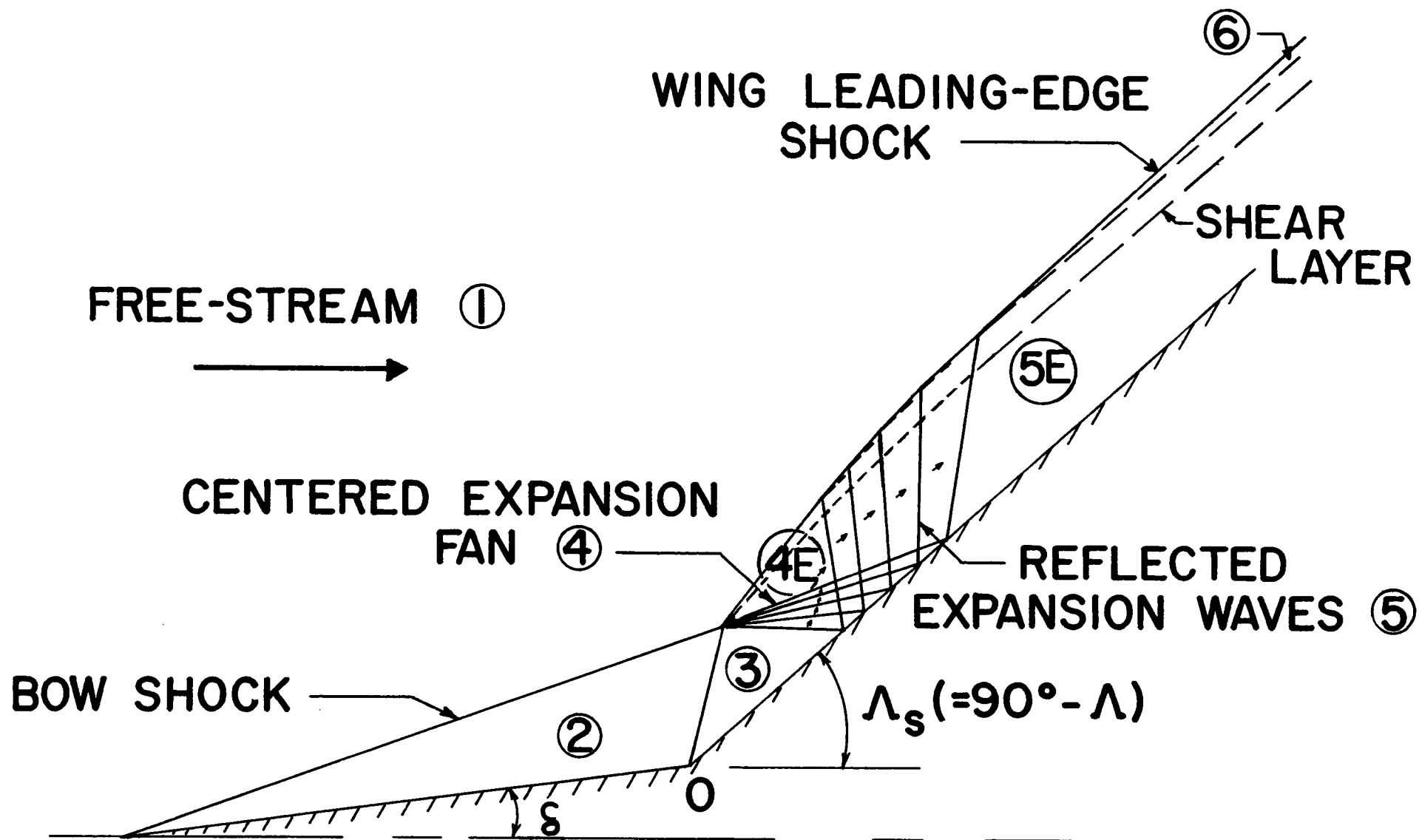


Figure 1. - Flow model of the Type VI shock-interference pattern for a double wedge.

Figure 2. - Calculated geometry of the Type VI shock-interference pattern; $U_\infty = 4330$ m/sec, $P_\infty = 0.333$ mmHg, $T_\infty = 273^\circ\text{K}$, $\Lambda = 60^\circ$.

The diagram illustrates the calculated geometry of a Type VI shock-interference pattern. It shows a series of shock waves and Mach lines originating from a curved surface. The flow is divided into several regions, labeled 1 through 6, and 4E, 5E. The shock waves are labeled with their respective S/R values: $S/R = 13.48$ and $S/R = 14.49$. The Mach lines are labeled with their respective Mach numbers: $M = 1.4$ and $M = 1.5$. The flow is assumed to be perfect gas.

(a) Perfect-gas solution

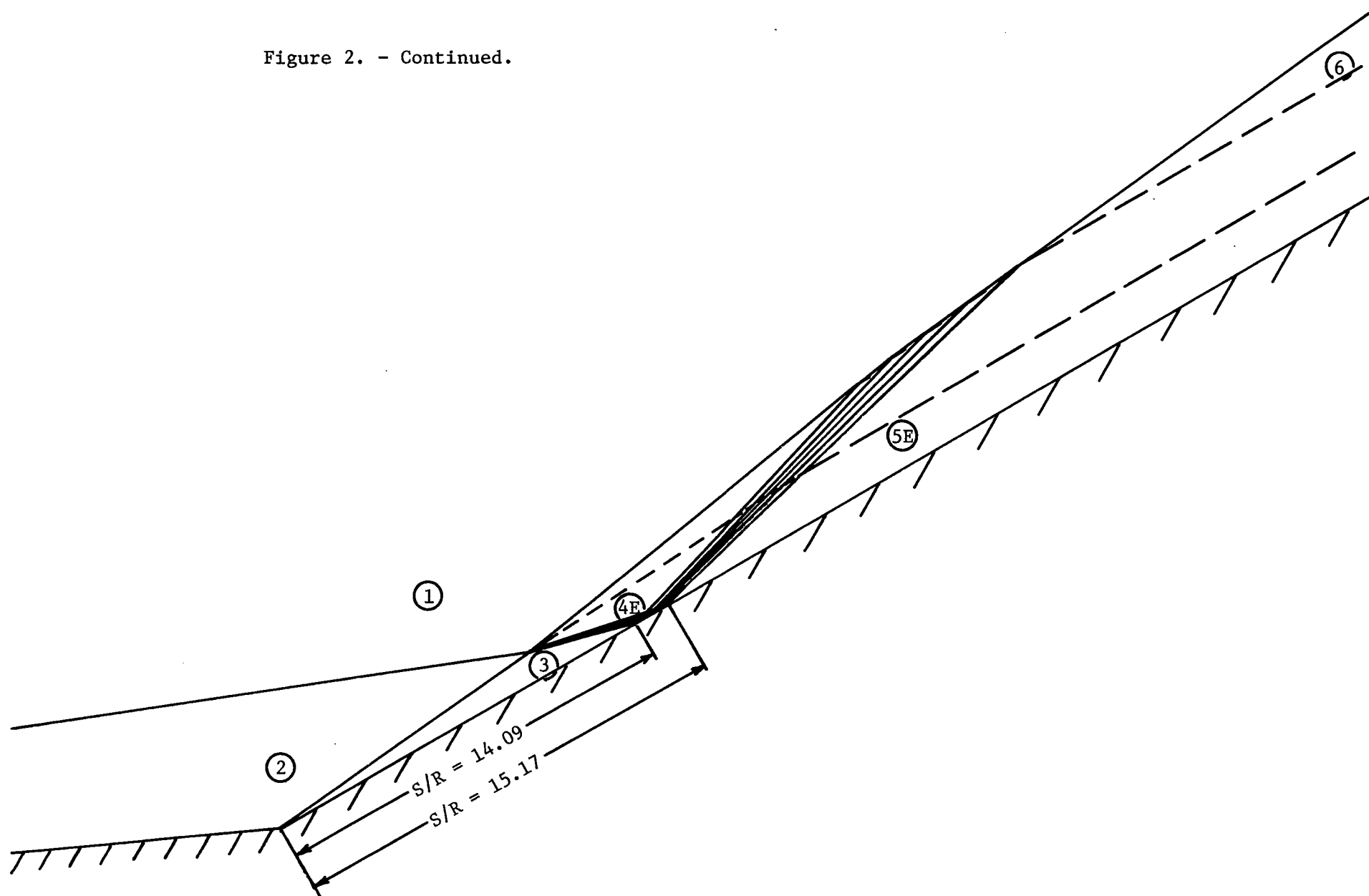
Figure 2. - Calculated geometry of the Type VI shock-interference pattern; $U_\infty = 4330$ m/sec, $P_\infty = 0.333$ mmHg, $T_\infty = 273^\circ\text{K}$, $\Lambda = 60^\circ$.

The diagram illustrates the calculated geometry of a Type VI shock-interference pattern. It shows a series of shock waves and Mach lines originating from a corner. The flow regions are labeled with circled numbers: 1, 2, 3, 4E, 5E, and 6. The shock waves are represented by solid lines, and the Mach lines by dashed lines. The flow direction is indicated by arrows. The diagram includes the following labels and dimensions:

- Region 1: The region above the first shock wave.
- Region 2: The region below the first shock wave and above the second shock wave.
- Region 3: The region between the second and third shock waves, with $S/R = 13.48$.
- Region 4E: The region between the third and fourth shock waves, with $S/R = 14.49$.
- Region 5E: The region between the fourth and fifth shock waves.
- Region 6: The region above the fifth shock wave.

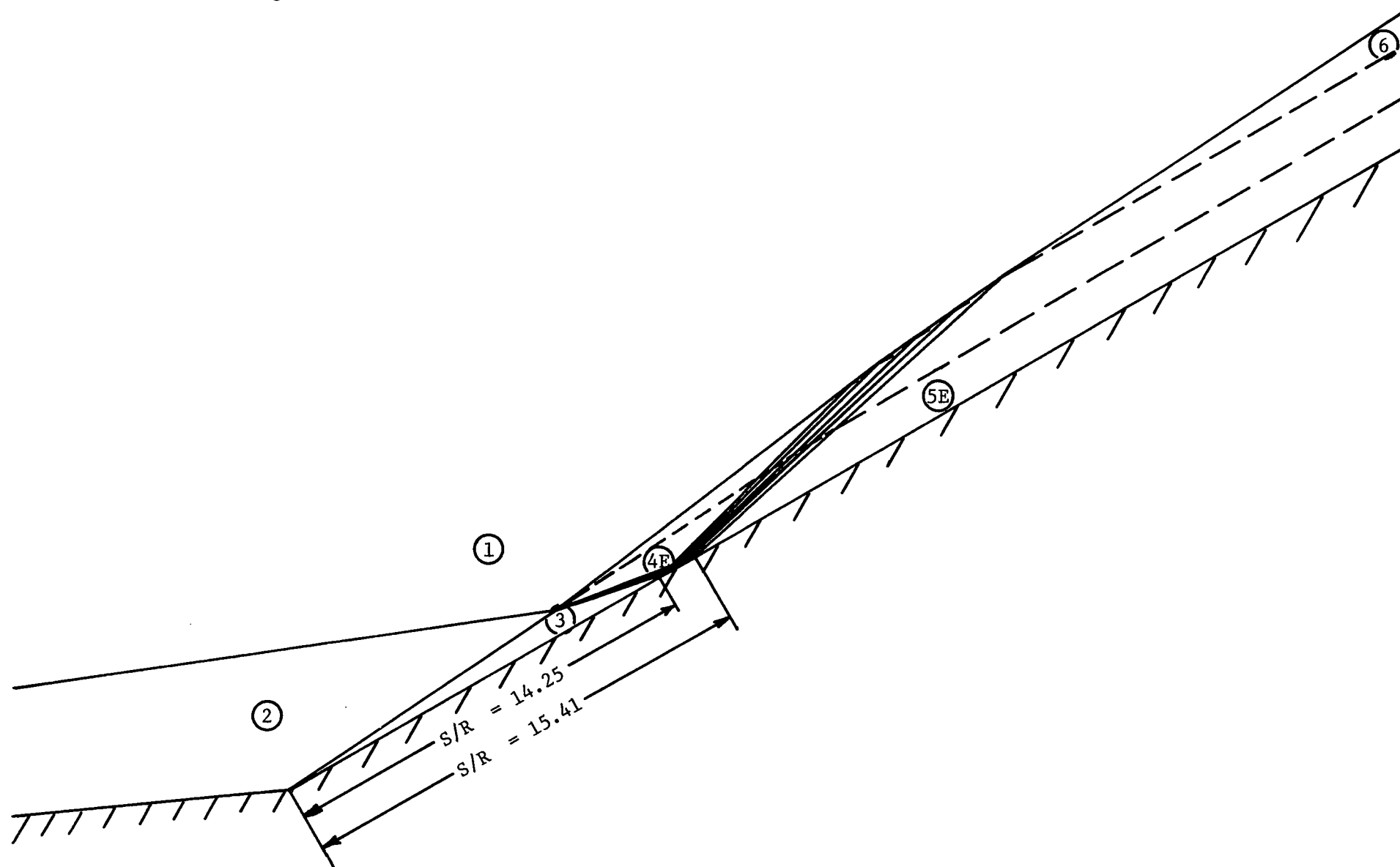
(a) Perfect-gas solution

Figure 2. - Continued.

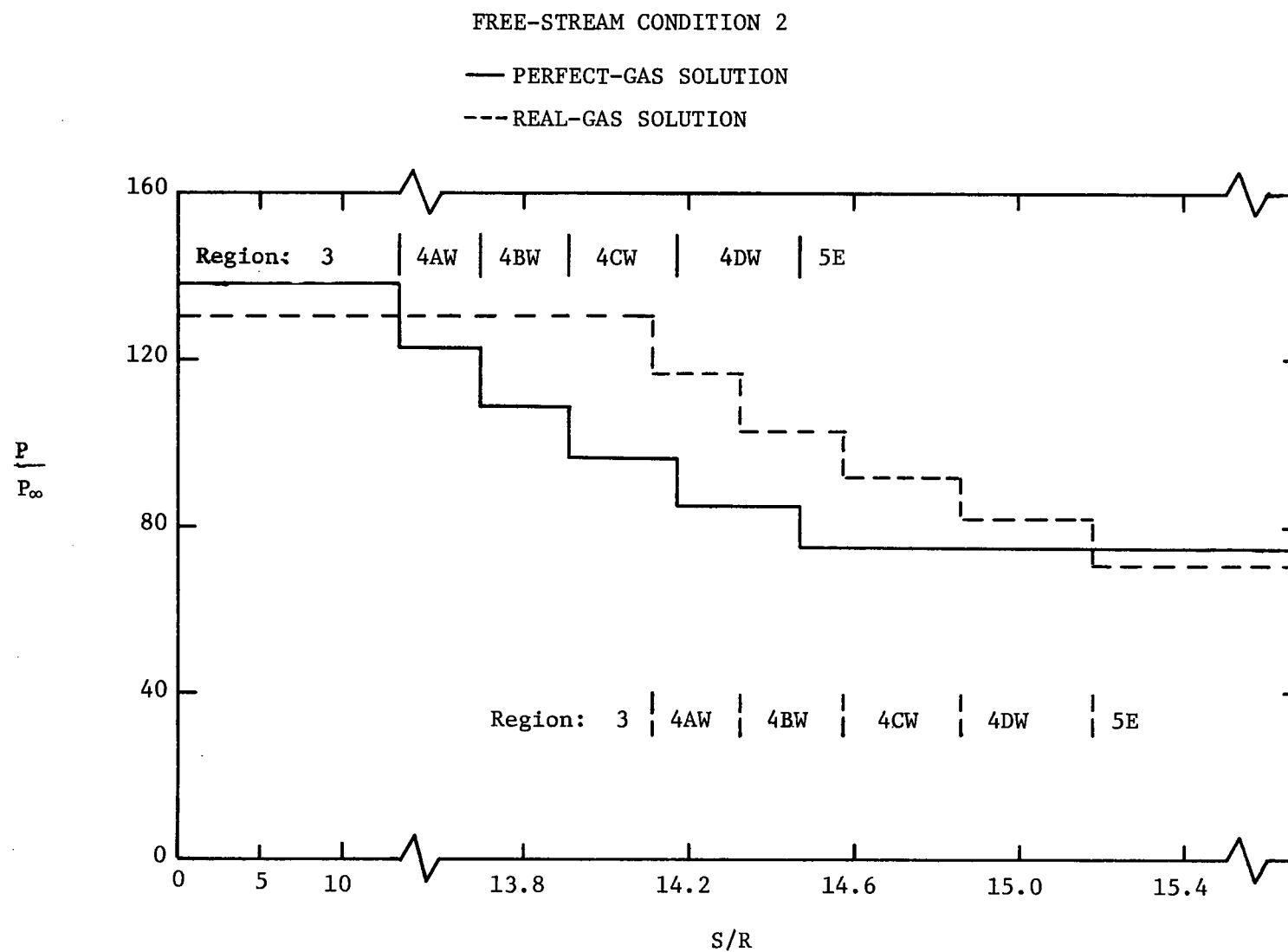


(b) Real-gas solution

Figure 2. - Concluded.

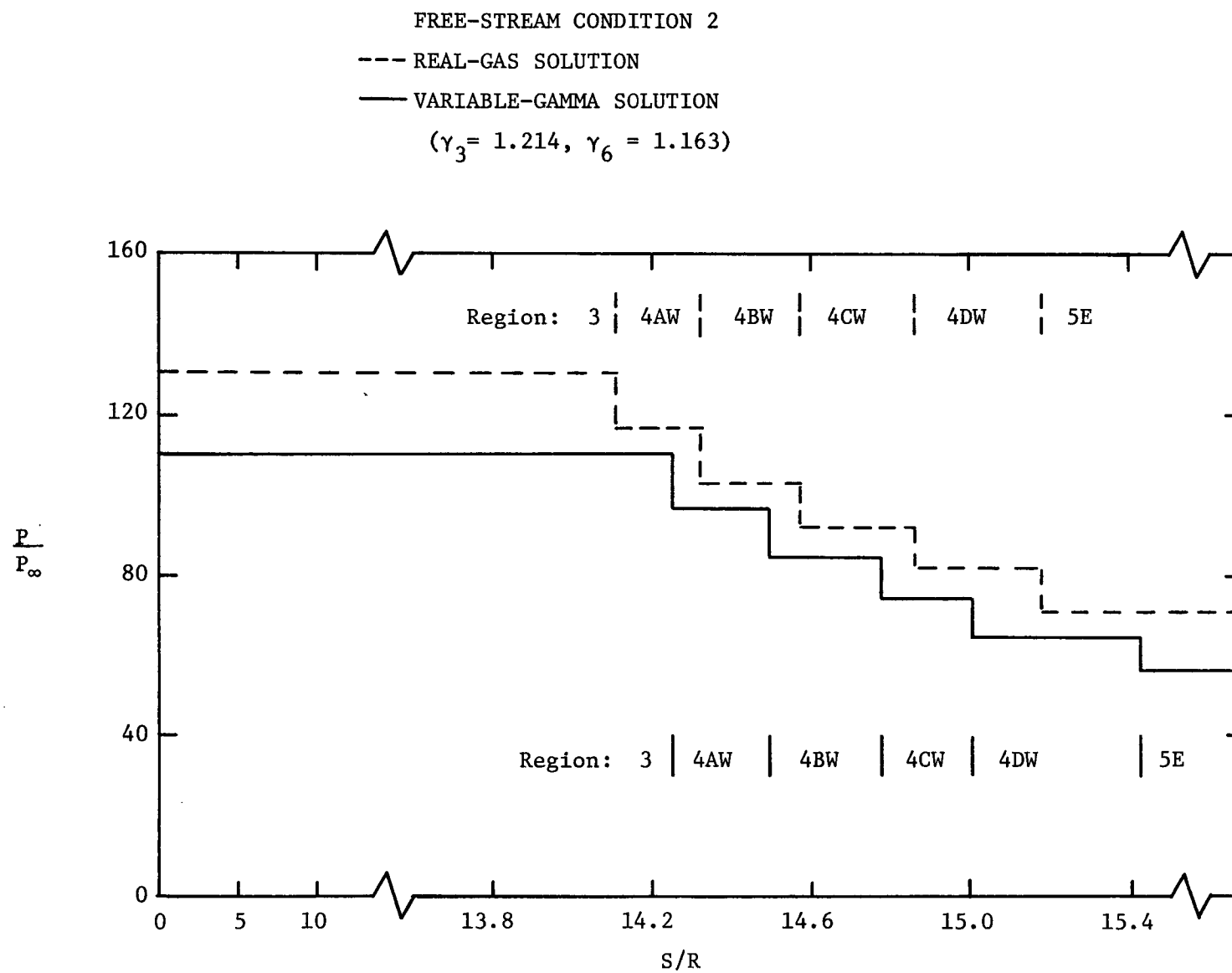


(c) Variable-gamma solution ($\gamma_3 = 1.214$, $\gamma_6 = 1.163$)

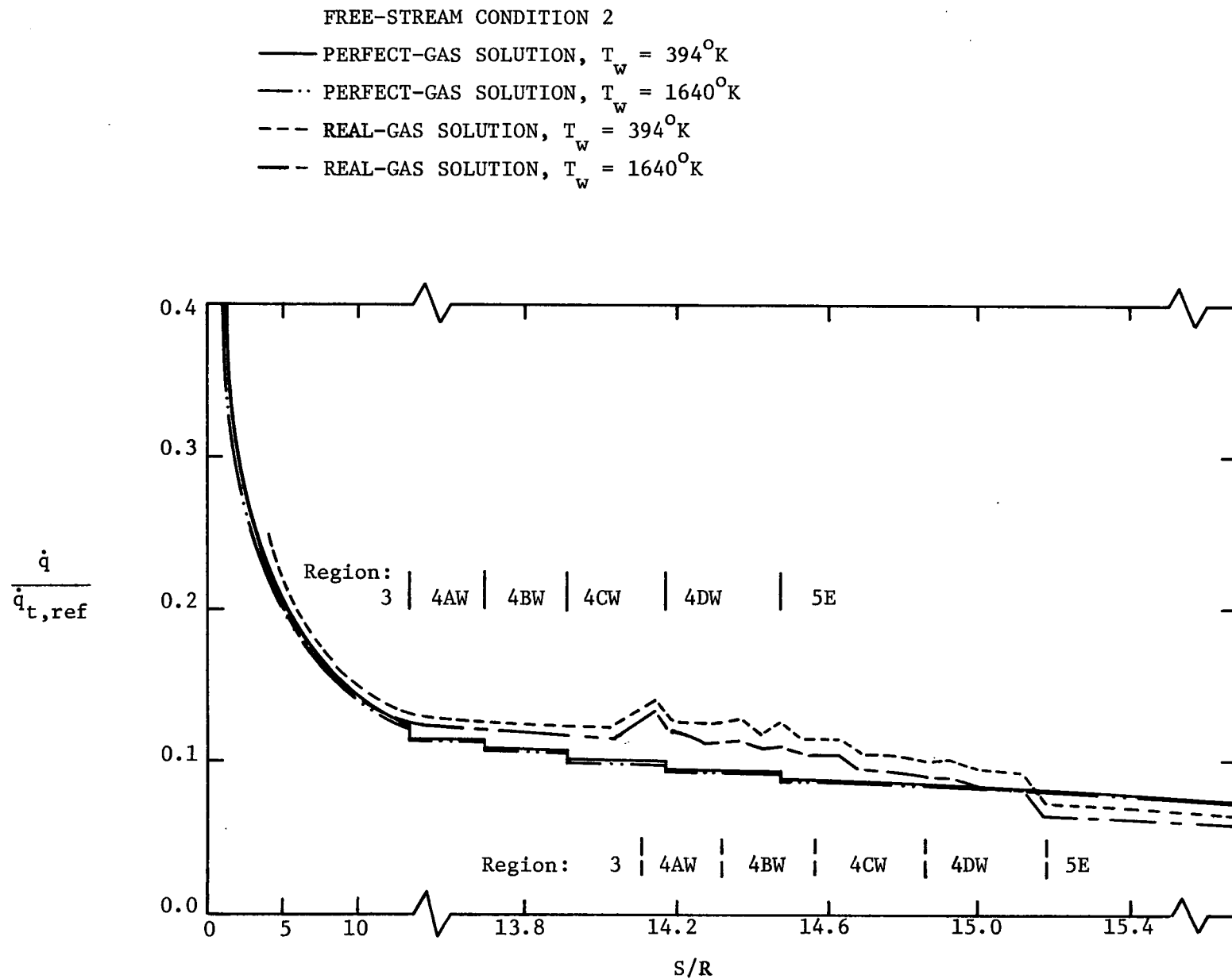


(a) Real-gas compared with perfect-gas

Figure 3. The pressure distributions for the wing leading-edge; $U_\infty = 4330$ m/sec, $P_\infty = 0.333$ mmHg, $T_\infty = 273^\circ\text{K}$, $\Lambda = 60^\circ$.



(b) Real-gas compared with variable-gamma



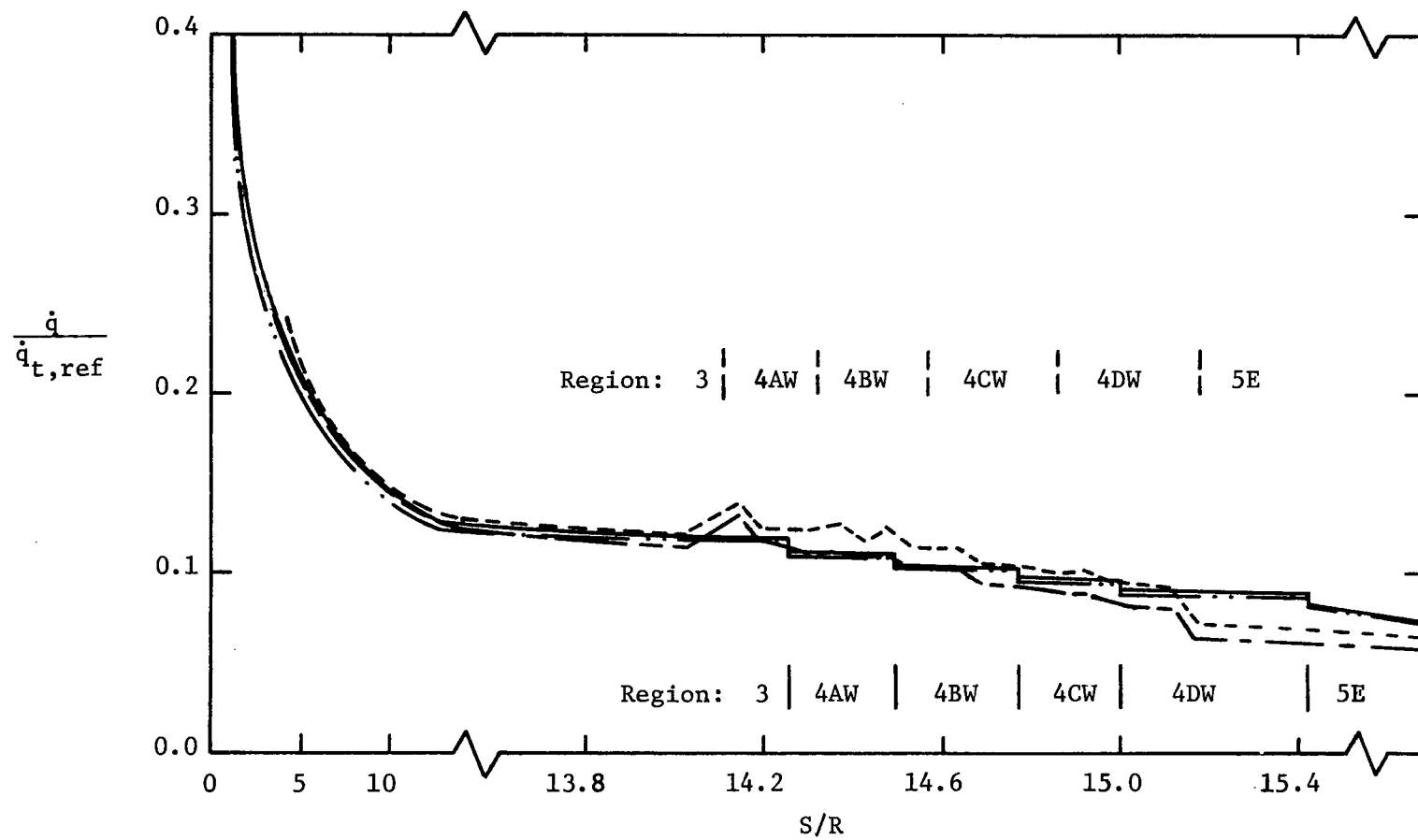
(a) Real-gas compared with perfect gas

Figure 4. - The heat-transfer distributions for the wing leading edge;

$$U_\infty = 4330 \text{ m/sec}, P_\infty = 0.333 \text{ mmHg}, T_\infty = 273^\circ\text{K}, \Lambda = 60^\circ$$

--- REAL-GAS SOLUTION, $T_w = 394^\circ\text{K}$
 --- REAL-GAS SOLUTION, $T_w = 1640^\circ\text{K}$
 — VARIABLE-GAMMA SOLUTION, $T_w = 394^\circ\text{K}$
 — VARIABLE-GAMMA SOLUTION, $T_w = 1640^\circ\text{K}$

$\left. \begin{array}{l} \\ \end{array} \right\} \gamma_3 = 1.214, \gamma_6 = 1.163$



(b) Real-gas compared with variable-gamma

Figure 4. - Concluded.

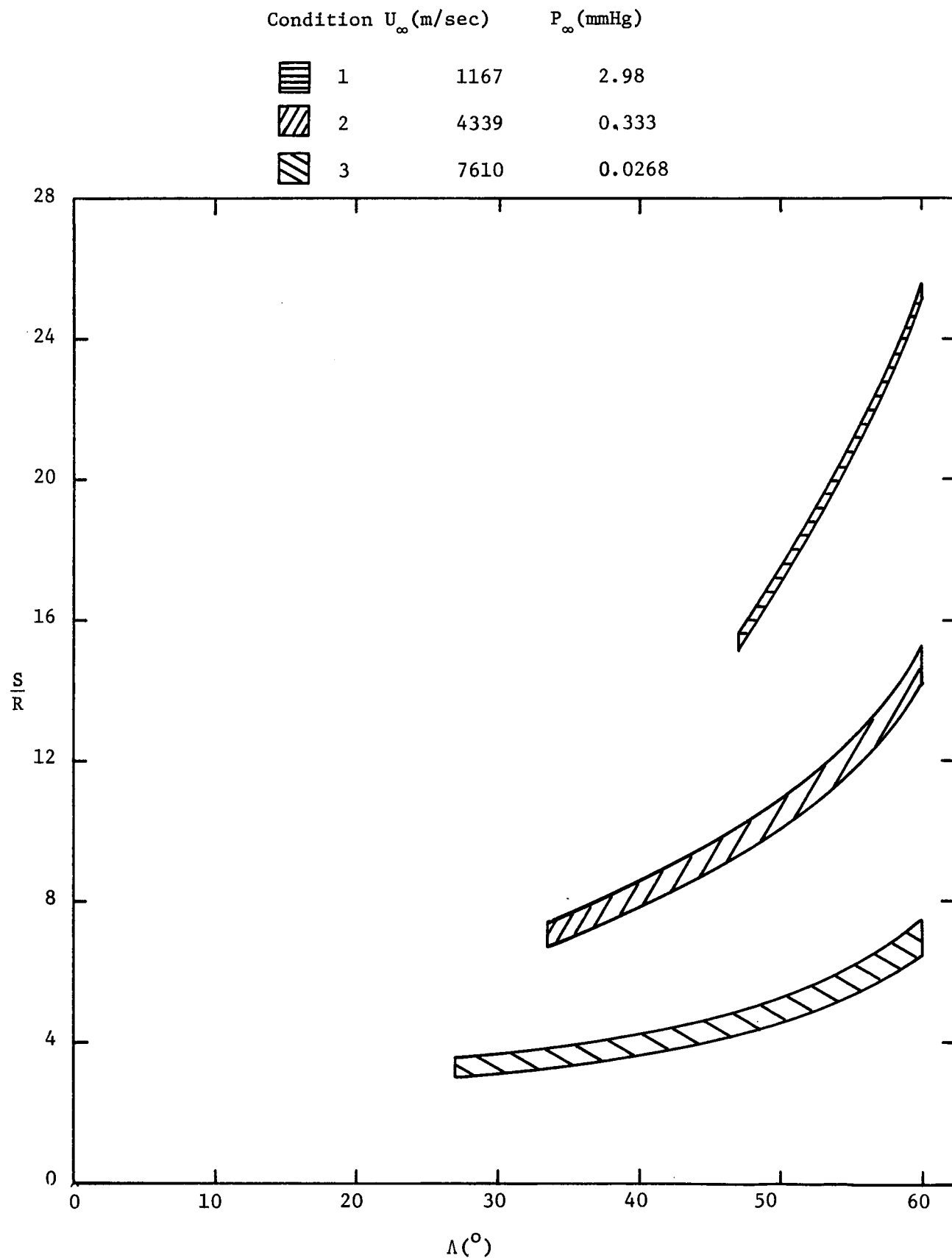
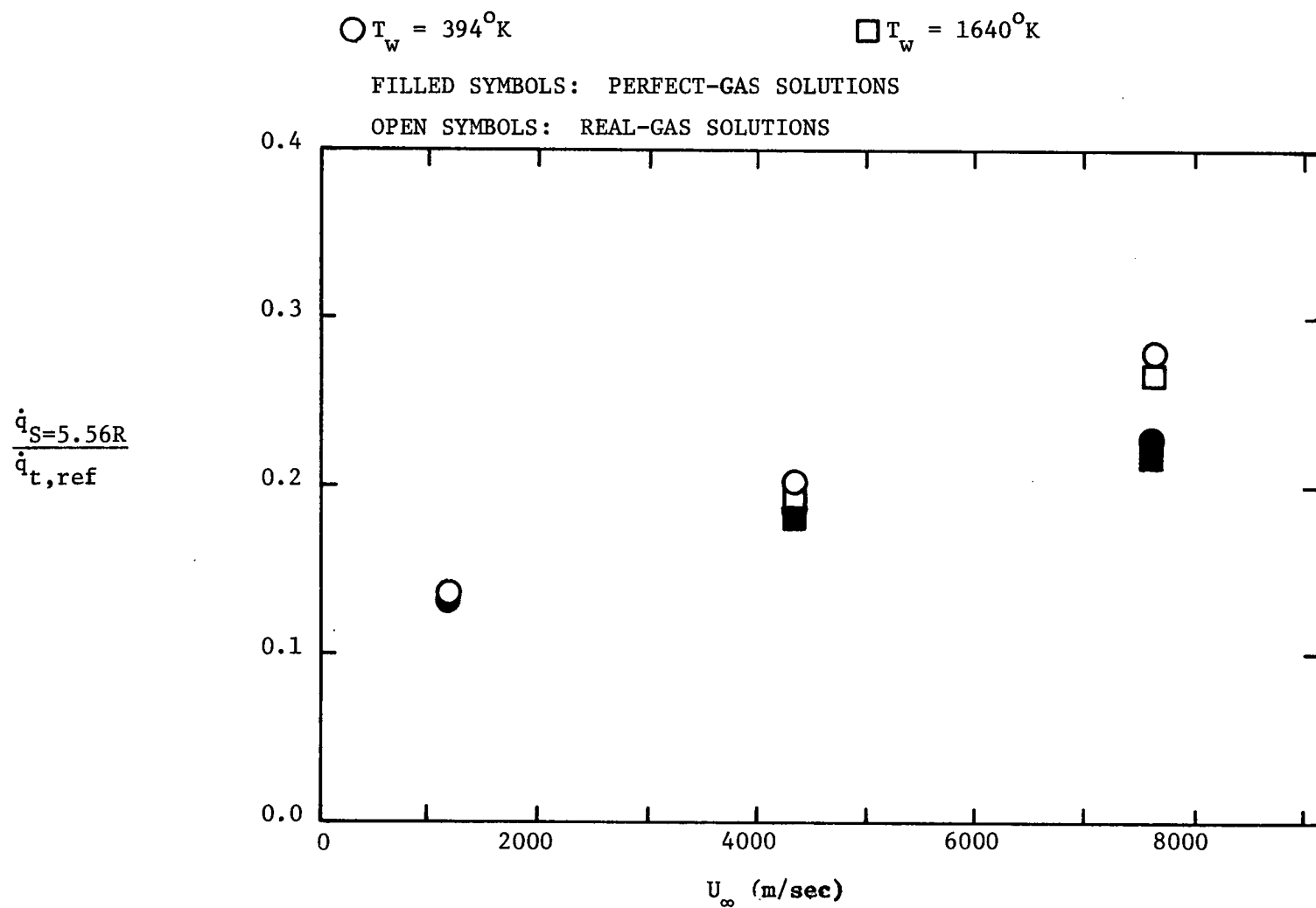


Figure 5. - The location and the extent of the interaction-perturbed region of the wing leading-edge as a function of leading-edge sweep (real-gas solutions).

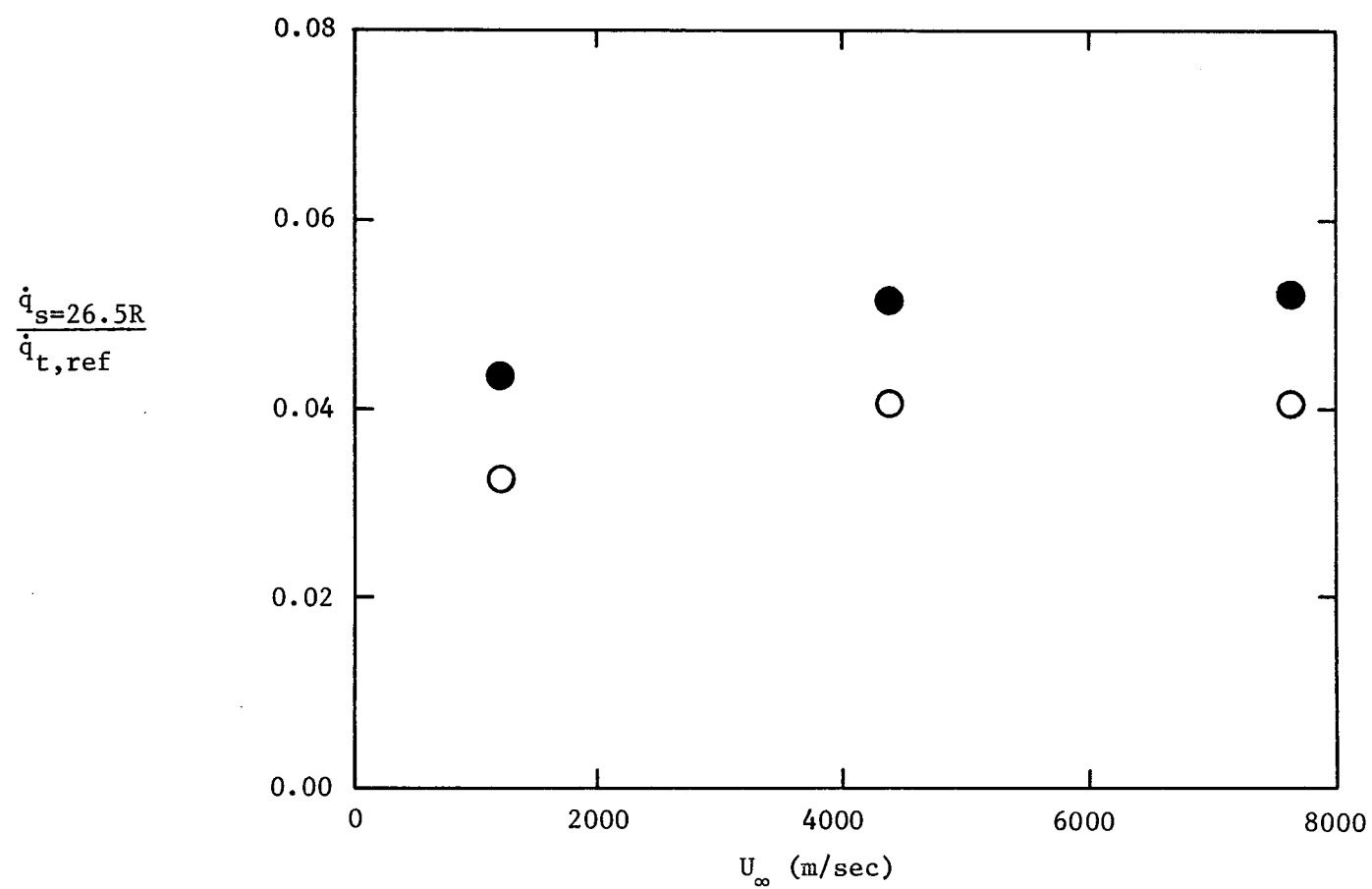


(a) Point in Region 3, $\Lambda = 60^\circ$.

Figure 6. - The effect of free-stream velocity and of wall temperature on the leading-edge heat-transfer.

FILLED SYMBOL: PERFECT-GAS SOLUTIONS

OPEN SYMBOL: REAL-GAS SOLUTIONS

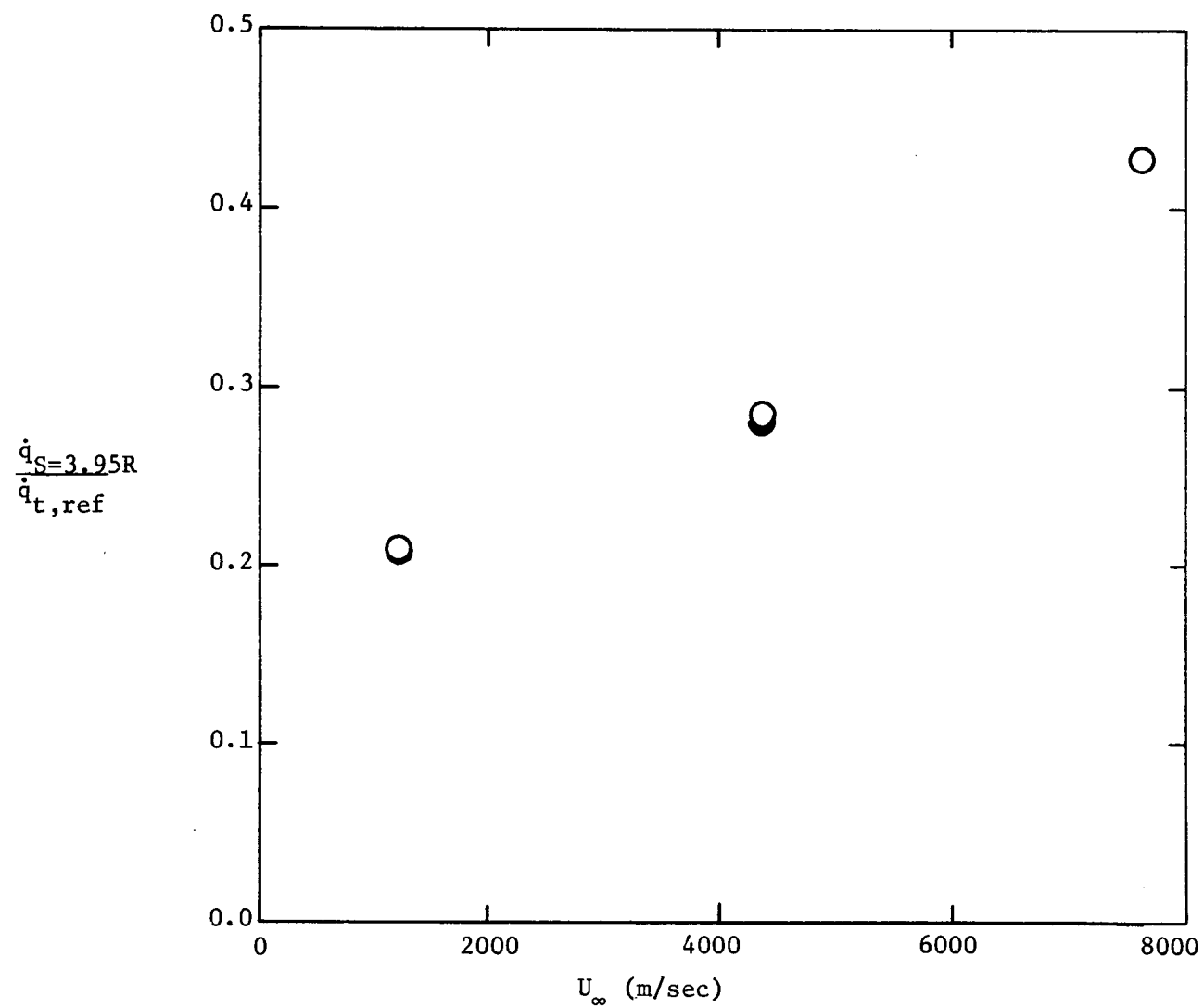


(b) Point in region 5E, $\Lambda = 60^\circ$ ($T_w = 394^\circ\text{K}$ only)

Figure 6. - Continued.

FILLED SYMBOLS: PERFECT-GAS SOLUTIONS

OPEN SYMBOLS: REAL-GAS SOLUTIONS

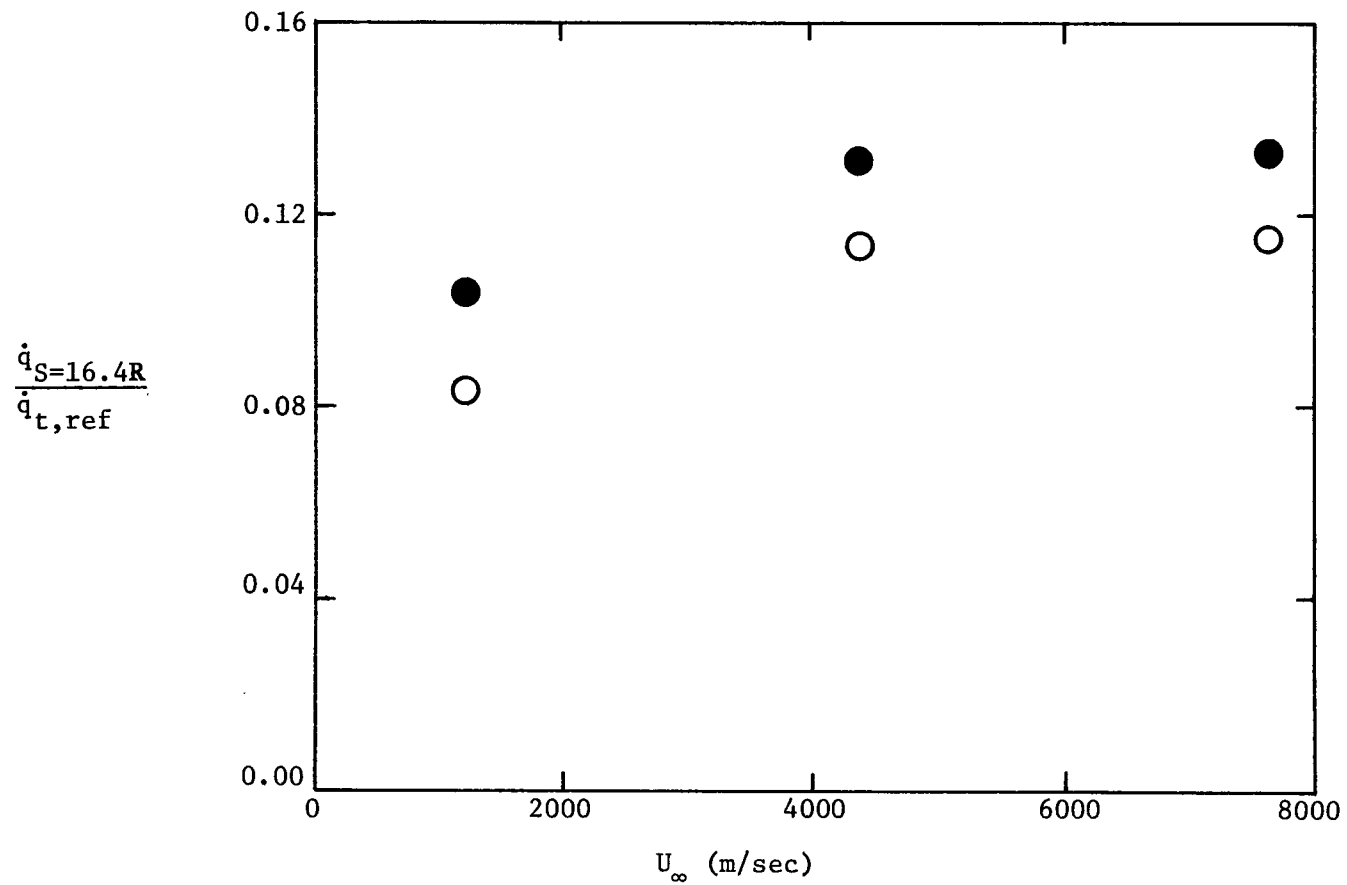


(c) Point in region 3, $\Lambda = 48^\circ$ ($T_w = 394^\circ\text{K}$ only)

Figure 6. - Continued.

FILLED SYMBOLS: PERFECT-GAS SOLUTIONS

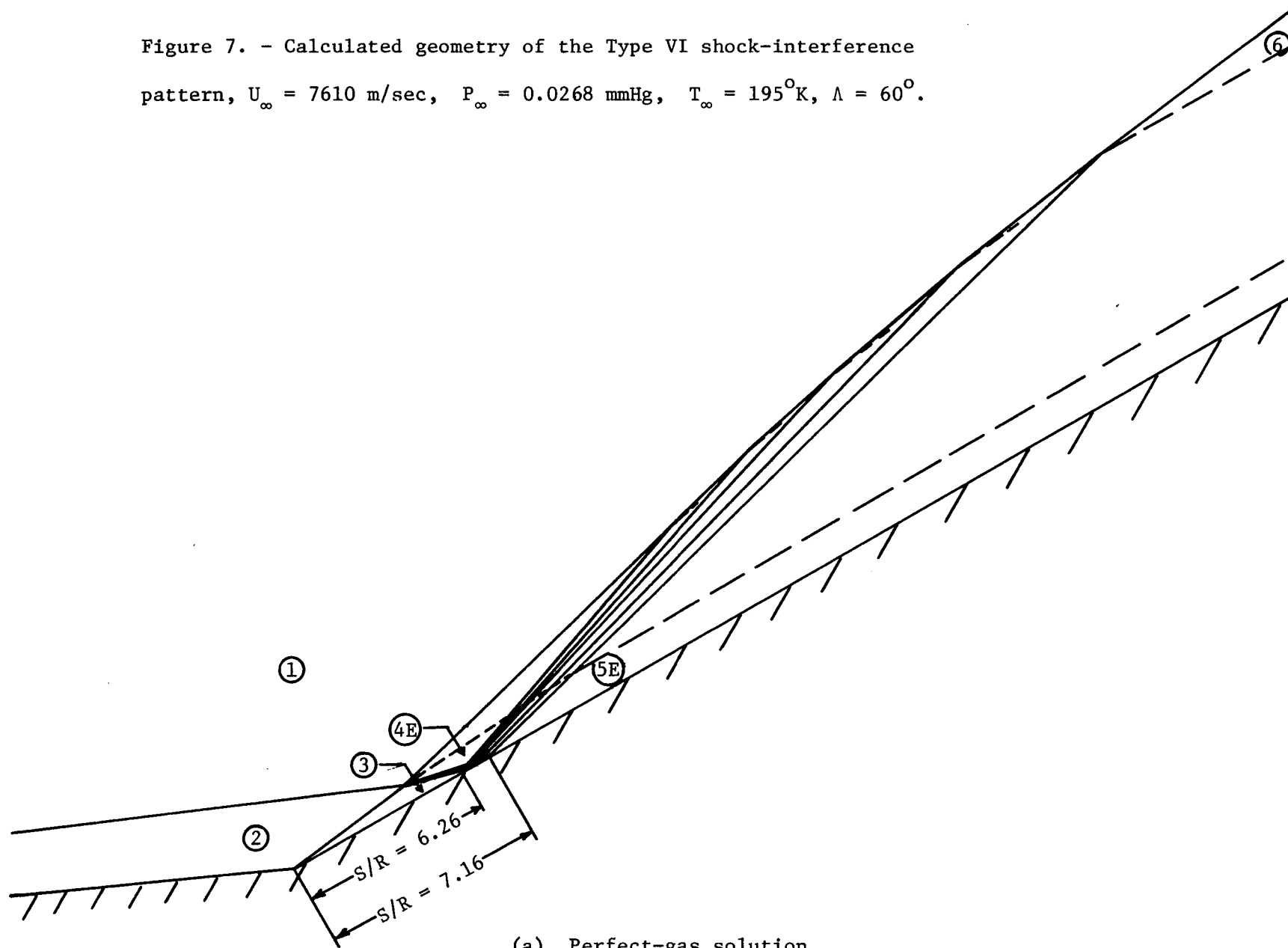
OPEN SYMBOLS: REAL-GAS SOLUTIONS



(d) Point in region 5E, $\Lambda = 48^\circ$ ($T_w = 394^\circ\text{K}$ only)

Figure 6. - Concluded.

Figure 7. - Calculated geometry of the Type VI shock-interference pattern, $U_{\infty} = 7610$ m/sec, $P_{\infty} = 0.0268$ mmHg, $T_{\infty} = 195^{\circ}\text{K}$, $\Lambda = 60^{\circ}$.



(a) Perfect-gas solution

Figure 7. - Continued.

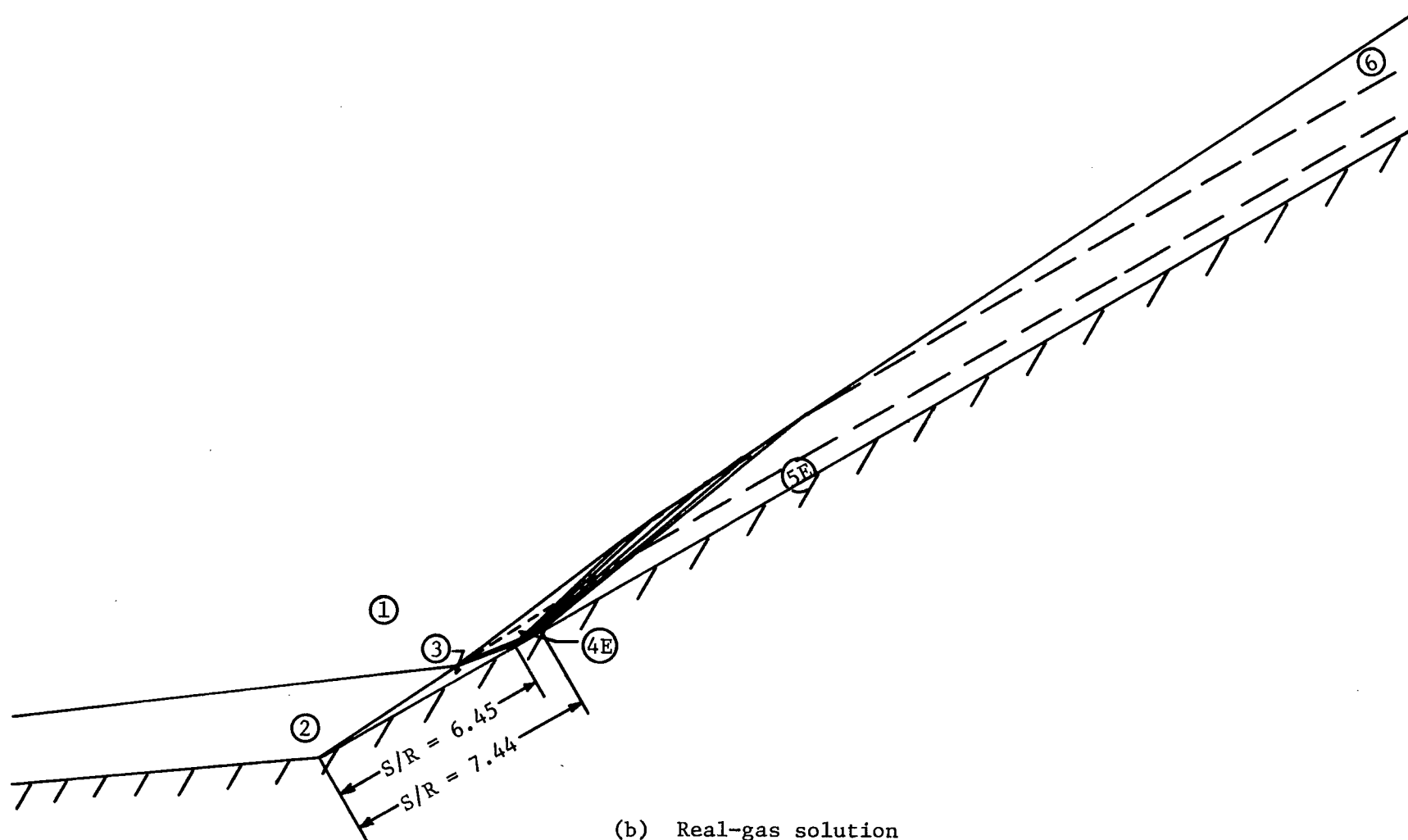
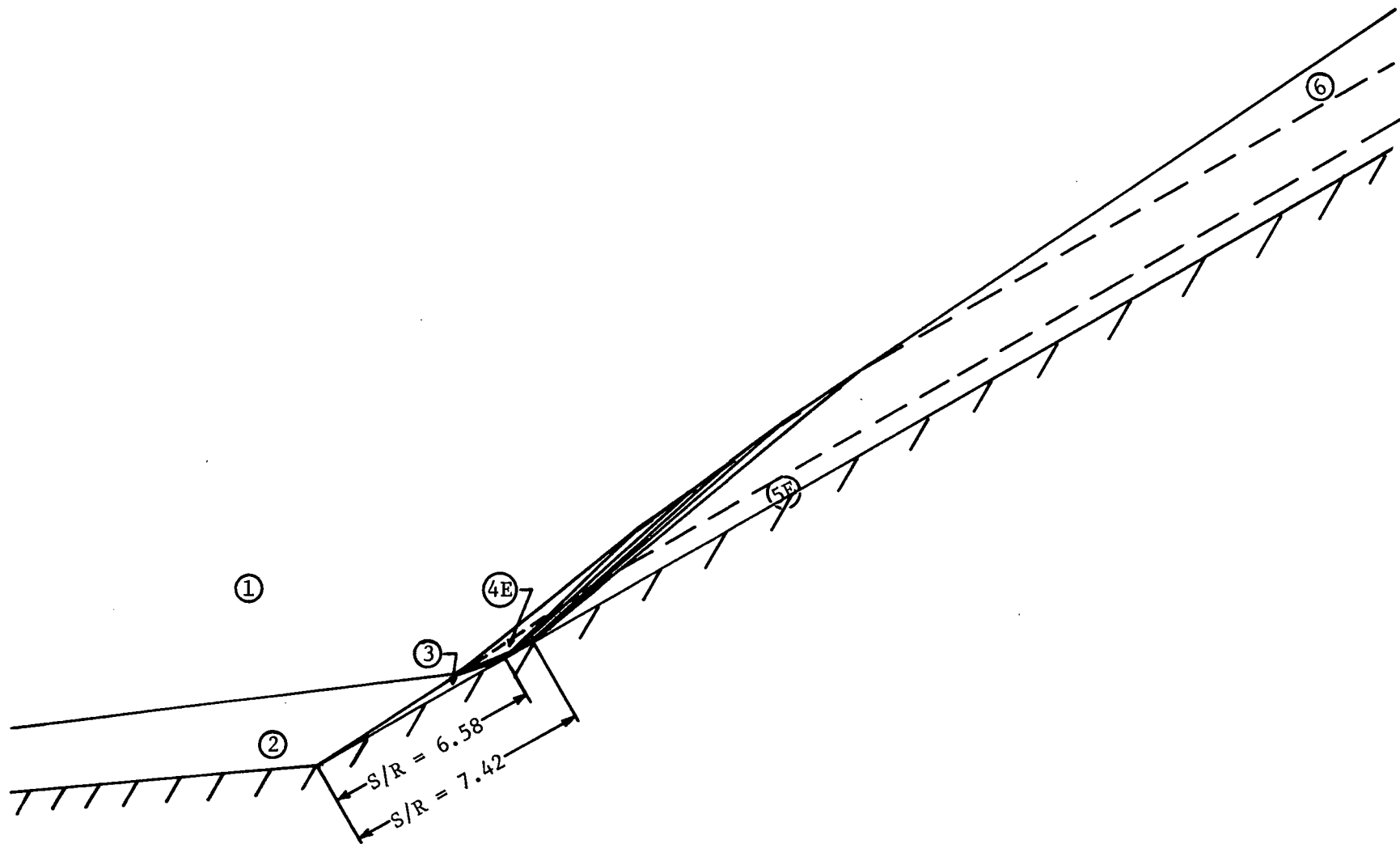
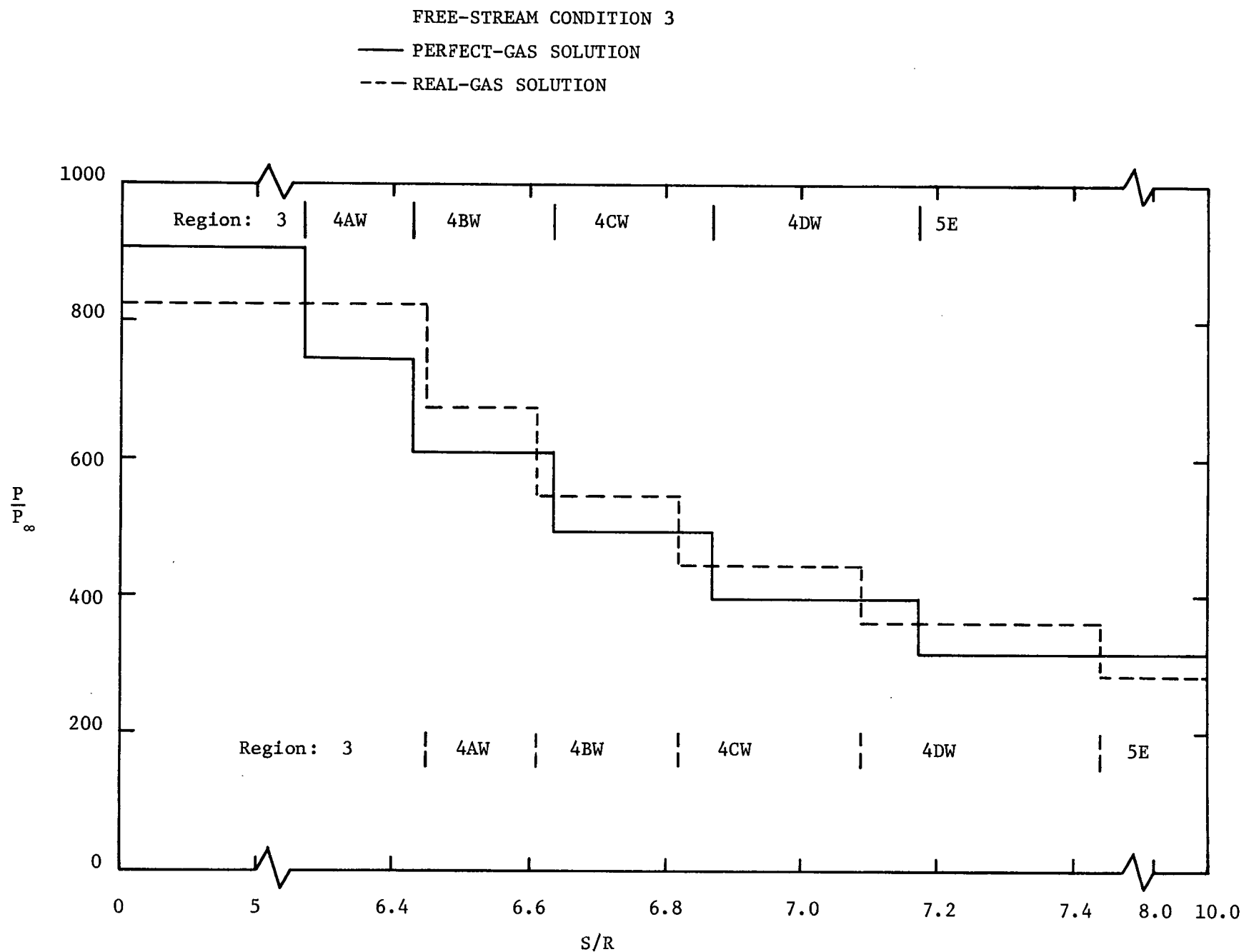


Figure 7. - Concluded.



(c) Variable-gamma solution ($\gamma_3 = 1.169$, $\gamma_6 = 1.216$)



(a) Real-gas compared with perfect-gas

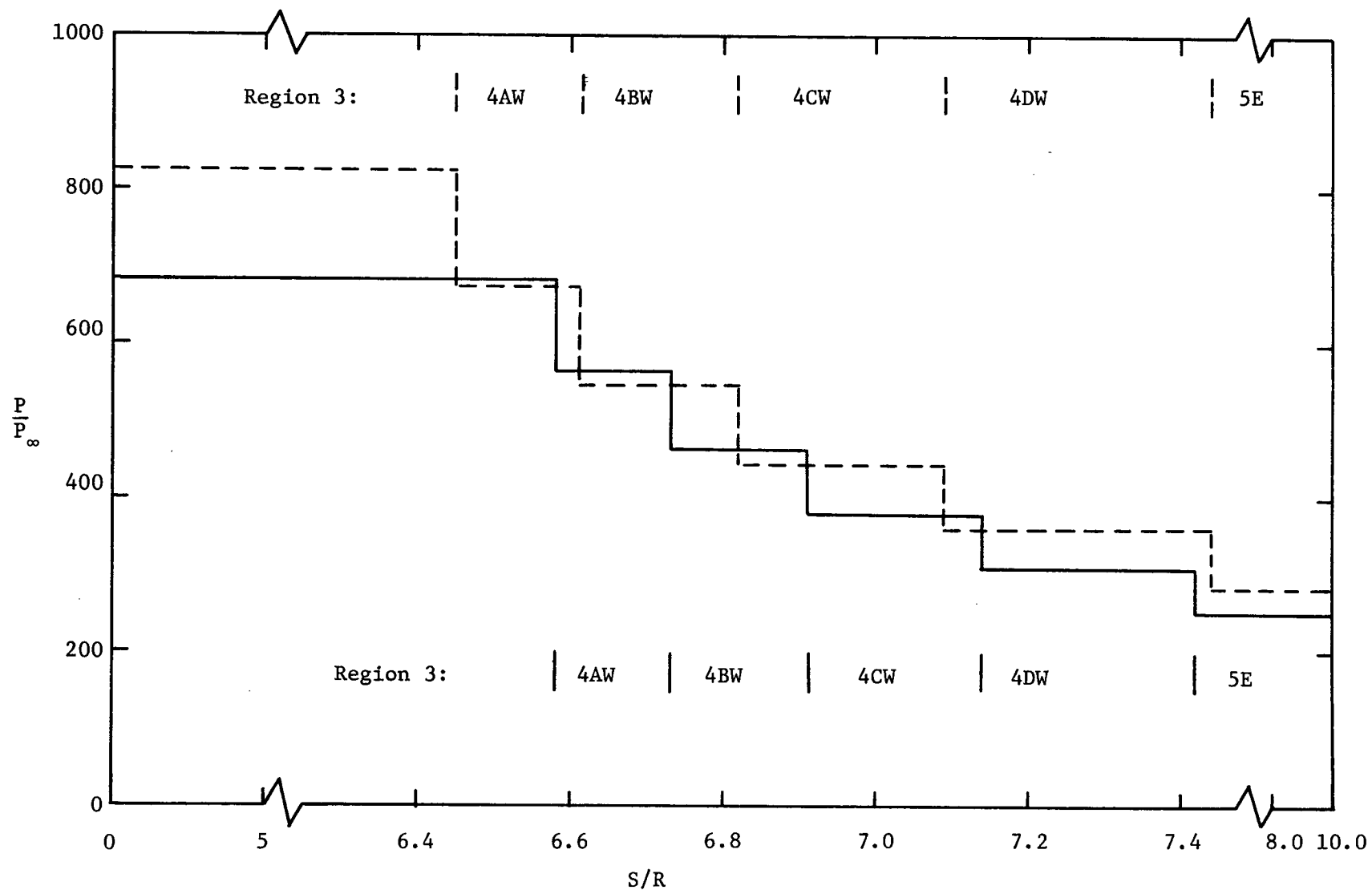
Figure 8. - The pressure distributions for the wing leading-edge; $U_{\infty} = 7610$ m/sec, $P_{\infty} = 0.0268$ mmHg, $T_{\infty} = 195^{\circ}\text{K}$, $\Lambda = 60^{\circ}$.

FREE-STREAM CONDITION 3

--- REAL-GAS SOLUTION

— VARIABLE-GAMMA SOLUTION

($\gamma_3 = 1.169$, $\gamma_6 = 1.216$)

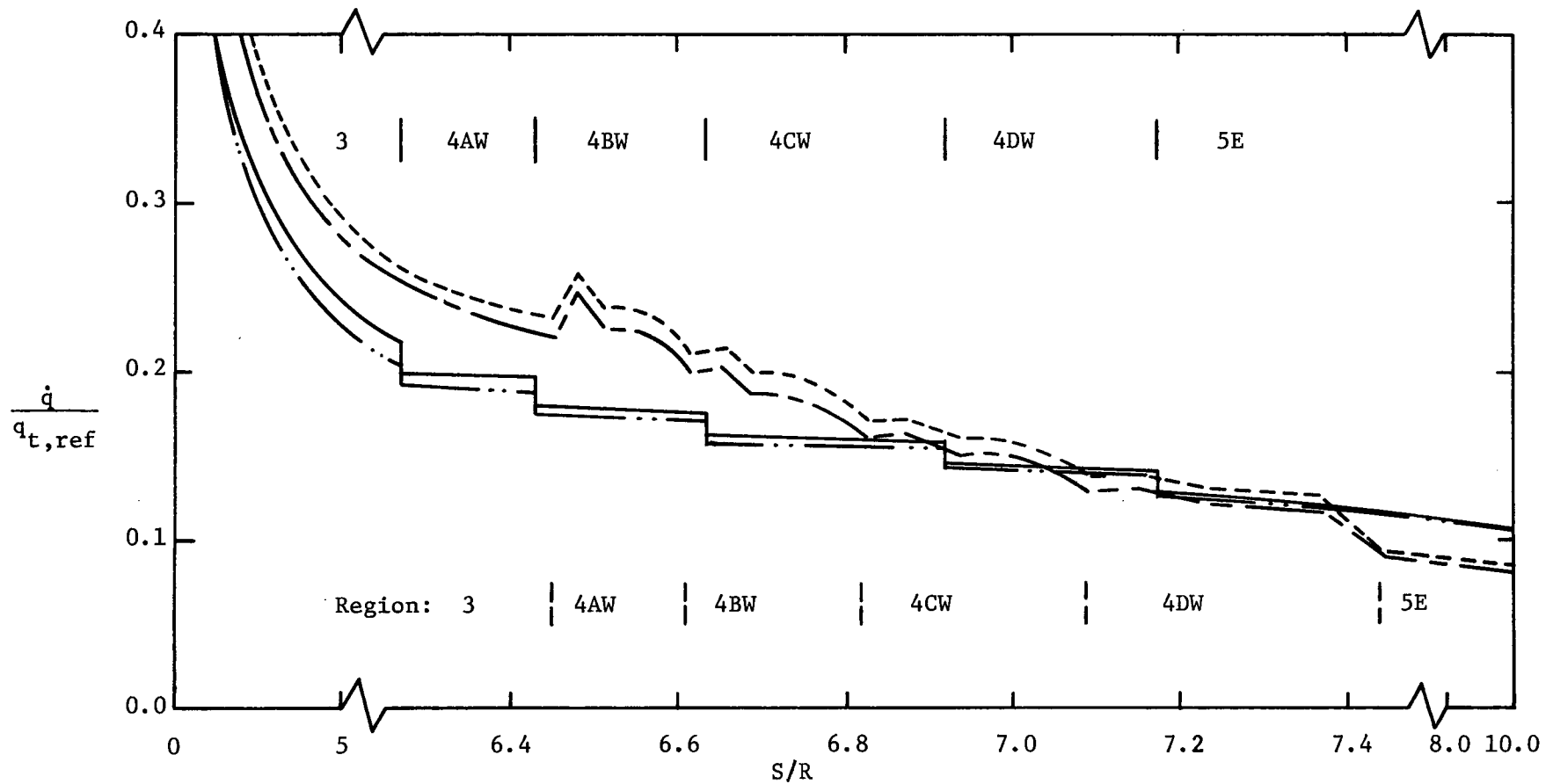


(b) Real-gas compared with variable-gamma

Figure 8. - Concluded.

FREE-STREAM CONDITION 3

- PERFECT-GAS SOLUTION, $T_w = 394^\circ\text{K}$
- · — PERFECT-GAS SOLUTION, $T_w = 1640^\circ\text{K}$
- - - REAL-GAS SOLUTION, $T_w = 394^\circ\text{K}$
- - - REAL-GAS SOLUTION, $T_w = 1640^\circ\text{K}$

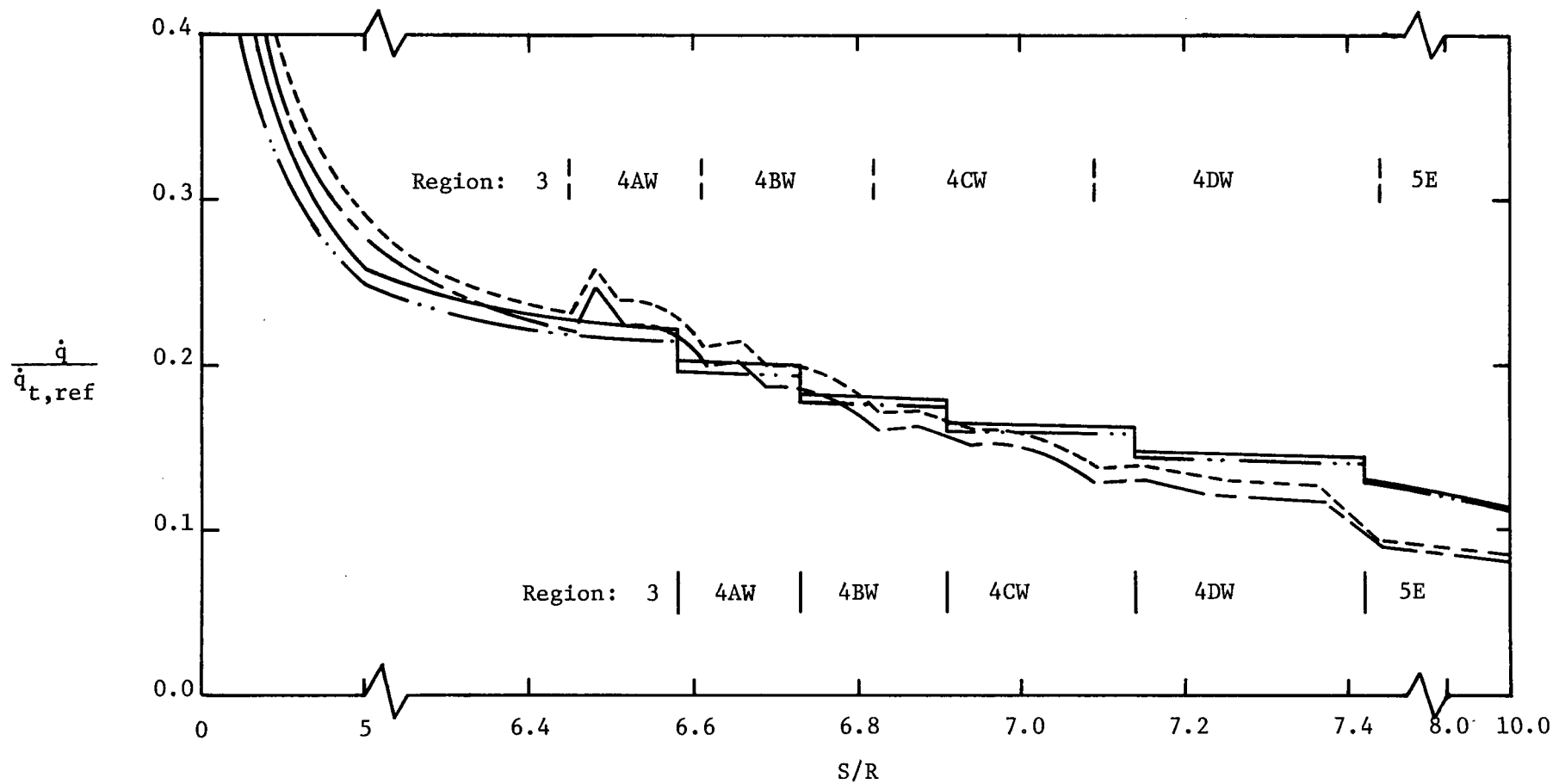


(a) Real-gas compared with perfect-gas

Figure 9. - The heat-transfer distributions for the wing leading-edge; $U_\infty = 7610$ m/sec, $P_\infty = 0.0268$ mmHg, $T_\infty = 195^\circ\text{K}$, $\Lambda = 60^\circ$.

--- REAL-GAS SOLUTION, $T_w = 394^\circ\text{K}$
 --- REAL-GAS SOLUTION, $T_w = 1640^\circ\text{K}$
 — VARIABLE-GAMMA SOLUTION, $T_w = 394^\circ\text{K}$
 - · - VARIABLE-GAMMA SOLUTION, $T_w = 1640^\circ\text{K}$

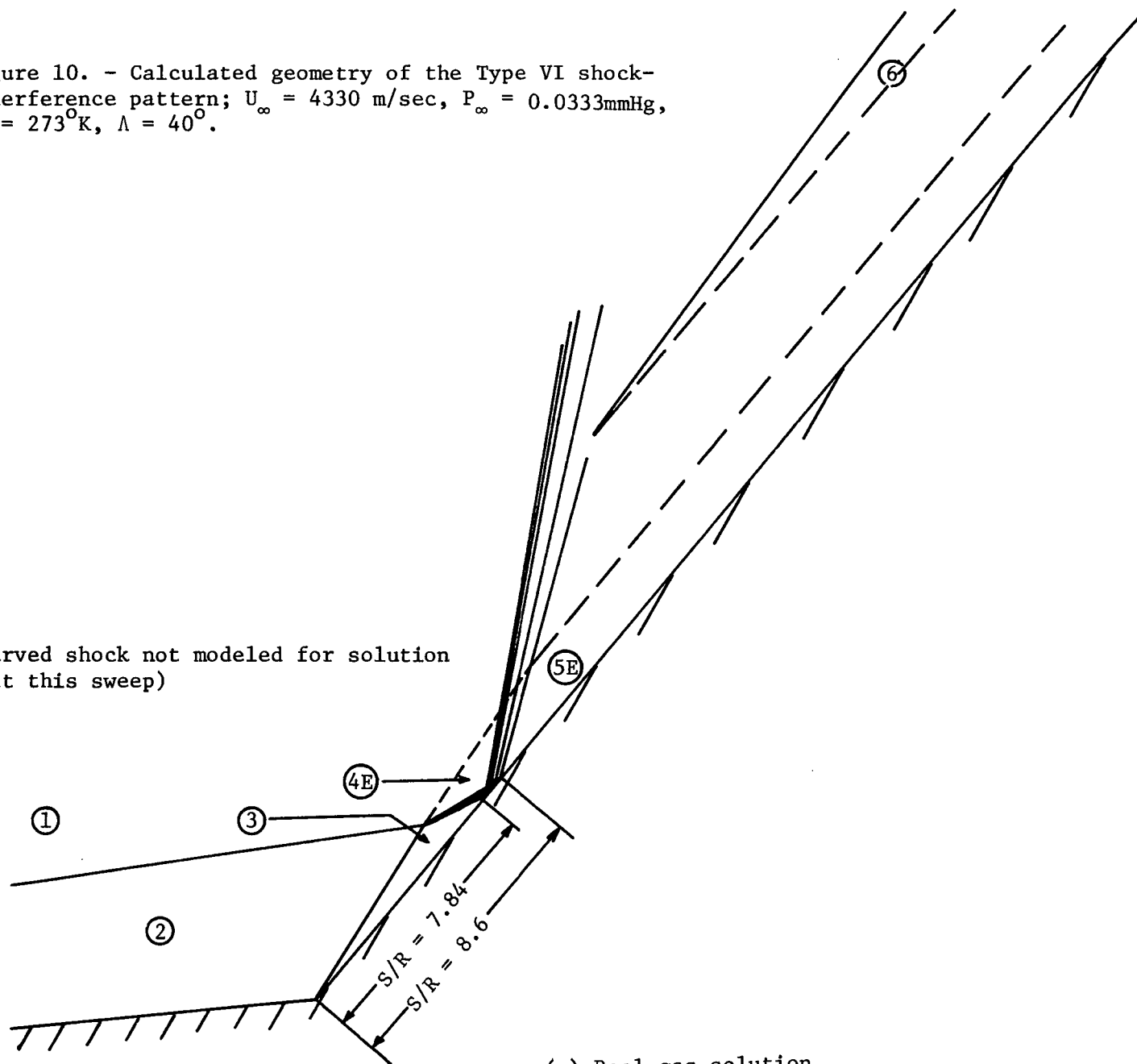
$\gamma_3 = 1.169, \quad \gamma_6 = 1.216$



(b) Real-gas compared with variable-gamma
 Figure 9. - Concluded.

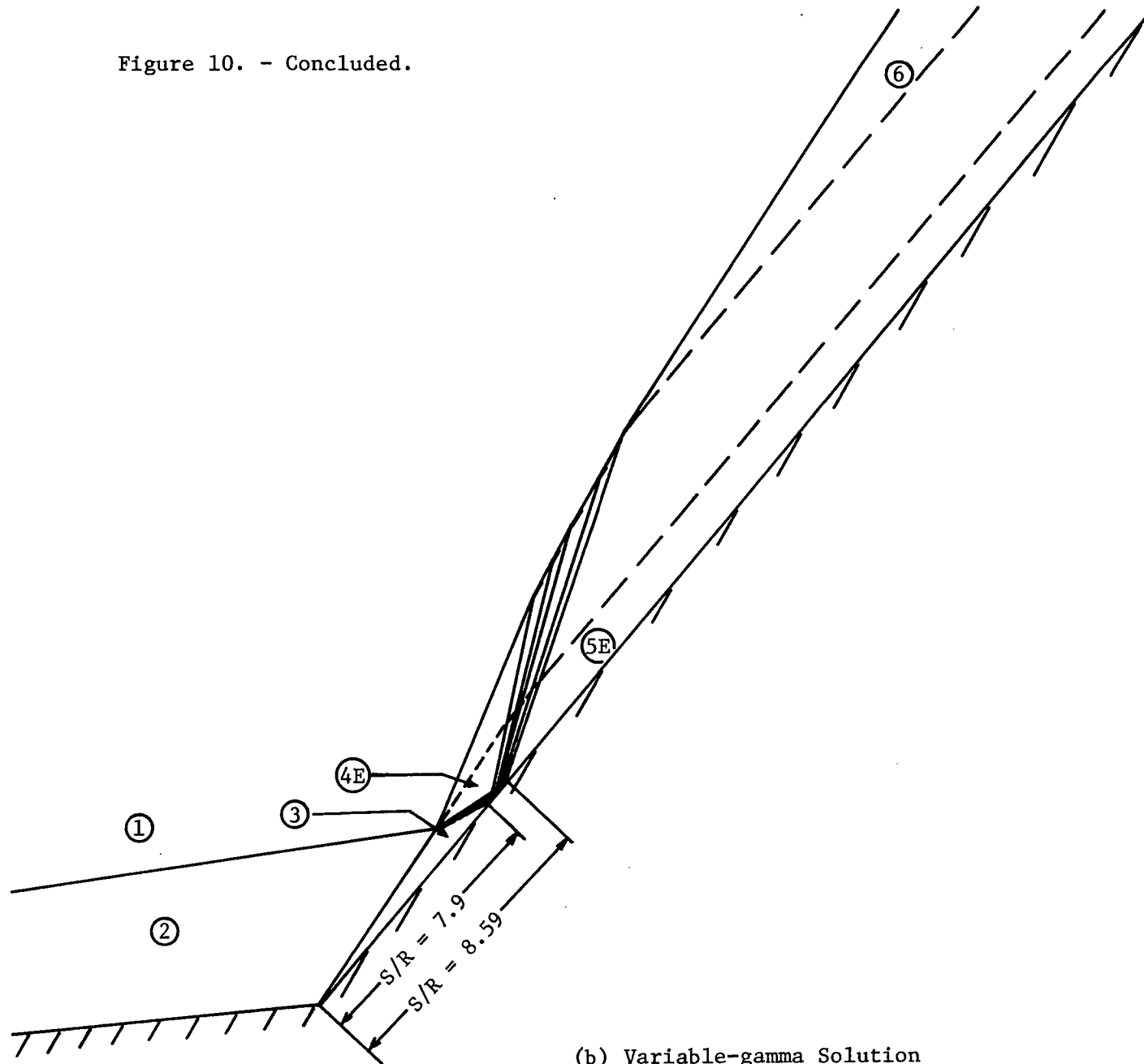
Figure 10. - Calculated geometry of the Type VI shock-interference pattern; $U_{\infty} = 4330$ m/sec, $P_{\infty} = 0.0333$ mmHg, $T_{\infty} = 273^{\circ}\text{K}$, $\Lambda = 40^{\circ}$.

Curved shock not modeled for solution
(at this sweep)



(a) Real-gas solution

Figure 10. - Concluded.



(b) Variable-gamma Solution
($\gamma_3 = 1.159$, $\gamma_6 = 1.158$)

FREE-STREAM CONDITION 2

--- REAL-GAS SOLUTION

— VARIABLE-GAMMA SOLUTION

($\gamma_3 = 1.159$, $\gamma_6 = 1.158$)

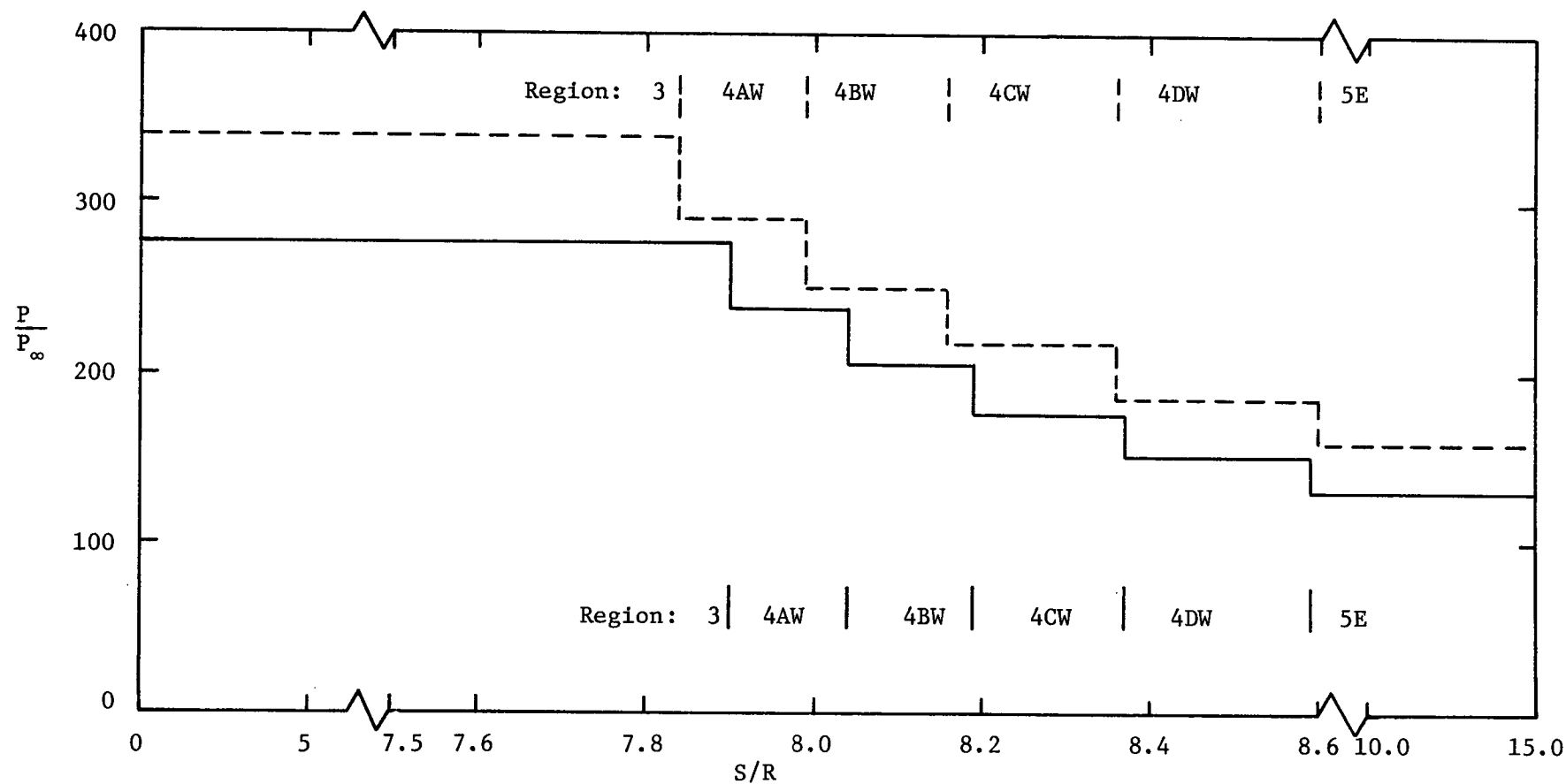


Figure 11. - A comparison of the real-gas and the variable-gamma pressure distribution for the wing leading-edge; $U_\infty = 4330$ m/sec, $P_\infty = 0.333$ mmHg, $T_\infty = 273^\circ\text{K}$, $\Lambda = 40^\circ$.

FREE-STREAM CONDITION 2

- REAL-GAS SOLUTION, $T_w = 394^\circ\text{K}$
 --- REAL-GAS SOLUTION, $T_w = 1640^\circ\text{K}$
 — VARIABLE-GAMMA SOLUTION, $T_w = 394^\circ\text{K}$
 —.. VARIABLE-GAMMA SOLUTION, $T_w = 1640^\circ\text{K}$
- $\left. \begin{array}{l} \text{--- REAL-GAS SOLUTION, } T_w = 394^\circ\text{K} \\ \text{--- REAL-GAS SOLUTION, } T_w = 1640^\circ\text{K} \\ \text{— VARIABLE-GAMMA SOLUTION, } T_w = 394^\circ\text{K} \\ \text{—.. VARIABLE-GAMMA SOLUTION, } T_w = 1640^\circ\text{K} \end{array} \right\} \gamma_3 = 1.159, \quad \gamma_6 = 1.158$

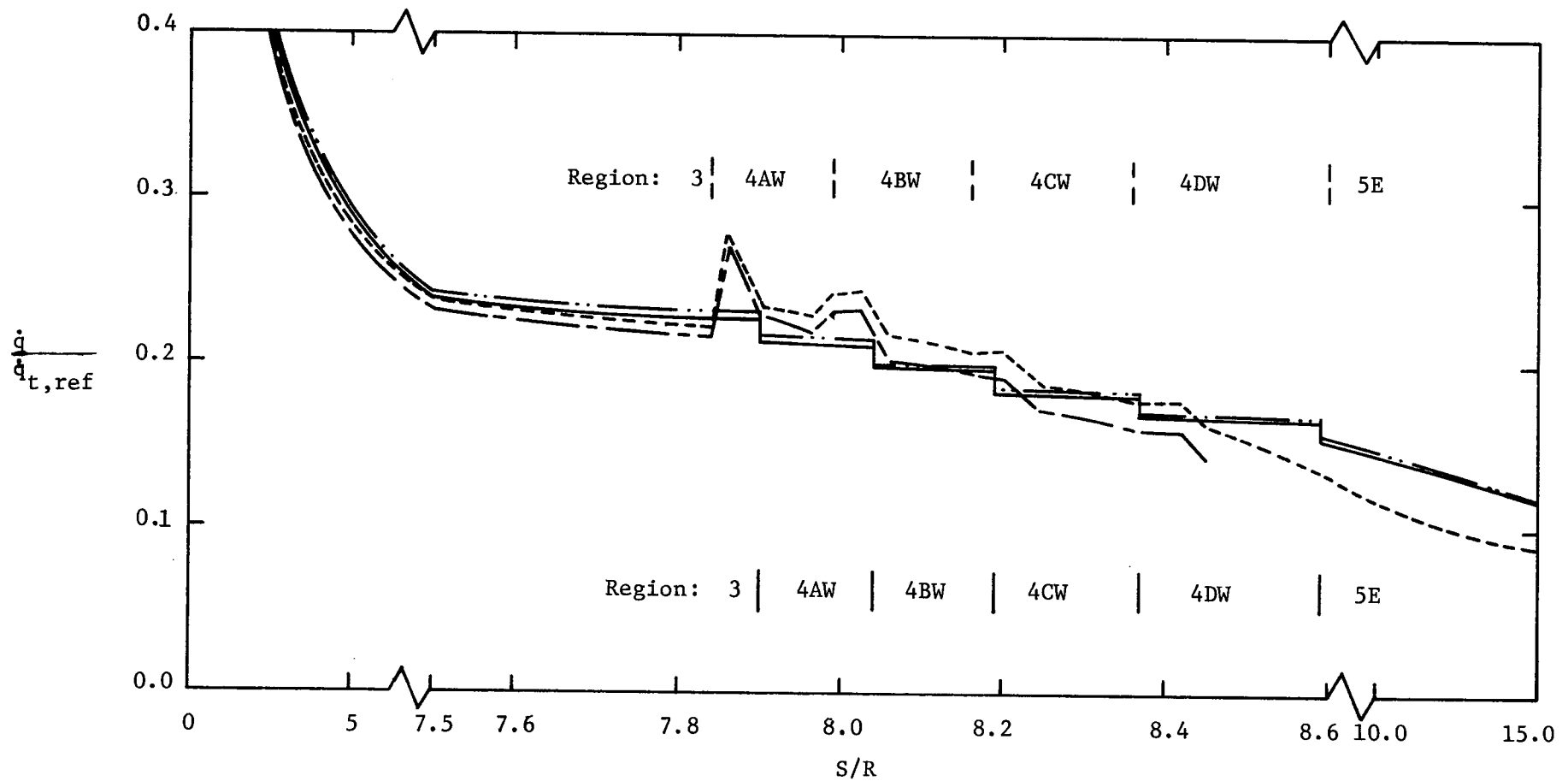

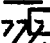
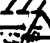



Figure 12. - A comparison of the real-gas and the variable-gamma heat-transfer distributions for the wing leading-edge; $U_\infty = 4330$ m/sec, $P_\infty = 0.333$ mmHg, $T_\infty = 273^\circ\text{K}$, $\Lambda = 40^\circ$.

-  PERFECT-GAS SOLUTIONS ($\gamma = 1.4$ THROUGHOUT)
-  REAL-GAS SOLUTIONS
-  VARIABLE-GAMMA SOLUTIONS
-  CONSTANT-GAMMA SOLUTIONS ($\gamma = 1.2$ THROUGHOUT)

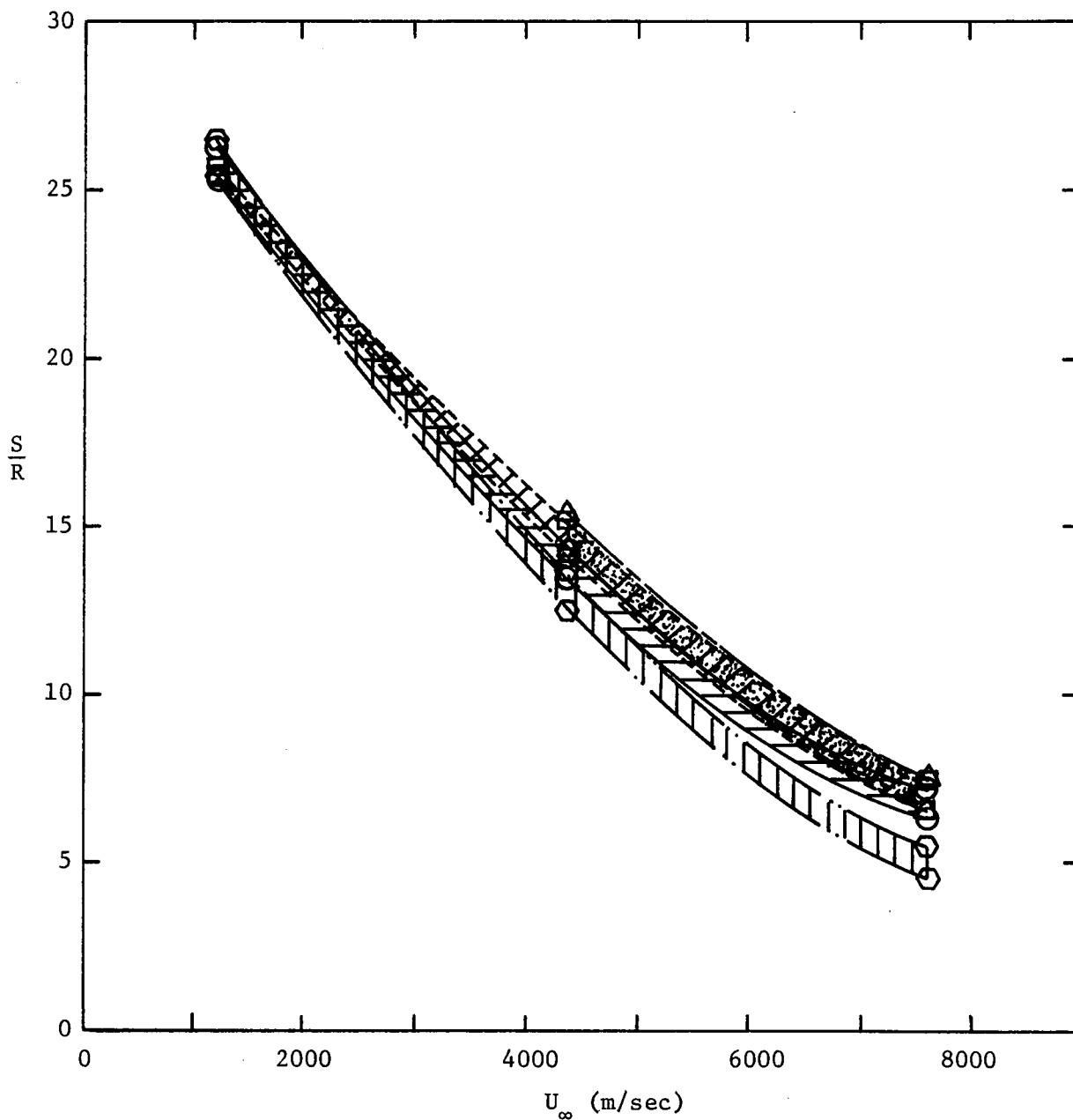
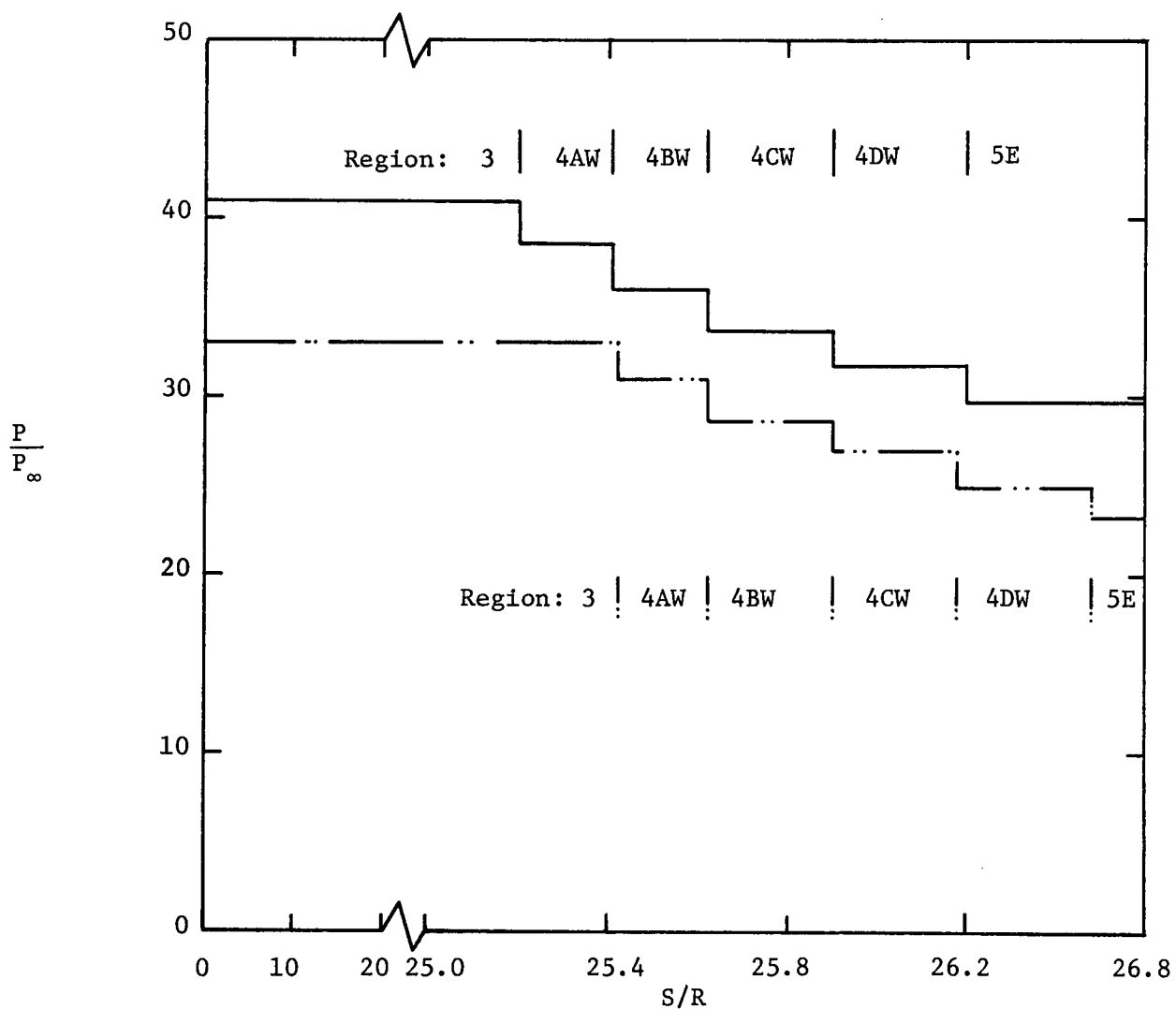


Figure 13. - The location of the interaction-perturbed region on the wing leading-edge as a function of velocity ($\Lambda = 60^\circ$).

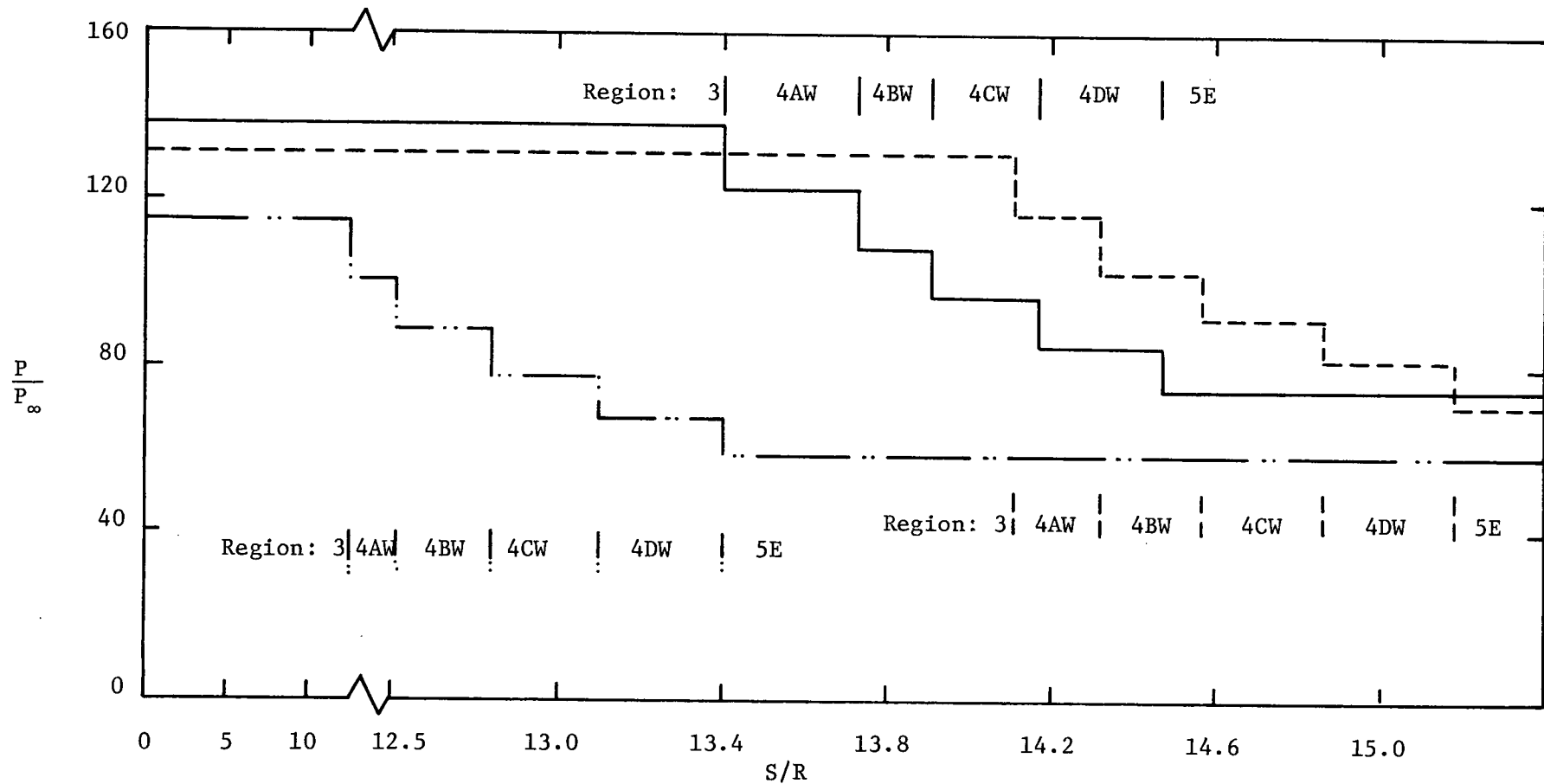
— PERFECT-GAS SOLUTION ($\gamma = 1.4$ THROUGHOUT)
 —·· CONSTANT-GAMMA SOLUTION ($\gamma = 1.2$ THROUGHOUT)



(a) Condition 1: $U_\infty = 1167$ m/sec, $P_\infty = 2.98$ mmHg, $T_\infty = 53^\circ\text{K}$

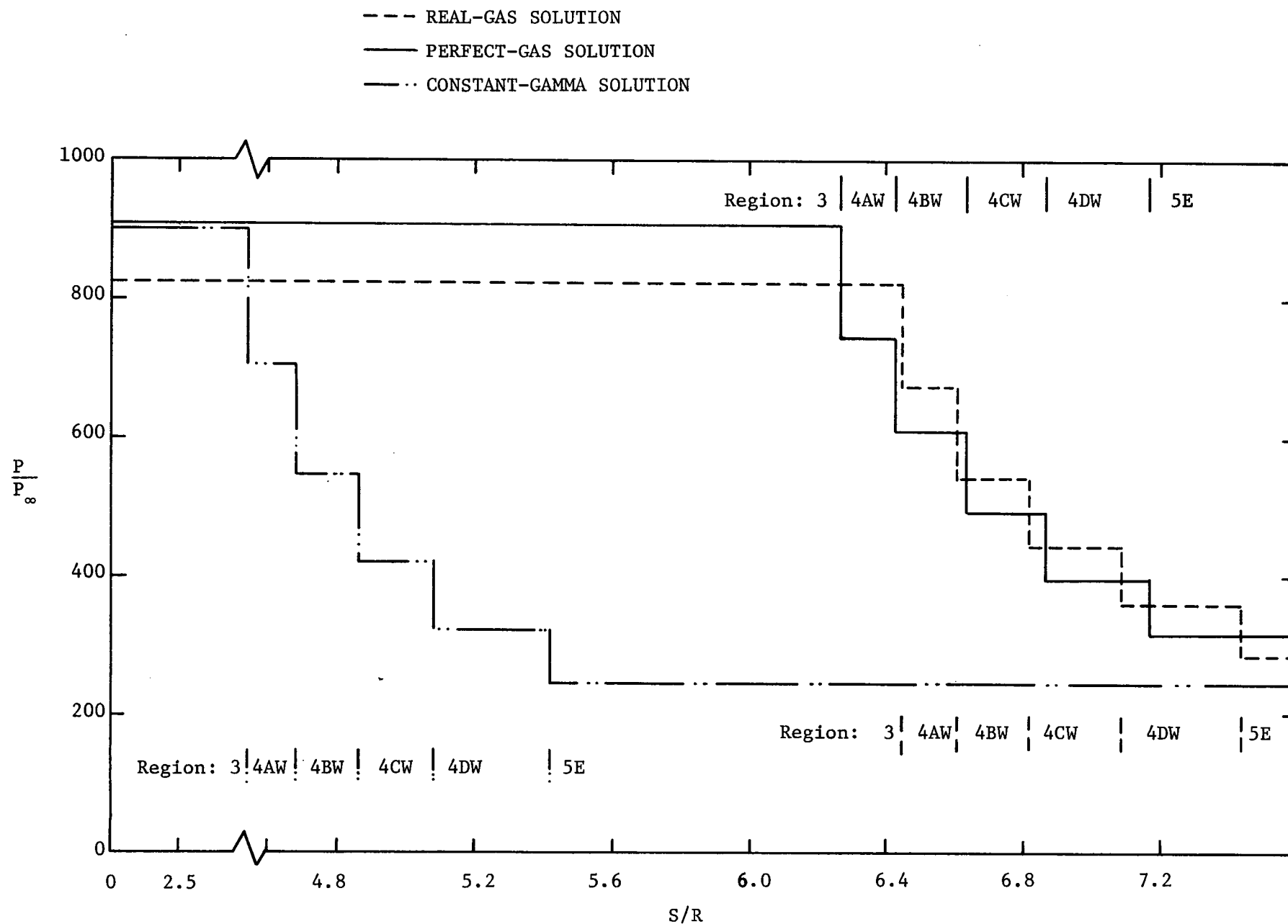
Figure 14. - The pressure-distribution along the wing leading-edge,
 $\Lambda = 60^\circ$.

--- REAL-GAS SOLUTION
 — PERFECT-GAS SOLUTION
 - · - CONSTANT-GAMMA SOLUTION



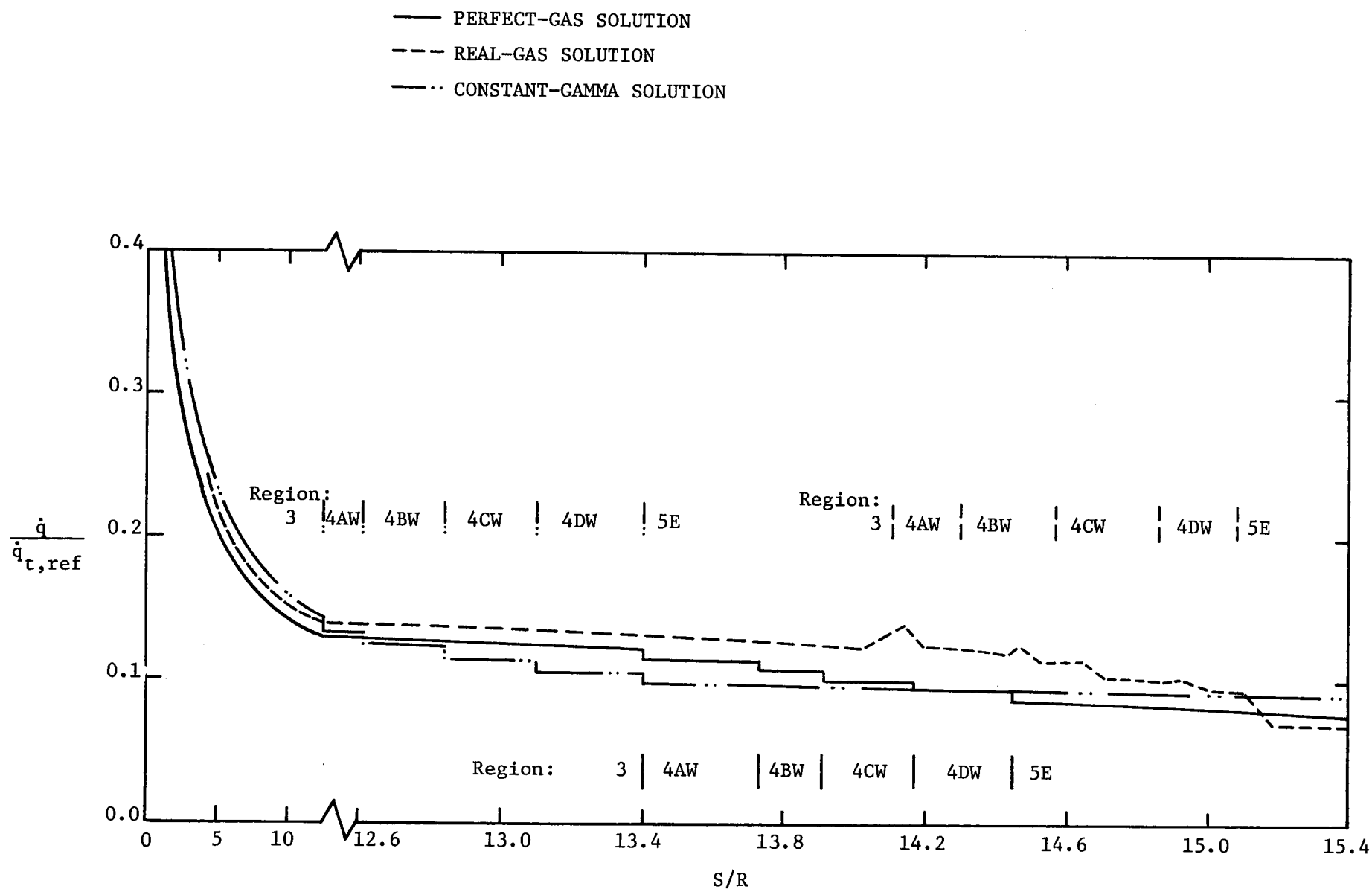
(b) Condition 2: $U_\infty = 4330$ m/sec, $P_\infty = 0.333$ mmHg, $T_\infty = 273^\circ\text{K}$

Figure 14. - Continued.



(c) Condition 3: $U_\infty = 7610$ m/sec, $P_\infty = 0.0268$ mmHg, $T_\infty = 195^\circ\text{K}$

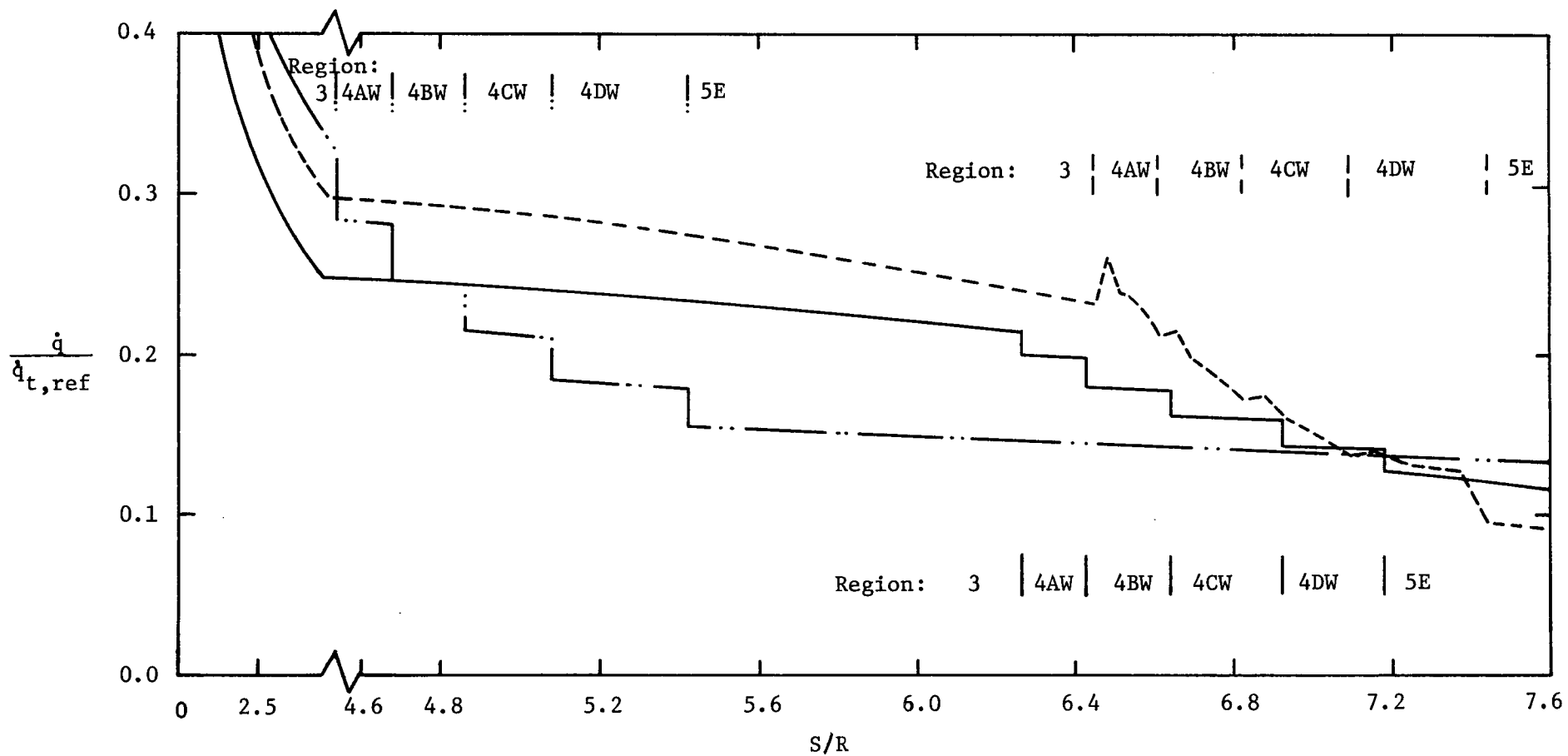
Figure 14. - Concluded.



(a) Condition 2: $U_{\infty} = 4330$ m/sec, $P_{\infty} = 0.333$ mmHg, $T_{\infty} = 273^{\circ}\text{K}$

Figure 15. - The heat-transfer distribution along the wing leading-edge for $\Lambda = 60^{\circ}$.

— PERFECT-GAS SOLUTION
 - - - REAL-GAS SOLUTION
 - · - · - CONSTANT-GAMMA SOLUTION



(b) Condition 3: $U_{\infty} = 7610$ m/sec, $P_{\infty} = 0.0268$ mmHg, $T_{\infty} = 195^{\circ}\text{K}$

Figure 15. - Concluded.

APPENDIX A. - GENERAL DESCRIPTION OF PERFECT GAS CODE

The general solution procedure for the perfect-gas code has been discussed previously. This section will provide a more detailed description of the governing equations and their place in the numerical routine. Input data for the perfect-gas code consists of the free-stream flow-field conditions of region 1 and the model geometry. The procedure used to calculate flow conditions in regions 2, 3, and 6 is to first call subroutine DELTAK, which solves for the shock wave angle, and second to call subroutine PTHETA, which calculates the flow conditions of regions 2, 3, and 6 using the computed shock wave angle.

Flow-Field Conditions in Regions 2, 3, and 6. The subroutine DELTAK uses the known turning angle δ to calculate the shock wave angle θ in the following equation:

$$\delta = \tan^{-1} \left\{ \frac{1}{\tan \theta \left[\frac{(\gamma+1)M_1^2}{2(M_1^2 \sin^2 \theta - 1)} \right] - 1} \right\} \quad (1)$$

where the subscript 1 denotes conditions upstream of the shock. A half-interval, iteration procedure is used to determine θ . The half-interval method is started by assuming θ to be an average between a lower limit, which is equal to δ , and an upper limit, equal to 90° . This average shock-wave angle is used to calculate the corresponding δ from equation (1). A comparison is then made between the calculated δ and the actual δ . If this comparison is not within a prespecified tolerance (i.e., 0.0001 radians) either the lower, or upper limit of θ , depending upon the comparison, is set equal to the previous iteration's average value of θ . A new average value of θ is computed using the new limit, and the procedure is repeated until the

calculated δ equals the actual δ (within the prespecified tolerance). Once the shock-wave angle has been determined the subroutine PTHETA uses this θ to calculate the pressure ratio by the following:

$$\frac{P_2}{P_1} \equiv \xi = \frac{2\gamma M_1^2 \sin^2 \theta - (\gamma - 1)}{\gamma + 1} \quad (2)$$

The subscript 2 denotes the conditions downstream of the shock. Thus, to solve for the flow-field conditions in region 3, conditions in region 2 are actually the conditions upstream of the shock, and conditions in region 3 are the conditions downstream of the shock. The density ratio and temperature ratio are then calculated as function of ξ as follows:

$$\frac{\rho_2}{\rho_1} = \frac{(\gamma + 1)\xi + (\gamma - 1)}{(\gamma - 1)\xi + (\gamma + 1)} \quad (3)$$

$$\frac{T_2}{T_1} = \xi \frac{(\gamma - 1)\xi + (\gamma + 1)}{(\gamma + 1)\xi + (\gamma - 1)} \quad (4)$$

The Mach numbers of regions downstream of the shock wave are calculated from the equation:

$$M_2 = \left[\frac{M_1^2 [(\gamma + 1)\xi + (\gamma - 1)] - 2(\xi^2 - 1)}{\xi[(\gamma - 1)\xi + (\gamma + 1)]} \right]^{1/2} \quad (5)$$

The pressure coefficient of each region is found from the equation:

$$C_P = \frac{P - P_1}{0.5\gamma_1 P_1 M_1^2} \quad (6a)$$

which, when combined with equation 2, yields the following relation for regions 2 and 6:

$$C_P = \frac{4(M_1^2 \sin^2 \theta - 1)}{(\gamma + 1) M_1^2} \quad (6b)$$

The procedure to compute the stagnation conditions for regions 1, 2, and

and 3 is to assume the flow decelerates isentropically to zero velocity. The equation for calculating the stagnation pressure is:

$$P_{ti} = P_i \left[1 + \frac{\gamma_i - 1}{2} M_i^2 \right]^{\frac{\gamma_i}{\gamma_i - 1}} \quad (7)$$

where these calculations are carried out for $i = 1$ (the free-stream), 2, and 3 (which serves as the stagnation pressure for the isentropic expansion).

Expansion Fan. The flow in region 3 is assumed to accelerate isentropically to subregion 5E. Region 3 is uniquely determined, as described above. Since the streamlines in the subregions from subregion 5E through region 6 are straight and parallel to the surface, i.e., not curved,

$$\frac{dP}{dn} = 0 \quad .$$

Thus, the static pressure in region 5E is equal to the static pressure in region 6, which is known. The isentropic assumption requires that the stagnation pressure in subregion 5E is equal to the stagnation pressure in region 3, which is known. Thus, the flow in subregion 5E is uniquely defined.

The flow field in the expansion fan is calculated in the subroutine EXPAN and the locations of the intersection points of the right running and left running waves of the fan are calculated by the subroutine INTRST. Since the waves are assumed to be linear, the subroutine INTRST requires the knowledge of two initial points and the angle between these points to the point of intersection. The intersection point can then be calculated using linear relations. The required angles are the shear layer angles and the expansion wave angles (i.e., Mach waves).

For the isentropic expansion from region 3 to region 5E, the Prandtl-Meyer expansion equations are used. First, the Prandtl-Meyer angle v for region 3 and for subregion 5E is calculated as follows:

$$v = \sqrt{\frac{\gamma+1}{\gamma-1}} \left\{ \tan^{-1} \sqrt{\frac{\gamma-1}{\gamma+1} (M^2-1)} \right\} - \tan^{-1} \sqrt{M^2-1} \quad (8)$$

(When using the variable-gamma option of the perfect-gas code, v both for region 3 and for subregion 5E is calculated using the gamma for region 3). The difference between these two Prandtl-Meyer angles is divided into ten equal parts to give the five waves in region 4 and the five waves in region 5. When crossing the right-running waves of the centered expansion fan, the change in the Prandtl-Meyer function is related to the change in the flow direction by

$$dv = d\theta \quad (9-a)$$

When crossing the left-running waves reflected from the wall,

$$dv = -d\theta \quad (9-b)$$

Thus, there is no net change in flow direction, satisfying the condition that the flow in subregion 5E is parallel to the surface. The subroutine EXPAN calculates the local Mach numbers of the expansion fan from which the local pressures can then be calculated. The local Prandtl-Meyer angle is calculated by adding one tenth of Δv to the v for the previous region. Then using equation (8), the local Mach number can be calculated using the half-interval iteration method. After all the local Mach numbers have been calculated, the local pressures are calculated using the following equation:

$$P_{ex} = \frac{P_{te}}{\left[1 + \frac{\gamma_3-1}{2} M_{ex}^2 \right] \frac{\gamma_3}{\gamma_3-1}} \quad (10)$$

The surface pressures have been calculated for the interaction between the right-running waves of the expansion fan (region 4) and the reflected left-running waves (region 5). See Figure A-1. The flow in subregion 4A is directed away from the surface by the angle $0.1\Delta v$. The expansion of the flow from 4A so that it is parallel to the surface in subregion 4AW is accomplished along right-running characteristics. Thus

$$v_{4AW} = v_{4A} - (\theta_{4AW} - \theta_{4A}) \quad (11)$$

A similar procedure is used for subregions 4BW, 4CW, and 4DW. Once the Prandtl-Meyer functions for these subregions are known, the remaining properties are calculated using EXPAN.

Wing Leading-Edge Heat-Transfer-Rate Calculations. After the wall pressures in regions 3, 4, and 5 have been found, the final step is to calculate the heat-transfer rate on the "wing leading-edge" in these regions. The subroutine ERTQDOT calculates the desired heat-transfer rate. The technique used to calculate the heat-transfer rate employs the Eckert's reference temperature equation for a laminar boundary-layer, as follows:

$$\dot{q} = 0.332(Re_x^*)^{0.5} (Pr^*)^{0.333} k^* (T_r - T_w) (x)^{-0.5} \quad (12)$$

This heat-transfer rate is divided by the reference stagnation-point heat-transfer rate to give a non-dimensionalized heat-transfer for use in correlation.

Calculation of the Stagnation Conditions Behind a Normal Shock and of the Reference Heating. In addition, the stagnation pressure across a normal

shock wave (which of course does not exist in the flow-field) is calculated for region 3 and for region 6 using the equation:

$$\frac{P_{t2}}{P_1} = \left[\frac{(\gamma+1)M_1^2}{2} \right]^{\frac{\gamma}{\gamma-1}} \left[\frac{\gamma+1}{2\gamma M_1^2 - (\gamma-1)} \right]^{\frac{1}{\gamma-1}} \quad (13)$$

with the proper subscription of pressures and Mach numbers. The stagnation temperature is constant throughout the regions and is calculated by the adiabatic perfect-gas equation:

$$T_t = T_1 \left[1 + \frac{\gamma-1}{2} M_1^2 \right] \quad (14)$$

These normal shock values of stagnation temperature and of stagnation pressure, in region 6 are used to calculate the stagnation point heat-transfer rate to a reference sphere.

The following equation is used:

$$\dot{q}_{t,ref} = 0.64(\rho_t \mu_t)^{0.4} (\rho_w \mu_w)^{0.1} (C_{pt} T_t - C_{pw} T_w) \left[\frac{du}{dx} \right]_t^{0.5} (Pr)^{-1} \quad (15)$$

where

$$\left[\frac{du}{dx} \right]_t = \sqrt{\frac{2 R_{gas} T_t}{R}} \quad (16)$$

and the subscript t refers to stagnation temperature, the subscript w refers to wall temperature, and R is the radius of the reference sphere.

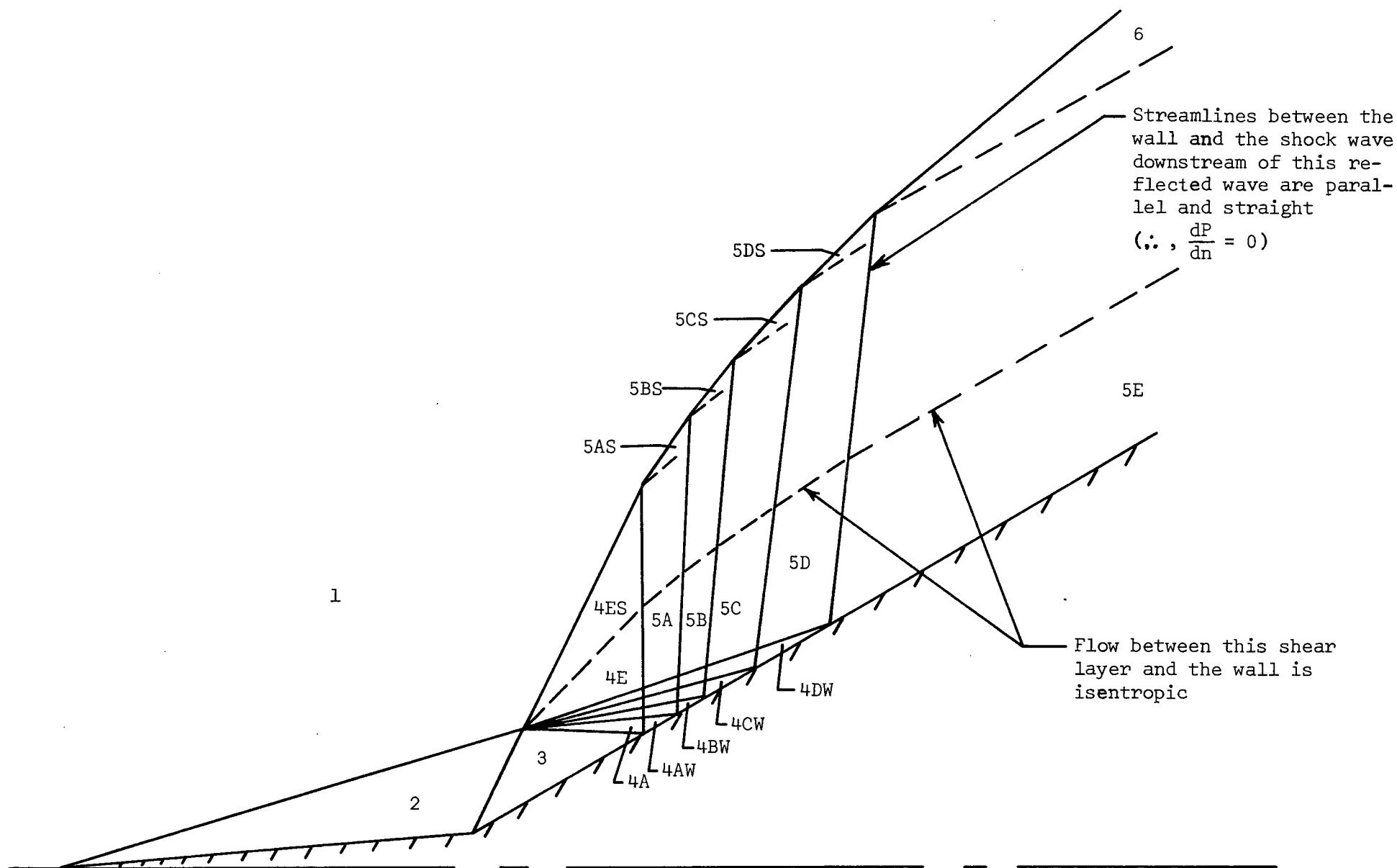
Calculation of the Shock-Wave Angles and the Intersection Points of the

Shock Wave with the Expansion Fan. Once the flow in subregion 5E is defined, the isentropic expansion flows inside of the shear layer in regions 4 and 5 is defined. It is not possible to match both the pressure and the flow direction across the "shear layer" which divides subregion 4ES, and subregion 4E (and, sequentially, 5AS, 5A; 5BS, 5B; 5CS, 5C; and 5DS, 5D). The actual flow

in subregions 4ES through 5DS is believed to be more complex than the flow-field model allows. The required pressure adjustment is assumed to be accomplished by the pressure gradient across curved streamlines:

$$\frac{dP}{dn} = \frac{\rho u^2}{r} \quad (17)$$

For the flow conditions studied, the radius of curvature is very large, i.e., only slight streamline curvature is needed. The subroutines DELTAK and PTHETA are used with the flow angle to generate approximate values of the shock-wave angle and the flow conditions in the subregions between the shock wave and the shear layer, i.e., subregions 4ES, 5AS, 5BS, 5CS, and 5DS. The intersection of the shock wave and the left-running expansion wave is computed using the subroutine INTRST. The expansion waves are assumed to be linear from their intersection with the shock wave. Because the pressure decreases in the expansion fan subregions, the shock-wave inclination decreases for each subsequent calculation. This results in the "curved" shock wave characteristic of the Type VI pattern, when the reflected waves interact with the wing leading-edge shock (see Figure 1).



Appendix A: Figure 1. - Flow model for Type VI showing regions for which flow conditions were determined using numerical codes

Input Cards

Card # 1 NC - number of cases

Card # 2 FSMACH - free-stream Mach number

 PINF - free-stream pressure (lbf/ft^2)

 TINF - free-stream temperature ($^{\circ}\text{R}$)

 LAMDAS - the deflection angle, i.e., complement
 of sweep angle ($^{\circ}$)

Card #3 RGAS - gas constant ($1716 \frac{\text{ft}^2}{\text{sec}^2 \text{ } ^{\circ}\text{R}}$)

 GAMMA - free-stream gamma (usually 1.4)

Card # 4 P2 - pressure in region 2 (lbf/ft^2)

 (optional)

 THETA - first shock wave angle ($^{\circ}$)

 (optional)

 DELTA - angle of first wedge ($^{\circ}$)

 KTHETA - does not equal zero if DELTA, δ , is known, equals
 zero if P_2 or THETA, θ , are known.

 KNØWN - does not equal zero if DELTA, δ , is known, equals
 zero if DELTA, δ , is unknown.

Card # 5 TW - wall temperature ($^{\circ}\text{R}$)

 RNØSE - radius of reference sphere (ft.)

 PRNØ - Prandtl number

Card # 6 CP0, CP1, CP2, CP3, CP4 - specific heat coefficients in the
 equation

$$C_p = C_{p0} + C_{p1}T + C_{p2}T^2 + C_{p3}T^3 + C_{p4}T^4 \left(\frac{\text{BTU}}{\text{slug}^{\circ}\text{R}} \right)$$

Card # 7 X0 - x-coordinate of "nose" (ft.)

 Y0 - y-coordinate of "nose" (ft.)

 X30 - x-coordinate of wedge intersection point (ft.)

 Y30 - y-coordinate of wedge intersection point (ft.)

Card # 8 GAMMA3 - gamma in region 3 (can be used to "simulate" real gas effects)

 GAMMA6 - gamma in region 6 (can be used to "simulate" real gas effects)

Card # 9 VISS0, VISS1, VISS2, VISS3, VISS4 - viscosity coefficients in the equation

$$\mu = \mu_0 + \mu_1 T + \mu_2 T^2 + \mu_3 T^3 + \mu_4 T^4 \quad \left(\frac{\text{lbf-sec}}{\text{ft}^2} \right)$$

(Note: Since the Prandtl number for air is approximately 0.7 for most temperatures and pressures,

$$K = \mu C_p / Pr$$

C_p and Pr are assumed constant for perfect air. Since μ is accurately calculated with the above polynomial, a reliable value for K is obtained).

PROGRAM SHOKINT (INPUT,OUTPUT)

*****THIS PROGRAM WILL CALCULATE SHOCKWAVE INTERSECTIONS AND THE
FLOW FIELD CONDITIONS BEHIND THE SHOCKWAVES GIVEN FREE-
STREAM CONDITIONS*****

```
REAL M1S, M2, M3, M6, LAMDAS, M2S
READ 111, NC
111 FORMAT(I5)
DO 99 IC=1,NC
  READ 101, FSMACH, PINF, TINF, LAMDAS
101 FORMAT(4E12.5)
  READ 102, RGAS, GAMMA
102 FORMAT(2E12.5)
  READ 103, P2, THETA, DELTA, KTHETA, KNOWN
103 FORMAT(3E12.5,2I5)
  READ 104, TW, RNOSE, PRNO
104 FORMAT(3E12.5)
  READ 105, CPU, CP1, CP2, CP3, CP4
105 FORMAT(5E12.5)
  READ 106, X0, Y0, X30, Y30
106 FORMAT(4E12.5)
  READ 107, GAMMA3, GAMMA6
107 FORMAT(2E12.5)
```

```
THETA=THETA/57.296
DELTA=DELTA/57.296
LAMDAS=LAMDAS/57.296
IF(KNOWN.EQ.0) GO TO 10
```

*****CALCULATING FLOW CONDITIONS IN REGION 2*****

```
CALL DELTAK(FSMACH,GAMMA,DELTA,THETA)
10 CALL PTHETA(FSMACH,M2,PINF,P2,PRAT21,DRAT21,TRAT21,THETA,DELTA,
1 PCOEF,GAMMA,KTHETA,KNOWN)
```

```
RHOINF=PINF/(RGAS*TINF)
P2=PRAT21*PINF
T2=TRAT21*TINF
RHO2=DRAT21*RHOINF
```

*****CALCULATING FLOW CONDITIONS IN REGION 3*****

```
DELTA3=LAMDAS-DELTA
CALL DELTAK(M2,GAMMA3,DELTA3,THETA3)
CALL PTHETA(M2,M3,P2,P3,PRAT32,DRAT32,TRAT32,THETA3,DELTA3,PCOEF3,
1 GAMMA3,KTHETA,KNOWN)
```

```
PRAT31=PRAT32*PRAT21
TRAT31=TRAT32*TRAT21
DRAT31=DRAT32*DRAT21
P3=PRAT31*PINF
T3=TRAT31*TINF
RHO3=DRAT31*RHOINF
PCOEF3=2.0*(PRAT31-1.0)/(GAMMA3*FSMACH*FSMACH)
```

```
G3P1=GAMMA3+1.0
G3M1=GAMMA3-1.0
PMF3=SQRT(G3P1/G3M1)*ATAN(SQRT((G3M1/G3P1)*(M3*M3-1.0)))-ATAN(SQRT
1 (M3*M3-1.0))
PTE=P3*((1.0+(G3M1/2.0)*M3*M3)**(GAMMA3/G3M1))
```

*****CALCULATING FLOW CONDITIONS IN REGION 6*****

DELTA6=LAMDAS
CALL DELTAK(FSMACH,GAMMA6,DELTA6,THETA6)
CALL PTHETA(FSMACH,M6,PINF,P6,PRAT61,DRAT61,TRAT61,THETA6,DELTA6,
PCOEF6,GAMMA6,KTHETA,KNOWN)

P6=PRAT61*PINF
T6=TRAT61*TINF
RH06=DRAT61*RHOINF

*****CALCULATING FLOW CONDITIONS IN REGION 5E*****

P5E=P6
PRAT5E=PTE/P5E
EXM5E=SQRT(2.0*((PRAT5E)**(G3M1/GAMMA3)-1.0)/G3M1)
PMF5E=SQRT(G3P1/G3M1)*ATAN(SQRT((G3M1/G3P1)*(EXM5E*EXM5E-1.0)))-
ATAN(SQRT(EXM5E*EXM5E-1.0))
DEXP=0.1*(PMF5E-PMF3)

*****COMPUTING STAGNATION CONDITIONS*****

M1S=FSMACH*FSMACH
M2S=M1S*M2
GM1=GAMMA-1.0
GP1=GAMMA+1.0
EXPON=GAMMA/GM1
PT1=PINF*((1.0+GM1*M1S/2.0)**EXPON)
PT2=P2*((1.0+GM1*M2S/2.0)**EXPON)
PT3=P2*((GP1*M2S/2.0)**EXPON)*((GP1/(2.0*GAMMA*M2S-GM1))**((1.0/GM1
1))
PT6=PINF*((GP1*M1S/2.0)**EXPON)*((GP1/(2.0*GAMMA*M1S-GM1))**((1.0/
1GM1))
TT=TINF*(1.0+GM1*M1S/2.0)
ITE=TT

CALL QDOT(PT6,RGAS,TW,TT,RNOSE,CP0,CP1,CP2,CP3,CP4,QTSR,PRNO)

*****FIND BOW AND WING SHOCKWAVE INTERSECTION*****

AGL3=THETA3+DELTA
CALL INTRST(X0,Y0,THETA,AGL3,X30,Y30,XI,YI)

*****FIND INTERSECTION FOR THE FIRST EXPANSION WAVE*****

*****EQUATION FOR THE ANGLE OF LINE 4A*****

WAVE3=ASIN(1.0/M3)
AGL4A=LAMDAS-WAVE3
CALL INTRST(XI,YI,AGL4A,LAMDAS,X30,Y30,X4A,Y4A)
THTA4A=LAMDAS+DEXP

*****LINE 4B*****

CALL EXPAN(PMF3,DEXP,GAMMA3,PMF4A,EXM4A,M3)
WAVE4A=ASIN(1.0/EXM4A)
AGL4B=LAMDAS+DEXP-WAVE4A
CALL INTRST(XI,YI,AGL4B,LAMDAS,X30,Y30,X4B,Y4B)
THTA4B=THTA4A+DEXP

C
C

*****LINE 4C*****

CALL EXPAN(PMF4A,DEXP,GAMMA3,PMF4B,EXM4B,EXM4A)
WAVE4B=ASIN(1.0/EXM4B)
AGL4C=LAMDAS+2.0*DEXP-WAVE4B
CALL INTRST(XI,YI,AGL4C,LAMDAS,X30,Y30,X4C,Y4C)
THTA4C=THTA4B+DEXP

C
C
C

*****LINE 4D*****

CALL EXPAN(PMF4B,DEXP,GAMMA3,PMF4C,EXM4C,EXM4B)
WAVE4C=ASIN(1.0/EXM4C)
AGL4D=LAMDAS+3.0*DEXP-WAVE4C
CALL INTRST(XI,YI,AGL4D,LAMDAS,X30,Y30,X4D,Y4D)
THTA4D=THTA4C+DEXP

C
C
C

*****LINE 4E*****

CALL EXPAN(PMF4C,DEXP,GAMMA3,PMF4D,EXM4D,EXM4C)
WAVE4D=ASIN(1.0/EXM4D)
AGL4E=LAMDAS+4.0*DEXP-WAVE4D
CALL INTRST(XI,YI,AGL4E,LAMDAS,X30,Y30,X4E,Y4E)
THTA4E=THTA4D+DEXP

C
C
C

*****LINE 5A*****

CALL EXPAN(PMF4D,DEXP,GAMMA3,PMF4E,EXM4E,EXM4D)
WAVE4E=ASIN(1.0/EXM4E)
AGL5A=THTA4E+WAVE4E
CALL INTRST(XI,YI,THTA4E,AGL5A,X4A,Y4A,X5A,Y5A)
THTA5A=THTA4E-DEXP

C
C
C

*****LINE 5B*****

CALL EXPAN(PMF4E,DEXP,GAMMA3,PMF5A,EXM5A,EXM4E)
WAVE5A=ASIN(1.0/EXM5A)
AGL5B=THTA5A+WAVE5A
CALL INTRST(X5A,Y5A,THTA5A,AGL5B,X4B,Y4B,X5B,Y5B)
THTA5B=THTA5A-DEXP

C
C
C

*****LINE 5C*****

CALL EXPAN(PMF5A,DEXP,GAMMA3,PMF5B,EXM5B,EXM5A)
WAVE5B=ASIN(1.0/EXM5B)
AGL5C=THTA5B+WAVE5B
CALL INTRST(X5B,Y5B,THTA5B,AGL5C,X4C,Y4C,X5C,Y5C)
THTA5C=THTA5B-DEXP

C
C
C

*****LINE 5D*****

CALL EXPAN(PMF5B,DEXP,GAMMA3,PMF5C,EXM5C,EXM5B)
WAVE5C=ASIN(1.0/EXM5C)
AGL5D=THTA5C+WAVE5C
CALL INTRST(X5C,Y5C,THTA5C,AGL5D,X4D,Y4D,X5D,Y5D)
THTA5D=THTA5C-DEXP

C
C
C

*****LINE 5E*****

CALL EXPAN(PMF5C,DEXP,GAMMA3,PMF5D,EXM5D,EXM5C)
WAVE5D=ASIN(1.0/EXM5D)
AGL5E=THTA5D+WAVE5D
CALL INTRST(X5D,Y5D,THTA5D,AGL5E,X4E,Y4E,X5E,Y5E)

WAVESE=ASIN(1.0/EXM5E)
THTASE=THTASD-DEXP

*****CALCULATING PRESSURES IN THE EXPANSION FAN*****

P4A=PTE/((1.0+(G3M1/2.0)*EXM4A*EXM4A)**(GAMMA3/G3M1))
P4B=PTE/((1.0+(G3M1/2.0)*EXM4B*EXM4B)**(GAMMA3/G3M1))
P4C=PTE/((1.0+(G3M1/2.0)*EXM4C*EXM4C)**(GAMMA3/G3M1))
P4D=PTE/((1.0+(G3M1/2.0)*EXM4D*EXM4D)**(GAMMA3/G3M1))
P4E=PTE/((1.0+(G3M1/2.0)*EXM4E*EXM4E)**(GAMMA3/G3M1))
P5A=PTE/((1.0+(G3M1/2.0)*EXM5A*EXM5A)**(GAMMA3/G3M1))
P5B=PTE/((1.0+(G3M1/2.0)*EXM5B*EXM5B)**(GAMMA3/G3M1))
P5C=PTE/((1.0+(G3M1/2.0)*EXM5C*EXM5C)**(GAMMA3/G3M1))
P5D=PTE/((1.0+(G3M1/2.0)*EXM5D*EXM5D)**(GAMMA3/G3M1))

*****CALCULATING FLOW ALONG THE WING IN THE EXPANSION REGION*****

EXP4AW=ABS(LAMDAS-THTA4A)
CALL EXPAN(PMF4A,EXP4AW,GAMMA3,PMF4AW,EXM4AW,EXM4A)
EXP4BW=ABS(LAMDAS-THTA4B)
CALL EXPAN(PMF4B,EXP4BW,GAMMA3,PMF4BW,EXM4BW,EXM4B)
EXP4CW=ABS(LAMDAS-THTA4C)
CALL EXPAN(PMF4C,EXP4CW,GAMMA3,PMF4CW,EXM4CW,EXM4C)
EXP4DW=ABS(LAMDAS-THTA4D)
CALL EXPAN(PMF4D,EXP4DW,GAMMA3,PMF4DW,EXM4DW,EXM4D)

P4AW=PTE/((1.0+(G3M1/2.0)*EXM4AW*EXM4AW)**(GAMMA3/G3M1))
P4BW=PTE/((1.0+(G3M1/2.0)*EXM4BW*EXM4BW)**(GAMMA3/G3M1))
P4CW=PTE/((1.0+(G3M1/2.0)*EXM4CW*EXM4CW)**(GAMMA3/G3M1))
P4DW=PTE/((1.0+(G3M1/2.0)*EXM4DW*EXM4DW)**(GAMMA3/G3M1))

*****COMPUTING SHOCK WAVE ANGLES AND INTERSECTING POINTS OF REGIONS
4E AND 5*****

CALL DELTAK(FSMACH,GAMMA6,THTA4E,THT4ES)
CALL PTHETA(FSMACH,EXM4ES,PINF,P4E,PR4E1, DR4E1,TR4E1,THT4ES,
1DELTA,X,PCOFF,GAMMA6,KTHETA,KNOWN)
CALL INTRST(XI,YI,THT4ES,AGL5A,X4A,Y4A,X5AS,Y5AS)
CALL DELTAK(FSMACH,GAMMA6,THTA5A,THT5AS)
CALL PTHETA(FSMACH,EXM5AS,PINF,P5A,PR5A1, DR5A1,TR5A1,THT5AS,
1DELTA,X,PCOFF,GAMMA6,KTHETA,KNOWN)
CALL INTRST(X5AS,Y5AS,THT5AS,AGL5B,X4B,Y4B,X5BS,Y5BS)
CALL DELTAK(FSMACH,GAMMA6,THTA5B,THT5BS)
CALL PTHETA(FSMACH,EXM5BS,PINF,P5B,PR5B1, DR5B1,TR5B1,THT5BS,
1DELTA,X,PCOFF,GAMMA6,KTHETA,KNOWN)
CALL INTRST(X5BS,Y5BS,THT5BS,AGL5C,X4C,Y4C,X5CS,Y5CS)
CALL DELTAK(FSMACH,GAMMA6,THTA5C,THT5CS)
CALL PTHETA(FSMACH,EXM5CS,PINF,P5C,PR5C1, DR5C1,TR5C1,THT5CS,
1DELTA,X,PCOFF,GAMMA6,KTHETA,KNOWN)
CALL INTRST(X5CS,Y5CS,THT5CS,AGL5D,X4D,Y4D,X5DS,Y5DS)
CALL DELTAK(FSMACH,GAMMA6,THTA5D,THT5DS)
CALL PTHETA(FSMACH,EXM5DS,PINF,P5D,PR5D1, DR5D1,TR5D1,THT5DS,
1DELTA,X,PCOFF,GAMMA6,KTHETA,KNOWN)
CALL INTRST(X5DS,Y5DS,THT5DS,AGL5E,X4E,Y4E,X5ES,Y5ES)

THT4ES=THT4ES*57.296
THT5AS=THT5AS*57.296
THT5BS=THT5BS*57.296
THT5CS=THT5CS*57.296
THT5DS=THT5DS*57.296

```

C      DELTA=DELTA*57.296
      THETA=THETA*57.296
      DELTA3=DELTA3*57.296
      THETA3=THETA3*57.296
      DELTA6=DELTA6*57.296
      THETA6=THETA6*57.296
      THETA5=THETA5*57.296

C
C      *****PRINTING THE SOLUTIONS*****
C
      PRINT 200
200  FORMAT(1H1)
      PRINT 299, IC
299  FORMAT(13X,*CASE =*,I2,///)
      PRINT 201
201  FORMAT(16X,*FREE-STREAM FLOW CONDITIONS*,///)
      PRINT 202
202  FORMAT(13X,*FSMACH*,11X,*P1*,14X,*T1*,12X,*RH01*,12X,*PT1*,12X,*TT
1*)
      PRINT 217
217  FORMAT(26X,*(LBF/SQFT)*,6X,* (RANKIN)*,8X,* (SLUGS/CUFT)*,/)
      PRINT 203, FSMACH, PINF, TINF, RH0INF, PT1, TT
203  FORMAT(10X,E12.5,3X,E12.5,4X,E12.5,3X,E12.5,4X,E12.5,4X,E12.5,///)
      PRINT 204
204  FORMAT(16X,*GAS CONSTANTS*,/)
      PRINT 205, RGAS, GAMMA, QTSPR
205  FORMAT(11X,*RGAS =*,E12.5,5X,*GAMMA =*,E12.5,5X,*QTSPR =*,E12.5,//
1/)
      PRINT 206
206  FORMAT(16X,*FLOW CONDITIONS IN REGION 2*,///)
      PRINT 207
207  FORMAT(15X,*M2*,14X,*P2/P1*,15X,*T2/T1*,14X,*RH02/RH01*,15X,*PCOEF
12*,/)
      PRINT 208, M2, PHAT21, TRAT21, URAT21, PCOEF
208  FORMAT(10X,E12.5,6X,E12.5,8X,E12.5,9X,E12.5,9X,E12.5,///)
      PRINT 212, P2, T2, RH02, PT2
212  FORMAT(11X,*P2 =*,E12.5,5X,*T2 =*,E12.5,5X,*RH02 =*,E12.5,5X,*PT2
1=*,E12.5,/)
      PRINT 209, DELTA, THETA
209  FORMAT(11X,*DELTA12 =*,E12.5,5X,*THETA12 =*,E12.5)
      PRINT 210
210  FORMAT(///,16X,*FLOW CONDITIONS IN REGION 3*,///)
      PRINT 213
213  FORMAT(15X,*M3*,14X,*P3/P1*,15X,*T3/T1*,14X,*RH03/RH01*,15X,*PCOEF
13*,/)
      PRINT 208, M3, PHAT31, TRAT31, URAT31, PCOEF3
      PRINT 215, P3, T3, RH03, PT3
215  FORMAT(11X,*P3 =*,E12.5,5X,*T3 =*,E12.5,5X,*RH03 =*,E12.5,5X,*PT3
1=*,E12.5,/)
      PRINT 218, DELTA3, THETA3, GAMMA3
218  FORMAT(11X,*DELTA23 =*,E12.5,5X,*THETA23 =*,E12.5,5X,*GAMMA3 =*,
1E12.5)
      PRINT 211
211  FORMAT(///,16X,*FLOW CONDITIONS IN REGION 6*,///)
      PRINT 214
214  FORMAT(15X,*M6*,14X,*P6/P1*,15X,*T6/T1*,14X,*RH06/RH01*,15X,*PCOEF
16*,/)
      PRINT 208, M6, PHAT61, TRAT61, URAT61, PCOEF6
      PRINT 216, P6, T6, RH06, PT6
216  FORMAT(11X,*P6 =*,E12.5,5X,*T6 =*,E12.5,5X,*RH06 =*,E12.5,5X,*PT6
1=*,E12.5,/)

```

```

      PRINT 219, DELTA6, THETA6, GAMMA6
219  FORMAT(11X,*DELTA16 =*,E12.5,5X,*THETA16 =*,E12.5,5X,*GAMMA6 =*,
      1E12.5)
      PRINT 220
220  FORMAT(///,16X,*POINTS OF INTEREST IN THE FLOW FIELD AND ON THE BO
      1DY (IN INCHES)*,///)
      PRINT 250,PTE,TTE
250  FORMAT(16X,*PTE =*,E12.5,5X,*TTE =*,E12.5,/)
      PRINT 221
221  FORMAT(13X,*INITIAL POINTS ON BOW SHOCKWAVE*)
      PRINT 222,X0,Y0
222  FORMAT(11X,*X =*,E12.5,5X,*Y =*,E12.5)
      PRINT 223
223  FORMAT(/,13X,*WING INTERSECTION POINT*)
      PRINT 222,X30,Y30
      PRINT 224
224  FORMAT(/,13X,*BOW SHOCK-WING SHOCK INTERSECTION POINT*)
      PRINT 222,X1,Y1
      PRINT 225
225  FORMAT(/,13X,*FIRST EXPANSION WAVE WING INTERSECTION POINT*)
      PRINT 222,X4A,Y4A
      PRINT 226
226  FORMAT(/,13X,*LINE 4B WING INTERSECTION POINT*)
      PRINT 222,X4B,Y4B
      PRINT 227
227  FORMAT(/,13X,*LINE 4C WING INTERSECTION POINT*)
      PRINT 222,X4C,Y4C
      PRINT 240
240  FORMAT(/,13X,*LINE 4D WING INTERSECTION POINT*)
      PRINT 222,X4D,Y4D
      PRINT 241
241  FORMAT(/,13X,*LINE 4E WING INTERSECTION POINT*)
      PRINT 222,X4E,Y4E
      PRINT 228
228  FORMAT(/,13X,*LINE 5A SHEAR INTERSECTION POINT*)
      PRINT 222,X5A,Y5A
      PRINT 229
229  FORMAT(/,13X,*LINE 5B SHEAR INTERSECTION POINT*)
      PRINT 222,X5B,Y5B
      PRINT 230
230  FORMAT(/,13X,*LINE 5C SHEAR INTERSECTION POINT*)
      PRINT 222,X5C,Y5C
      PRINT 242
242  FORMAT(/,13X,*LINE 5D SHEAR INTERSECTION POINT*)
      PRINT 222,X5D,Y5D
      PRINT 243
243  FORMAT(/,13X,*LINE 5E SHEAR INTERSECTION POINT*)
      PRINT 222,X5E,Y5E
      PRINT 231
231  FORMAT(/,13X,*FLOW IN REGION 5E FROM EXPANSION*)
      PRINT 232,THETA5E,EXM5E,P5E
232  FORMAT(11X,*THETA =*,E12.5,5X,*M5E =*,E12.5,5X,*P5E =*,E12.5)
      PRINT 233
233  FORMAT(/,13X,*MACH NUMBERS IN EXPANSION FAN*)
      PRINT 234, EXM4A,EXM4B,EXM4C
234  FORMAT(11X,*M4A =*,E12.5,5X,*M4B =*,E12.5,5X,*M4C =*,E12.5)
      PRINT 244,EXM4D,EXM4E
244  FORMAT(11X,*M4D =*,E12.5,5X,*M4E =*,E12.5)
      PRINT 235,EXM5A,EXM5B,EXM5C
235  FORMAT(11X,*M5A =*,E12.5,5X,*M5B =*,E12.5,5X,*M5C =*,E12.5)
      PRINT 245,EXM5D
245  FORMAT(11X,*M5D =*,E12.5)

```



```

      PRINT 236
236  FORMAT(/,13X,*PRESSURES IN THE EXPANSION FAN*)
      PRINT 237,P4A,P4B,P4C
237  FORMAT(11X,*P4A =*,E12.5,5X,*P4B =*,E12.5,5X,*P4C =*,E12.5)
      PRINT 246,P4D,P4E
246  FORMAT(11X,*P4D =*,E12.5,5X,*P4E =*,E12.5)
      PRINT 238,P5A,P5B,P5C
238  FORMAT(11X,*P5A =*,E12.5,5X,*P5B =*,E12.5,5X,*P5C =*,E12.5)
      PRINT 247,P5D
247  FORMAT(11X,*P5D =*,E12.5)
      PRINT 400
400  FORMAT(1H1,16X,*FLOW ALONG THE WING IN THE EXPANSION REGION*,///)
      PRINT 401
401  FORMAT(13X,*MACH NUMBERS*,/)
      PRINT 402,EXM4AW,EXM4BW,EXM4CW,EXM4DW
402  FORMAT(11X,*M4AW =*,E12.5,3X,*M4BW =*,E12.5,3X,*M4CW =*,E12.5,3X,
1*M4DW =*,E12.5,/)
      PRINT 403
403  FORMAT(13X,*PRESSURES*,/)
      PRINT 404,P4AW,P4BW,P4CW,P4DW
404  FORMAT(11X,*P4AW =*,E12.5,3X,*P4BW =*,E12.5,3X,*P4CW =*,E12.5,3X,
1*P4DW =*,E12.5)
      PRINT 300
300  FORMAT(///,13X,*FLOW IN THE SHOCKED REGION OF EXPANSION FAN*,///)
      PRINT 301
301  FORMAT(26X,*REGION 4ES*,/)
      PRINT 302,THT4ES,X5AS,Y5AS
302  FORMAT(16X,*THETA =*,E12.5,5X,*X =*,E12.5,5X,*Y =*,E12.5)
      PRINT 303,PR4E1,DR4E1,TR4E1,EXM4ES
303  FORMAT(/,16X,*PR =*,E12.5,5X,*DR =*,E12.5,5X,*TR =*,E12.5,5X,
1*M =*,E12.5,/)
      PRINT 304
304  FORMAT(26X,*REGION 5AS*,/)
      PRINT 302,THT5AS,X5BS,Y5BS
      PRINT 303,PR5A1,DR5A1,TR5A1,EXM5AS
      PRINT 305
305  FORMAT(26X,*REGION 5BS*,/)
      PRINT 302,THT5BS,X5CS,Y5CS
      PRINT 303,PR5B1,DR5B1,TR5B1,EXM5BS
      PRINT 306
306  FORMAT(26X,*REGION 5CS*,/)
      PRINT 302,THT5CS,X5DS,Y5DS
      PRINT 303,PR5C1,DR5C1,TR5C1,EXM5CS
      PRINT 307
307  FORMAT(26X,*REGION 5DS*,/)
      PRINT 302,THT5DS,X5ES,Y5ES
      PRINT 303,PR5D1,DR5D1,TR5D1,EXM5DS

```

```

C
C
C      *****CALCULATING HEAT-TRANSFER ALONG WING-LEADING EDGE*****

```

```

      CALL ERTQD01(PTE,TTE,P3,GAMMA3,RGAS,X30,X4A,X4B,X4C,X4D,X4E,Y30,
1Y4A,Y4B,Y4C,Y4D,Y4E,P4AW,P4BW,P4CW,P4DW,P5E,QTSPR,PINF)
99  CONTINUE
      END

```

```

      SUBROUTINE DELTAK(FSMACH,GAMMA,DELTA,THETA)

```

```

C
C
C      *****SOLVING FOR THETA GIVEN DELTA*****

```

```

      REAL M1S
      CONV=0.0001
      M1S=FSMACH*FSMACH
      GP1=GAMMA+1.0

```

```

    THETA=DELTA
    THETA=1.571
5  THETA=(THETA+THETA)/2.0
    DELTAC=ATAN(1.0/(TAN(THETA)*(((GP1*M1S)/(2.0*(M1S*((SIN(THETA))**2
    1)-1.0)))-1.0)))
    DIFF=DELTAC-DELTA
    IF (ABS(DIFF).LE.CONV) GO TO 2
    IF (DIFF) 3,2,4
3  THETA=THETA
    GO TO 5
4  THETA=THETA
    GO TO 5
2  CONTINUE
    RETURN
    END

```

```

SUBROUTINE PTHETA(FSMACH,M2,PINF,P2,PRAT21,DRAT21,TRAT21,THETA,
1 DELTA,PCOEF,GAMMA,KTHETA,KNOWN)

```

```

C *****SOLVING FOR FLOW CONDITIONS BEHIND A WEDGE SHOCK GIVEN EITHER
C P2 OR THETA*****
C

```

```

    REAL M1S, M2
    M1S=FSMACH*FSMACH
    GP1=GAMMA+1.0
    GM1=GAMMA-1.0
    IF (KTHETA.EQ.0) GO TO 2
    PRAT21=(2.0*GAMMA*M1S*((SIN(THETA))**2)-GM1)/GP1
    IF (KNOWN.NE.0) GO TO 4
    GO TO 3
2  PRAT21=P2/PINF
    THETA=ASIN(SQRT((GP1*PRAT21+GM1)/(2.0*GAMMA*M1S)))
3  DELTA=ATAN(1.0/(TAN(THETA)*(((GP1*M1S)/(2.0*(M1S*((SIN(THETA))**2
    1)-1.0)))-1.0)))
4  M2=SQRT(((M1S*(GP1*PRAT21+GM1))-2.0*(PRAT21**2-1.0))/(PRAT21*(GM1*
    1PRAT21+GP1)))
    DRAT21=(GP1*PRAT21+GM1)/(GM1*PRAT21+GP1)
    TRAT21=PRAT21*((GM1*PRAT21+GP1)/(GP1*PRAT21+GM1))
    PCOEF=(4.0*(M1S*((SIN(THETA))**2)-1.0)/(GP1*M1S)
    RETURN
    END

```

```

SUBROUTINE QDOT(PTREF, RGAS, TW, TT, RNOSE, CP0, CP1, CP2, CP3, CP4, QTSR,
1 PRNO)

```

```

C *****SUBROUTINE TO CALCULATE THE REFERENCE HEAT TRANSFER*****
C
C

```

```

    RHO=PTREF/(RGAS*TW)
    RHOT=PTREF/(RGAS*TT)
    VIST=2.27E-08*(TT**1.5)/(TT+198.6)
    VISW=2.27E-08*(TW**1.5)/(TW+198.6)
    DUEDX=((2.0*RGAS*TT)**0.5)/RNOSE
    CPW=CP0+CP1*TW+CP2*TW*TW+CP3*(TW**3)+CP4*(TW**4)
    CPT=CP0+CP1*TT+CP2*TT*TT+CP3*(TT**3)+CP4*(TT**4)
    DELH=CPT*TT-CPW*TW
    QTSR=0.67*((RHOT*VIST)**0.4)*((RHO*VISW)**0.1)*DELH*(DUEDX**0.5)
1/PRNO
    RETURN
    END

```

```

SUBROUTINE INTRSI(X1,Y1,A1,A2,X2,Y2,XI,YI)

```

```

C *****SUBROUTINE TO FIND THE INTERSECTION POINT OF THE SHOCKWAVES
C AND THE INTERSECTION POINTS IN THE EXPANSION FAN*****
C
C

```

```

XI=(Y2-Y1+X1*TAN(A1)-X2*TAN(A2))/(TAN(A1)-TAN(A2))
YI=Y1+(XI-X1)*TAN(A1)
RETURN
END

```

```

SUBROUTINE EXPAN(PMFI,DEXP,GAMMA,PMFO,EXMACH,EXMI)

```

```

*****SUBROUTINE TO CALCULATE MACH NUMBERS IN THE EXPANSION FAN*****

```

```

GM1=GAMMA-1.0
GP1=GAMMA+1.0
PMFO=PMFI+DEXP
A=SQRT(GP1/GM1)
PCONV=0.0001
STM=EXMI
RM=1.1*STM
5 EXMACH=(STM+RM)/2.0
EXMS=EXMACH*EXMACH
PMFOG=A*ATAN(SQRT((EXMS-1.0)*GM1/GP1))-ATAN(SQRT(EXMS-1.0))
PDIFF=PMFOG-PMFO
IF(ABS(PDIFF).LE.PCONV) GO TO 2
IF(PDIFF) 3,2,4
3 STM=EXMACH
GO TO 5
4 RM=EXMACH
GO TO 5
2 CONTINUE
RETURN
END

```

```

SUBROUTINE ERTQDOT(PTE,TIE,P3,G,R,XI,X4A,X4B,X4C,X4D,X4E,YI,Y4A,
1Y4B,Y4C,Y4D,Y4E,P4A,P4B,P4C,P4D,P5E,QTSPR,PINF)

```

```

*****SUBROUTINE TO CALCULATE FLOW PARAMETERS ALONG WING-LEADING
EDGE*****

```

```

DIMENSION S(150),QDOT(150),PE(150),TW(150),TE(150),EM(150),ISTAR(
1150),VIS2(150),ICON(150),RHOS(150),AF(150),UE(150),RENOS(150),TR(
2150),PRG(150),VISE(150),RHOF(150),RES(150),QDOTR(150),PRAT(150)
READ ,PR,TWALL,DELS,J,LL
1 FORMAT(3E12.5,2I10)
READ 12,VISS0,VISS1,VISS2,VISS3,VISS4
12 FORMAT(5E12.5)
X1=XI-X4A
X2=XI-X4B
X3=XI-X4C
X4=XI-X4D
X5=XI-X4E
Y1=YI-Y4A
Y2=YI-Y4B
Y3=YI-Y4C
Y4=YI-Y4D
Y5=YI-Y4E
S(1)=0.0
SDELT=DELS
S4A=SQRT(X1*X1+Y1*Y1)/12.0
S4B=SQRT(X2*X2+Y2*Y2)/12.0
S4C=SQRT(X3*X3+Y3*Y3)/12.0
S4D=SQRT(X4*X4+Y4*Y4)/12.0
S4E=SQRT(X5*X5+Y5*Y5)/12.0
DELT5=0.02*(S4E-S4A)
REC=SQRT(PR)
DO 6 I=2,J
S(I)=S(I-1)+SDEL I

```

```

    TW(I)=TWALL
    IF(S(I).LE.S4A) GO TO 41
    IF(LL.EQ.2) GO TO 47
    IF(LL.EQ.1) GO TO 47
    SDEL=DELTS
    S(I)=S4A-0.5*SDEL
    PE(I)=P3
    LL=1
    GO TO 44
47 CONTINUE
    IF(S(I).LE.S4B) GO TO 42
    IF(S(I).LE.S4C) GO TO 43
    IF(S(I).LE.S4D) GO TO 45
    IF(S(I).LE.S4E) GO TO 46
    PE(I)=P5F
    IF(LL.EQ.2) GO TO 44
    SDEL=DEL
    LL=2
    GO TO 44
41 PE(I)=P3
    GO TO 44
42 PE(I)=P4A
    GO TO 44
43 PE(I)=P4B
    GO TO 44
45 PE(I)=P4C
    GO TO 44
46 PE(I)=P4D
44 CONTINUE
    IF(I)=TTF*((PE(I)/PTE)**((G-1.)/G))
    PRG(I)=(PTE/PE(I))**((G-1.)/G)
    EM(I)=SQRT((PRG(I)-1.)*2./(G-1.))
    TSTAR(I)=.5*(TE(I)+TW(I))+.22*REC*(EM(I)**2.)*TE(I)*((G-1.)/2.)
    VISE(I)=(VISS0+VISS1*TE(I)+VISS2*TE(I)*TE(I)+VISS3*(TE(I)**3)+
1 VISS4*(TE(I)**4))
    VIS2(I) = (VISS0 + VISS1*TSTAR(I) + VISS2*TSTAR(I)*TSTAR(I) +
1 VISS3*TSTAR(I)*TSTAR(I)*TSTAR(I) + VISS4*TSTAR(I)*TSTAR(I)*TSTAR(I)
2)*TSTAR(I))
    TCON(I)=0.24*32.176*VIS2(I)/Ph
    RHOS(I)=P(I)/(R*TSTAR(I))
    RHOE(I)=PE(I)/(R*TE(I))
    AE(I)=SQRT(G*R*TE(I))
    UE(I)=EM(I)*AE(I)
    RENOS(I)=RHOS(I)*UE(I)/(VIS2(I))
    RES(I)=RHOE(I)*UE(I)*S(I)/VISE(I)
    TR(I)=TE(I)*(1.0+REC*((G-1.0)/2.0)*(EM(I)**2.0))
    QDOT(I)=.332*SQRT(RENOS(I))*(PR**.333)*TCON(I)*(TR(I)-TW(I))/SQRT(
1 S(I))
    QDOTR(I)=QDOT(I)/QTSPR
    PRAT(I)=PE(I)/PINF
6 CONTINUE
    PRINT 60
60 FORMAT (1H1)
    PRINT 77
77 FORMAT(26X,*FLOW PARAMETERS ALONG WING-LEADING EDGE*,//)
    PRINT 7
7 FORMAT(14X,*S(I)*,7X,*PE(I)*,7X,*RES(I)*,9X,*QDOT(I)*,7X,*QDOTR(I)
1*,7X,*PRAT(I)*,/)
    DO 10 I=2,J
    PRINT 8,S(I),PE(I),RES(I),QDOT(I),QDOTR(I),PRAT(I)
8 FORMAT(10X,F10.5,F10.5,3X,E12.5,3X,F12.5,3X,E12.5,3X,E12.5)
10 CONTINUE

```

RETURN
END

DESCRIPTION OF OUTPUT

The output for the perfect-gas code includes the flow conditions from each region of the flow-field model, the geometry of the shock waves and the expansion waves, and the heat-transfer distribution along the second wedge, i.e., the wing leading-edge. The units for a particular parameter in any region will be the same as the free-stream parameter, unless otherwise noted. The output for the free-stream flow includes:

- FSMACH - free-stream Mach number
- P1 - free-stream static pressure (lbf/ft^2)
- T1 - free-stream temperature ($^{\circ}\text{R}$)
- RH01 - free-stream density (slugs/ft^3)
- PT1 - free-stream stagnation pressure (lbf/ft^2)
- TT - stagnation temperature of entire flow model ($^{\circ}\text{R}$)
- RGAS - gas constant ($\text{ft}^2/\text{sec}^2\text{-}^{\circ}\text{R}$)
- GAMMA - γ for the free-stream and region 2
- QTSPR - reference heating rate ($\text{Btu/ft}^2\text{-sec}$)

The following flow conditions are output for each region "I", where I = 2, 3, or 6:

- MI - the Mach number of the region
- PI/P1 - the static pressure ratio
- TI/T1 - the temperature ratio
- RH0I/RH01 - the density ratio
- PCOEFI - the pressure coefficient
- PI - the static pressure
- TI - the temperature
- RH0I - the density
- PTI - the stagnation pressure

DELTAJI - the change in flow-direction between two consecutive regions,
in degrees.

THETAJI - the shock wave angle between two consecutive regions, in
degrees

GAMMAI - the γ of the region

The output for the expansion fan region includes the following stagnation
condition and intersection points:

PTE - stagnation pressure at the edge of the boundary layer

TTE - stagnation temperature at the edge of the boundary layer

Intersection points include:

INITIAL POINTS ON BOW SHOCK WAVE, i.e., the origin of the coordinate
system, or the nose.

WING INTERSECTION POINT, i.e., intersection of the two wedges

BOW-SHOCK:WING-SHOCK INTERSECTION POINT, i.e., the intersection of
the shock of the first wedge with the shock of the second
wedge

Next Five Points - the intersections of the centered expansion fan
with the wing leading edge

Last Five Points - the intersection of the reflected waves with the
inboard shear layer

Output for the flow in region 5E include:

THETA - the flow direction, in degrees

M5E - the Mach number

P5E - the static pressure

The Mach numbers and pressures of each of the other nine subregions of re-
gions 4 and 5 are the output under the next two headings.

Output listed for the interaction region between the left running and right

running expansion fan waves includes:

EXM4IW - the Mach number

P4IW - the static pressure

where "I" = A, B, C, and D.

Output for the subregions between the inboard shear-layer and the "curved" shock wave include:

THETA - shock wave angle

X - x-coordinate point of the intersection of the shock wave
and the left-running expansion wave

Y - y-coordinate point of the intersection of the shock wave and
the left-running expansion wave

PR - pressure ratio with respect to region 1

DR - density ratio with respect to region 1

TR - temperature ratio with respect to region 1

M - Mach number

The output for the flow parameters and the heat-transfer distribution along with wing leading edge include:

S(I) - distance along wing leading edge

PE(I) - pressure at the edge of the boundary layer

RES(I) - Reynolds number

QDOT(I) - heat transfer rate

QDOTR(I) - heat transfer rate ratio with reference heat transfer rate

PRAT(I) - pressure ratio with respect to region 1

where the (I) index refers to the station for which the calculations are made.

CASE = 1

FREE-STREAM FLOW CONDITIONS

FSMACH	P1 (LBF/SQFT)	T1 (RANKINE)	RH01 (SLUGS/CUFT)	PT1	TT
1.31000E+01	9.29874E-01	4.90569E+02	1.10460E-06	2.43547E+05	1.73279E+04

GAS CONSTANTS

RGAS = 1.71600E+03 GAMMA = 1.40000E+00 QTSR = 5.89275E+02

FLOW CONDITIONS IN REGION 2

M2	P2/P1	T2/T1	RH02/RH01	PCOEF2
1.02440E+01	4.03662E+00	1.60644E+00	2.51277E+00	2.52784E-02

P2 = 3.75355E+00 T2 = 7.88071E+02 RH02 = 2.77562E-06 PT2 = 1.87100E+05
DELTA12 = 5.00000E+00 THETA12 = 8.33116E+00

FLOW CONDITIONS IN REGION 3

M3	P3/P1	T3/T1	RH03/RH01	PCOEF3
3.39620E+00	1.37609E+02	1.06815E+01	1.28829E+01	1.13720E+00

P3 = 1.27959E+02 T3 = 5.24002E+03 RH03 = 1.42305E-05 PT3 = 5.08890E+02
DELTA23 = 2.50000E+01 THETA23 = 3.19361E+01 GAMMA3 = 1.40000E+00

FLOW CONDITIONS IN REGION 6

M6	P6/P1	T6/T1	RH06/RH01	PCOEF6
2.83044E+00	7.56203E+01	1.35735E+01	5.57119E+00	6.21179E-01

P6 = 7.03174E+01 T6 = 6.65873E+03 RH06 = 6.15396E-06 PT6 = 2.05891E+02

DELTA16 = 3.00000E+01 THETA16 = 3.79703E+01 GAMMA6 = 1.40000E+00

POINTS OF INTEREST IN THE FLOW FIELD AND ON THE BODY (IN INCHES)

PTE = 8.41422E+03 TTE = 1.73279E+04

INITIAL POINTS ON BOW SHOCKWAVE

X = 0. Y = 0.

WING INTERSECTION POINT

X = 9.00000E+00 Y = 8.10000E-01

BOW SHOCK-WING SHOCK INTERSECTION POINT

X = 9.83909E+00 Y = 1.44083E+00

FIRST EXPANSION WAVE WING INTERSECTION POINT

X = 1.02588E+01 Y = 1.53677E+00

LINE 4B WING INTERSECTION POINT

X = 1.02787E+01 Y = 1.54827E+00

LINE 4C WING INTERSECTION POINT

X = 1.03007E+01 Y = 1.56097E+00

LINE 4D WING INTERSECTION POINT

X = 1.03252E+01 Y = 1.57508E+00

LINE 4E WING INTERSECTION POINT

X = 1.03526E+01 Y = 1.59093E+00

LINE 5A SHEAR INTERSECTION POINT

X = 1.06104E+01 Y = 1.94685E+00

LINE 5B SHEAR INTERSECTION POINT

X = 1.06574E+01 Y = 1.97692E+00

LINE 5C SHEAR INTERSECTION POINT

X = 1.07080E+01 Y = 2.00846E+00

LINE 5D SHEAR INTERSECTION POINT

X = 1.07626E+01 Y = 2.04166E+00

LINE 5E SHEAR INTERSECTION POINT

X = 1.08216E+01 Y = 2.07662E+00

FLOW IN REGION 5E FROM EXPANSION

THETA = 3.00000E+01 M5E = 3.82344E+00 P5E = 7.03174E+01

MACH NUMBERS IN EXPANSION FAN

M4A = 3.43600E+00	M4B = 3.47627E+00	M4C = 3.51700E+00
M4D = 3.55890E+00	M4E = 3.60131E+00	
M5A = 3.64421E+00	M5B = 3.68763E+00	M5C = 3.73228E+00
M5D = 3.77748E+00		

PRESSURES IN THE EXPANSION FAN

P4A = 1.20858E+02	P4B = 1.14106E+02	P4C = 1.07689E+02
P4D = 1.01494E+02	P4E = 9.56184E+01	
P5A = 9.00470E+01	P5B = 8.47671E+01	P5C = 7.96868E+01
P5D = 7.48814E+01		

FLOW ALONG THE WING IN THE EXPANSION REGION

MACH NUMBERS

M4AW = 3.47627E+00 M4BW = 3.55910E+00 M4CW = 3.64408E+00 M4DW = 3.73268E+00

PRESSURES

P4AW = 1.14106E+02 P4BW = 1.01467E+02 P4CW = 9.00633E+01 P4DW = 7.96434E+01

FLOW IN THE SHOCKED REGION OF EXPANSION FAN

REGION 4ES

THETA = 4.24924E+01 X = 1.14125E+01 Y = 2.88224E+00
PR = 9.11872E+01 DR = 5.63987E+00 TR = 1.61683E+01 M = 2.43377E+00

REGION 5AS

THETA = 4.15671E+01 X = 1.16193E+01 Y = 3.06559E+00
PR = 8.79715E+01 DR = 5.62755E+00 TR = 1.56323E+01 M = 2.50954E+00

REGION 5BS

THETA = 4.06615E+01 X = 1.18523E+01 Y = 3.26571E+00
PR = 8.48364E+01 DR = 5.61469E+00 TR = 1.51097E+01 M = 2.58621E+00

REGION 5CS

THETA = 3.97480E+01 X = 1.21149E+01 Y = 3.48414E+00
PR = 8.16890E+01 DR = 5.60086E+00 TR = 1.45851E+01 M = 2.66626E+00

REGION 5DS

THETA = 3.88555E+01 X = 1.24107E+01 Y = 3.72243E+00
PR = 7.86319E+01 DR = 5.58644E+00 TR = 1.40755E+01 M = 2.74724E+00

FLOW PARAMETERS ALONG WING-LEADING EDGE

S(I)	PE(I)	RES(I)	QDOT(I)	QDOTR(I)	PRAT(I)
.00400	127.95874	4.32403E+02	3.93434E+02	6.67658E-01	1.37609E+02
.00800	127.95874	8.64807E+02	2.78200E+02	4.72105E-01	1.37609E+02
.01200	127.95874	1.29721E+03	2.27149E+02	3.85472E-01	1.37609E+02
.01600	127.95874	1.72961E+03	1.96717E+02	3.33829E-01	1.37609E+02
.02000	127.95874	2.16202E+03	1.75949E+02	2.98586E-01	1.37609E+02
.02400	127.95874	2.59442E+03	1.60619E+02	2.72570E-01	1.37609E+02
.02800	127.95874	3.02682E+03	1.48704E+02	2.52351E-01	1.37609E+02
.03200	127.95874	3.45923E+03	1.39100E+02	2.36053E-01	1.37609E+02
.03600	127.95874	3.89163E+03	1.31145E+02	2.22553E-01	1.37609E+02
.04000	127.95874	4.32403E+03	1.24415E+02	2.11132E-01	1.37609E+02
.04400	127.95874	4.75644E+03	1.18625E+02	2.01306E-01	1.37609E+02
.04800	127.95874	5.18884E+03	1.13575E+02	1.92736E-01	1.37609E+02
.05200	127.95874	5.62124E+03	1.09119E+02	1.85175E-01	1.37609E+02
.05600	127.95874	6.05365E+03	1.05150E+02	1.78439E-01	1.37609E+02
.06000	127.95874	6.48605E+03	1.01584E+02	1.72388E-01	1.37609E+02
.06400	127.95874	6.91845E+03	9.83584E+01	1.66914E-01	1.37609E+02
.06800	127.95874	7.35086E+03	9.54217E+01	1.61931E-01	1.37609E+02
.07200	127.95874	7.78326E+03	9.27332E+01	1.57368E-01	1.37609E+02
.07600	127.95874	8.21566E+03	9.02599E+01	1.53171E-01	1.37609E+02
.08000	127.95874	8.64807E+03	8.79745E+01	1.49293E-01	1.37609E+02
.08400	127.95874	9.08047E+03	8.58543E+01	1.45695E-01	1.37609E+02
.08800	127.95874	9.51287E+03	8.38804E+01	1.42345E-01	1.37609E+02
.09200	127.95874	9.94528E+03	8.20366E+01	1.39216E-01	1.37609E+02
.09600	127.95874	1.03777E+04	8.03093E+01	1.36285E-01	1.37609E+02
.10000	127.95874	1.08101E+04	7.86867E+01	1.33532E-01	1.37609E+02
.10400	127.95874	1.12425E+04	7.71587E+01	1.30938E-01	1.37609E+02
.10800	127.95874	1.16749E+04	7.57164E+01	1.28491E-01	1.37609E+02
.11200	127.95874	1.21073E+04	7.43520E+01	1.26175E-01	1.37609E+02
.11600	127.95874	1.25397E+04	7.30588E+01	1.23981E-01	1.37609E+02
.12000	127.95874	1.29721E+04	7.18308E+01	1.21897E-01	1.37609E+02
.12104	127.95874	1.30843E+04	7.15222E+01	1.21373E-01	1.37609E+02
.12122	114.10592	1.23735E+04	6.77579E+01	1.14985E-01	1.22711E+02
.12140	114.10592	1.23919E+04	6.77075E+01	1.14900E-01	1.22711E+02
.12158	114.10592	1.24103E+04	6.76572E+01	1.14814E-01	1.22711E+02
.12176	114.10592	1.24288E+04	6.76070E+01	1.14729E-01	1.22711E+02
.12194	114.10592	1.24472E+04	6.75570E+01	1.14644E-01	1.22711E+02
.12212	114.10592	1.24656E+04	6.75070E+01	1.14560E-01	1.22711E+02
.12230	114.10592	1.24840E+04	6.74572E+01	1.14475E-01	1.22711E+02
.12248	114.10592	1.25025E+04	6.74074E+01	1.14391E-01	1.22711E+02
.12266	114.10592	1.25209E+04	6.73578E+01	1.14306E-01	1.22711E+02
.12284	114.10592	1.25393E+04	6.73083E+01	1.14222E-01	1.22711E+02
.12302	114.10592	1.25578E+04	6.72589E+01	1.14138E-01	1.22711E+02
.12320	101.46675	1.18532E+04	6.36267E+01	1.07975E-01	1.09119E+02
.12338	101.46675	1.18706E+04	6.35801E+01	1.07896E-01	1.09119E+02
.12357	101.46675	1.18880E+04	6.35336E+01	1.07817E-01	1.09119E+02
.12375	101.46675	1.19053E+04	6.34873E+01	1.07738E-01	1.09119E+02
.12393	101.46675	1.19227E+04	6.34410E+01	1.07659E-01	1.09119E+02
.12411	101.46675	1.19401E+04	6.33949E+01	1.07581E-01	1.09119E+02
.12429	101.46675	1.19574E+04	6.33488E+01	1.07503E-01	1.09119E+02
.12447	101.46675	1.19748E+04	6.33028E+01	1.07425E-01	1.09119E+02
.12465	101.46675	1.19922E+04	6.32570E+01	1.07347E-01	1.09119E+02
.12483	101.46675	1.20096E+04	6.32112E+01	1.07270E-01	1.09119E+02
.12501	101.46675	1.20269E+04	6.31656E+01	1.07192E-01	1.09119E+02
.12519	90.06329	1.13369E+04	5.96954E+01	1.01303E-01	9.68554E+01
.12537	90.06329	1.13532E+04	5.96524E+01	1.01230E-01	9.68554E+01
.12555	90.06329	1.13696E+04	5.96095E+01	1.01157E-01	9.68554E+01

.12573	90.06329	1.13859E+04	5.95666E+01	1.01085E-01	9.65554E+01
.12591	90.06329	1.14023E+04	5.95239E+01	1.01012E-01	9.68554E+01
.12609	90.06329	1.14186E+04	5.94813E+01	1.00940E-01	9.68554E+01
.12627	90.06329	1.14350E+04	5.94388E+01	1.00868E-01	9.68554E+01
.12645	90.06329	1.14513E+04	5.93963E+01	1.00796E-01	9.68554E+01
.12663	90.06329	1.14677E+04	5.93540E+01	1.00724E-01	9.68554E+01
.12681	90.06329	1.14840E+04	5.93117E+01	1.00652E-01	9.68554E+01
.12700	90.06329	1.15004E+04	5.92695E+01	1.00580E-01	9.68554E+01
.12718	90.06329	1.15167E+04	5.92274E+01	1.00509E-01	9.68554E+01
.12736	90.06329	1.15331E+04	5.91854E+01	1.00438E-01	9.68554E+01
.12754	79.64335	1.08464E+04	5.58286E+01	9.47412E-02	8.56496E+01
.12772	79.64335	1.08618E+04	5.57891E+01	9.46742E-02	8.56496E+01
.12790	79.64335	1.08771E+04	5.57497E+01	9.46074E-02	8.56496E+01
.12808	79.64335	1.08925E+04	5.57104E+01	9.45407E-02	8.56496E+01
.12826	79.64335	1.09078E+04	5.56712E+01	9.44741E-02	8.56496E+01
.12844	79.64335	1.09232E+04	5.56321E+01	9.44077E-02	8.56496E+01
.12862	79.64335	1.09385E+04	5.55930E+01	9.43414E-02	8.56496E+01
.12880	79.64335	1.09539E+04	5.55540E+01	9.42753E-02	8.56496E+01
.12898	79.64335	1.09692E+04	5.55151E+01	9.42093E-02	8.56496E+01
.12916	79.64335	1.09846E+04	5.54763E+01	9.41434E-02	8.56496E+01
.12934	79.64335	1.10000E+04	5.54376E+01	9.40777E-02	8.56496E+01
.12952	79.64335	1.10153E+04	5.53990E+01	9.40121E-02	8.56496E+01
.12970	79.64335	1.10307E+04	5.53604E+01	9.39466E-02	8.56496E+01
.12988	79.64335	1.10460E+04	5.53219E+01	9.38813E-02	8.56496E+01
.13006	79.64335	1.10614E+04	5.52835E+01	9.38162E-02	8.56496E+01
.13025	70.31739	1.03907E+04	5.21023E+01	8.84176E-02	7.56203E+01
.13425	70.31739	1.07098E+04	5.13202E+01	8.70904E-02	7.56203E+01
.13825	70.31739	1.10289E+04	5.05723E+01	8.58212E-02	7.56203E+01
.14225	70.31739	1.13480E+04	4.98561E+01	8.46059E-02	7.56203E+01
.14625	70.31739	1.16671E+04	4.91696E+01	8.34409E-02	7.56203E+01
.15025	70.31739	1.19862E+04	4.85107E+01	8.23227E-02	7.56203E+01
.15425	70.31739	1.23053E+04	4.78775E+01	8.12482E-02	7.56203E+01
.15825	70.31739	1.26244E+04	4.72685E+01	8.02148E-02	7.56203E+01
.16225	70.31739	1.29435E+04	4.66822E+01	7.92198E-02	7.56203E+01
.16625	70.31739	1.32627E+04	4.61172E+01	7.82610E-02	7.56203E+01
.17025	70.31739	1.35818E+04	4.55722E+01	7.73361E-02	7.56203E+01
.17425	70.31739	1.39009E+04	4.50461E+01	7.64433E-02	7.56203E+01
.17825	70.31739	1.42200E+04	4.45378E+01	7.55807E-02	7.56203E+01
.18225	70.31739	1.45391E+04	4.40463E+01	7.47466E-02	7.56203E+01
.18625	70.31739	1.48582E+04	4.35707E+01	7.39396E-02	7.56203E+01
.19025	70.31739	1.51773E+04	4.31103E+01	7.31582E-02	7.56203E+01
.19425	70.31739	1.54964E+04	4.26641E+01	7.24010E-02	7.56203E+01
.19825	70.31739	1.58155E+04	4.22315E+01	7.16669E-02	7.56203E+01

APPENDIX B. - GENERAL DESCRIPTION OF REAL-GAS CODE

As has been discussed previously, philosophically the real-gas code is approached in the same way as the perfect-gas code. As with the perfect-gas code, the free-stream conditions and the model geometry serve as input. The real-gas code uses a Mollier gas table to find the flow-field conditions in place of the perfect gas relations of the perfect-gas code.

Calculation of Flow-Field Conditions. The flow conditions of regions 2, 3, and 6 are calculated in subroutine RELGAS. The procedure of this subroutine is to assume an initial value for the shock wave angle θ , and solve for the density as follows.

$$\rho_2 = \frac{\rho_1 \tan \theta}{\tan(\theta - \delta)} \quad (18)$$

The velocity behind the shock wave can then be determined by using the conservation of mass equation:

$$U_{2n} = \frac{\rho_1 U_{1n}}{\rho_2} \quad (19)$$

The pressure is then calculated from the conservation of normal momentum equation:

$$P_2 = P_1 + \rho_1 U_{1n}^2 - \rho_2 U_{2n}^2 \quad (20)$$

Then the enthalpy behind the shock wave is calculated using the conservation of energy equation:

$$h_2 = h_1 + 0.5 U_{1n}^2 - 0.5 U_{2n}^2 \quad (21)$$

Once the static pressure and the static enthalpy are known, the remaining flow properties behind the shock wave can be found by using the subroutine MØLIER. MØLIER, which incorporates the gas table, needs only two properties as

input to find the remaining flow field properties. The density found from MØLIER is compared to the density behind the shock wave calculated from equation (18). If the comparison is not acceptable (to within a prespecified tolerance), a half-interval iteration method is used to redetermine the shock wave angle. The procedure to calculate the flow condition behind the shock wave is then repeated until successive values of the densities converge.

Calculation of Stagnation Conditions. The stagnation conditions are calculated after the flow conditions in regions 2, 3, and 6 are calculated, by first calculating the stagnation enthalpy by the following equation:

$$H = h_1 + 0.5 U_1^2 \quad (22)$$

Using the stagnation enthalpy and the entropy of regions 1, 2, 3, and 6, the stagnation conditions for an isentropic deceleration of the local flow are found from MØLIER.

Calculation of Expansion Fan Flow. To calculate the expansion fan flow, the flow is assumed to expand isentropically from region 3 to region 5E. Thus, the entropy of region 3 defines the entropy of the expansion fan. Therefore, the two properties serving as input for the MØLIER subroutine, are the local static enthalpy and the entropy.

As before, the streamlines for subregion 5E through region 6 are parallel and straight for the assumed flow model. Therefore,

$$\frac{dP}{dn} = 0 \quad (23)$$

and the static pressure of subregion 5E is equal to the static pressure of region 6. The enthalpy of region 5E is found by using the static pressure of region 6 and the entropy of region 3. To calculate the enthalpy of each of the other nine regions in the expansion fan, the difference between the

enthalpies of region 3 and 5E is divided by ten to get ten equal increments. The enthalpy of region 4A is, therefore, the enthalpy of region 3 plus the above increment. The enthalpies of the remaining subregions are gotten by appropriately incrementing the previous enthalpy.

As a check to the above procedure the Prandtl-Meyer angle for the subregion of interest was calculated using the equation:

$$v - v_3 = \frac{1}{2} \int_{\text{Reg. 3}} \left[\frac{2(H-h)}{a^2} - 1 \right]^{1/2} \frac{d(H-h)}{H-h} \quad (24)$$

When crossing a right-running wave, the change in the Prandtl-Meyer angle is equal to the change in the flow direction, i.e.,

$$dv = d\theta \quad (25a)$$

When crossing the reflected left-running waves,

$$dv = -d\theta \quad (25b)$$

Thus, since the flow in region 3 is parallel to the wall, the sum of the change in v through region 4 should equal to the sum of the change in v through region 5. For all cases computed thus far, the difference between the v -sums has been small. Thus, the net change in flow angle has been essentially zero, as it should. The intersection points of the shock waves and expansion fan waves are calculated the same way as in the perfect gas code using the subroutine INTRST.

The flow properties at the wall account for the waves of the centered expansion fan, i.e., region 4, and of the reflected left-running waves, i.e., region 5. As noted before,

$$v_{4AW} = v_{4A} - (\theta_{4AW} - \theta_{4A}) \quad (26)$$

so that

$$v_{4AW} = v_{4B} \quad (27a)$$

Similarly,

$$v_{4BW} = v_{4D} \quad (27b)$$

$$v_{4CW} = v_{5A} \quad (27c)$$

and

$$v_{4DW} = v_{5C} \quad (27d)$$

Once the Prandtl-Meyer functions are known, the remaining properties are readily calculated, since flow in this region is isentropic.

Wing Leading-Edge Heat-Transfer Rate Calculations. After the inviscid flow-field conditions have all been calculated, the heat-transfer rate along the "wing leading-edge" is calculated. The procedure for calculating the heat-transfer is to first use the numerical routine as described in ref. 15 to set up the initial boundary-layer profile.

This initial profile serves as an input into the NONSIMBL code (ref. 11). Several modifications were made to this numerical routine for a laminar boundary-layer. One modification was to eliminate the need for user "experience" in establishing the initial, input guesses for the wall values of the shear function, $f''(0)$, and of the heat-transfer function, $g'(0)$. Instead, since the temperature of the edge of the boundary layer and at the wall in region 3 were known from the previous subroutines, the initial value of $g'(0)$ was assumed to be

$$g'(0) = \left[1 - \frac{T_w}{T_{t3}} \right] 0.6$$

The initial guess for the shear function was assumed to be: $f''(0) = 0.47$, which seemed to provide reasonable results over the entire velocity range (in the absence of gas injection of the wall).

Another modification was to incorporate into the routine a procedure for calculating alpha (i.e., the coordinate transformation parameter).

The above procedure is designated subroutine PIGYBAK and transforms the distribution of the dimensionless velocity function F and the temperature ratio θ (THETA) into the new coordinate using α (α). The transformation is

$$n = 1 - e^{-\alpha\eta}$$

where n is the newly transformed y -coordinate (ref. 11) and η is the transformed y -coordinate using the standard Lees-Dorodnitsyn transformation. To calculate the appropriate value of α , the value of η where $u = 0.99u_e$ in the similar solution for the first station was identified. Then, the value of α was calculated to be the value which makes the product $\alpha\eta$ equal to three at this point, i.e., $n = 0.95$.

This viscous-layer profile for a similar boundary-layer which is subject to the flow conditions at the initial point in region 3 is used as an initial condition for the subroutine EJØYCE, which solves the nonsimilar boundary layer. This subroutine is actually the numerical code described in ref. 11 with modifications. Modifications were made to this code so that one could obtain real gas values of density, thermal conductivity, viscosity, and specific heat of air. The MØLLIER subroutine was used to calculate the density in the boundary layer. The tabulated values of Hansen (ref. 9) for thermal conductivity, viscosity, and specific heat were input as a function of temperature. Then, the subroutine SPLNTRP was used to calculate the transport properties at the desired temperatures. SPLNTRP is a curve fitting subroutine. The final output of EJØYCE gives boundary layer profiles, heat-transfer rates, and other data for five points in each of the six regions and subregions on the "wing leading-edge".

Calculation of the Shock-Wave Angles and the Intersection Points of the Shock Wave with the Expansion Fan.

As was the case for the perfect-gas code the flow direction in subregions 4E, 5A, 5B, 5C, and 5D of the expansion

fan are used as boundary conditions for computing the shock waves in this region. The subroutine RELGAS is used to generate the shock wave angle and the flow conditions in the subregions between the shock wave and the shear layer, i.e., subregion 4ES, 5AS, 5BS, 5CS, and 5DS. The intersection of the shock wave and the left-running expansion wave is computed using the subroutine INTRST using the same procedure as discussed in the perfect-gas section.

Input Cards

Card # 1 NC - number of cases

Card # 2 X0 - x-location of "nose" (ft)
 Y0 - y-location of "nose" (ft)
 X30 - x-location of wedges intersection point (ft)
 Y30 - y-location of wedges intersection point (ft)

Card # 3 U1 - free-stream velocity (ft/sec)
 P1 - free-stream pressure (lbf/ft²)
 H1 - free-stream enthalpy (ft²/sec²)
 DELTA - angle of the first wedge (°)
 LAMDAS - complement of sweep angle (°)
 NØPT - option in MØLIER for the two input properties enthalpy
 and pressure (°)

Card # 4 TWALL - wall temperature (°R)
 RADIUS - radius of reference sphere (ft)
 PR - Prandtl number

Card # 5 E - convergence criterion on boundary condition (typically .0005)
 DELT - step size in y-direction (typically .05)
 EPS - convergence criterion when variable step size is used.

Card # 6 KEY - equals 1 if using variable step size (equals 0 for the
 fixed size routine)

Card # 7 IN - number of y-points
 ALF - coordinate transformation parameter

Card # 8 PIGYBK - if equals 1.0 edge properties are not read in as input

Card # 9 MM - number of x-points for calculations
 N - number of y-points in boundary layer
 KK - equals 0 for two-dimensional flow, equals 1 for
 axi-symmetrical flow
 NØPRINT - if equals 0 output will be printed.

Card # 10 WMI - molecular weight of injectant

 WMS - molecular weight of stream (WMI = WMS for this routine)

Card # 11-13 TEMP - temperature ($^{\circ}\text{R}$), fifteen temperatures on three cards

Card # 14-16 VISC - viscosity ($\frac{\text{lb} \cdot \text{sec}}{\text{ft}^2}$) fifteen viscosities corresponding to above temperatures.

Card # 17-19 TC - thermal conductivity ($\frac{\text{BTU}}{\text{ft} \cdot \text{sec} \cdot ^{\circ}\text{R}}$), fifteen thermal conductivities corresponding to above temperatures

Card # 20-22 CP - specific heat ($\frac{\text{BTU}}{\text{slug} \cdot ^{\circ}\text{R}}$), fifteen specific heats corresponding to above temperatures

Card # 23 equals Card # 3 if NC > 1

Card # 24 equals Card # 4 if NC > 1

```

PROGRAM REALGAS (INPUT,OUTPUT)
  DIMENSION H*(50),P4(50),T4(50),R4(50),G4(50),A4SU(50),Y(50),
  1UNU(50),Z4(50)
  DIMENSION WAVE4(50),AGL4(50),X4(50),Y4(50),THTA4(50),U4(50),
  1EXM4(50),SIGUNU(50)
  DIMENSION THTS4(11),XS4(11),YS4(11),US4(11),PS4(11),TS4(11),
  1RS4(11),HS4(11),GS4(11),ZS4(11),SS4(11)
  COMMON/KONSI/TWALL,RADIUS,PR
  COMMON/WING/PT3,TT3,U3,T3,P3,X30,Y30,X4,Y4,P4,P6,T4,U4,T5E
  COMMON/CASE/NCASE
  COMMON/SHOCK/NFLUB,ISHOCK,JSHOCK
  REAL LAMDAS
  READ 222, NC
222 FORMAT(I5)
  READ 101,X0,Y0,X30,Y30
101 FORMAT(4E12.5)
  DO 99 II=1,NC
  READ 200,U1,P1,H1,DELTA,LAMDAS,NOPT
200 FORMAT(5E12.5,I5)
  READ 102, TWALL, RADIUS, PR
102 FORMAT(3E12.5)
C
  H1=H1/(32.176*778.0)
  CALL MOLIER(H1,P1,NOPT,T1,Z1,S1,RH01,GAMMA1)
  H1=H1*32.176*778.0
C
C *****CALCULATING FLOW CONDITIONS IN REGION 2*****
  CALL RELGAS (U1,P1,RH01,H1,DELTA,NOPT,U2,P2,RH02,H2,T2,Z2,GAMMA2,
  1THETA,S2)
C
C *****CALCULATING FLOW CONDITIONS IN REGION 3*****
  DELTA3=LAMDAS-DELTA
  CALL RELGAS(U2,P2,RH02,H2,DELTA3,NOPT,U3,P3,RH03,H3,T3,Z3,GAMMA3,
  1THETA3,S3)
C
C *****CALCULATING FLOW CONDITIONS IN REGION 6*****
  DELTA6=LAMDAS
  NFLUB=1
  CALL RELGAS(U1,P1,RH01,H1,DELTA6,NOPT,U6,P6,RH06,H6,T6,Z6,GAMMA6,
  1THETA6,S6)
C
C *****COMPUTING STAGNATION CONDITIONS*****
C
  HSTAG=H1+0.5*U1*U1
  HSTAG=HSTAG/(32.176*778.0)
  CALL MOLIER(HSTAG,PT1,3,TT1,ZT1,S1,RT1,GT1)
  CALL MOLIER(HSTAG,PT2,3,TT2,ZT2,S2,RT2,GT2)
  CALL MOLIER(HSTAG,PT3,3,TT3,ZT3,S3,RT3,GT3)
  CALL MOLIER(HSTAG,PT6,3,TT6,ZT6,S6,RT6,GT6)
C
  PRAT21=P2/P1
  PRAT31=P3/P1
  PRAT61=P6/P1
  TRAT21=T2/T1
  TRAT31=T3/T1
  TRAT61=T6/T1
  DRAT21=RH02/RH01
  DRAT31=RH03/RH01
  DRAT61=RH06/RH01
C
  H1=H1/(32.176*778.0)

```

H2=H2/(32.176*778.0)
H3=H3/(32.176*778.0)
H6=H6/(32.176*778.0)

*****COMPUTING EXPANSION FAN FLOW*****

IF(ISHOCK.EQ.1) GO TO 703
CALL MOLIER(H5E,P6,1,T5E,Z5E,S3,RH05E,G5E)
A3SQ=P3*GAMMA3/RH03
A5ESQ=P6*G05E/RH05E
A3SQ=A3SQ/(32.176*778.0)
A5ESQ=A5ESQ/(32.176*778.0)
ETA1=HSTAG-H3
ETAN=HSTAG-H5E
N=11
Y(1)=SQRT(2.0*ETA1/A3SQ-1.0)/(2.0*ETA1)
Y(N)=SQRT(2.0*ETAN/A5ESQ-1.0)/(2.0*ETAN)
M=N-1
HSTEP=(ETAN-ETA1)/M
ETA=ETA1

DO 98 I=2,M
ETA=ETA+HSTEP
H4(I)=HSTAG-ETA
CALL MOLIER(H4(I),P4(I),3,T4(I),Z4(I),S3,R4(I),G4(I))
A4SQ(I)=P4(I)*G4(I)/R4(I)
A4SQ(I)=A4SQ(I)/(32.176*778.0)
Y(I)=SQRT(2.0*ETA/A4SQ(I)-1.0)/(2.0*ETA)

98 CONTINUE

SIGDNU(1)=0.0
SIGDNU(2)=SIGDNU(1)+(Y(1)+Y(2))*HSTEP/2.0
DO 97 J=3,N,2
SIGDNU(J)=SIGDNU(J-2)+(Y(J-2)+4.0*Y(J-1)+Y(J))*HSTEP/3.0
IF((J+1).GT.M) GO TO 97
SIGDNU(J+1)=SIGDNU(J-1)+(Y(J-1)+4.0*Y(J)+Y(J+1))*HSTEP/3.0

97 CONTINUE

DO 90 JP=2,N
DNU(JP)=SIGDNU(JP)-SIGDNU(JP-1)

90 CONTINUE

DNU4=DNU(2)+DNU(3)+DNU(4)+DNU(5)+DNU(6)
DNU5=DNU(7)+DNU(8)+DNU(9)+DNU(10)+DNU(11)
DNU4IF=DNU4-DNU5

*****FINDING VELOCITIES AND MACH NUMBERS IN THE EXPANSION FAN*****

HSTAG=HSTAG*32.176*778.0
DO 96 K=2,M
H4(K)=H4(K)*32.176*778.0
U4(K)=SQRT(2.0*(HSTAG-H4(K)))
A4SQ(K)=A4SQ(K)*32.176*778.0
EXM4(K)=U4(K)/SQRT(A4SQ(K))
H4(K)=H4(K)/(32.176*778.0)

96 CONTINUE

H5E=H5E*32.176*778.0
A5ESQ=A5ESQ*32.176*778.0
U4(N)=SQRT(2.0*(HSTAG-H5E))
EXM4(N)=U4(N)/SQRT(A5ESQ)
H5E=H5E/(32.176*778.0)

*****FINDING INTERSECTION POINTS OF SHOCK WAVES AND EXPANSION FAN*****

```

THETA=THETA/57.296
THETA3=THETA3/57.296
LAMDAS=LAMDAS/57.296
DELTA=DELTA/57.296
DELTA6=DELTA6/57.296

```

C

```

AGL3=THETA3+DELTA
CALL INTRST(X0,Y0,THETA,AGL3,X30,Y30,X1,Y1)

```

C

```

A3SQ=A3SQ*32.176*778.0
WAVE3=ASJ (1.0/(0.3/SGRT(A3SQ)))
AGL4A=LAMDAS-WAVE3
CALL INTRST(X1,Y1,AGL4A,LAMDAS,X30,Y30,X4A,Y4A)

```

C

```

EXM4(1)=0.3/SGRT(A3SQ)
X4(2)=X4A
Y4(2)=Y4A
AGL4(2)=AGL4A
LL=1
NN=(N+1)/2
DO 95 L=2,M
WAVE4(L)=ASIN(1./EXM4(L))
IF(NN-L)94,93,92
92 AGL4(L+1)=LAMDAS+SIGDNU(L)-WAVE4(L)
CALL INTRST(X1,Y1,AGL4(L+1),LAMDAS,X30,Y30,X4(L+1),Y4(L+1))
GO TO 95
94 LL=LL+1
THTA4(L)=THTA4(L-1)-DNU(L)
AGL4(L+1)=THTA4(L)+WAVE4(L)
CALL INTRST(X4(L),Y4(L),THTA4(L),AGL4(L+1),X4(LL),Y4(LL),X4(L+1),
Y4(L+1))
GO TO 95
93 THTA4(L)=LAMDAS+SIGDNU(L)
LL=LL+1
AGL4(L+1)=THTA4(L)+WAVE4(L)
CALL INTRST(X1,Y1,THTA4(L),AGL4(L+1),X4(LL),Y4(LL),X4(L+1),Y4(L+1))
1)
95 CONTINUE

```

C
C*****CALCULATING FLOW CONDITIONS IN SHOCKED REGIONS 4E AND 5*****
C

```

L=1
NFLUB=2
H1=H1*32.176*778.0
DO 77 I=6,M
THTA4(I)=THTA4(I)*57.296
CALL RELGAS(U1,P1,RHC1,H1,THTA4(I),NOPI,US4(I),PS4(I),RS4(I),
MS4(I),LS4(I),ZS4(I),GS4(I),THTS4(I),SS4(I))
THTS4(I)=THTS4(I)/57.296
L=L+1
IF(I.GT.6) GO TO 75
CALL INTRST(X1,Y1,THTS4(I),AGL4(I+1),X4(L),Y4(L),XS4(I+1),YS4(I+1))
1)
GO TO 76
75 CALL INTRST(XS4(I),YS4(I),THTS4(I),AGL4(I+1),X4(L),Y4(L),XS4(I+1),
YS4(I+1))
76 THTS4(I)=THTS4(I)*57.296
77 CONTINUE
H1=H1/(32.176*778.0)

```

C
C


```

    THETA3=THETA3*57.296
    LAMDA5=LAMDA5*57.296
    DELTA =DELTA6*57.296
    DELTA=DELTA*57.296
    THETA=THETA*57.296
703 CONTINUE
    PRINT 100
100 FORMAT(1H1)
    PRINT 200, I1
300 FORMAT(33X,*CASE =*,I2,/)
    PRINT 201
201 FORMAT(16X,*FREE-STREAM FLOW CONDITIONS*,///)
    PRINT 202
202 FORMAT(13X,* U1 *,11X,*P1*,14X,*T1*,12X,*RH01*,12X,*PT1*,12X,*TT
11*)
    PRINT 217
217 FORMAT(26X,*(LBF/SQFT)*,6X,*(RANKINE)*,8X,*(SLUGS/CUFT)*,/)
    PRINT 203, U1, P1, T1, RH01, PT1, TT1
203 FORMAT(10X,E12.5,3X,E12.5,4X,E12.5,3X,E12.5,4X,E12.5,4X,E12.5,/)
    PRINT 204, GAMMA1, H1, Z1
204 FORMAT(11X,*GAMMA1 =*,E12.5,5X,*H1 =*,E12.5,5X,*Z1 =*,E12.5,///)
    PRINT 206
206 FORMAT(16X,*FLOW CONDITIONS IN REGION 2*,///)
    PRINT 207
207 FORMAT(15X,*U2*,14X,*P2/P1*,15X,*T2/T1*,14X,*RH02/RH01*,/)
    PRINT 208, U2, PRAT21, TRAT21, URAT21
208 FORMAT(10X,E12.5,6X,E12.5,8X,E12.5,9X,E12.5,/)
    PRINT 212, P2, T2, RH02, PT2
212 FORMAT(11X,*P2 =*,E12.5,5X,*T2 =*,E12.5,5X,*RH02 =*,E12.5,5X,*PT2
1=*,E12.5,/)
    PRINT 205, T2, H2, Z2, GAMMA2
205 FORMAT(11X,*T2 =*,E12.5,5X,*H2 =*,E12.5,5X,*Z2 =*,E12.5,5X,*GAMMA
12 =*,E12.5,/)
    PRINT 209, DELTA, THETA
209 FORMAT(11X,*DELTA =*,E12.5,5X,*THETA =*,E12.5)
    PRINT 210
210 FORMAT(///,16X,*FLOW CONDITIONS IN REGION 3*,///)
    PRINT 213
213 FORMAT(15X,*U3*,14X,*P3/P1*,15X,*T3/T1*,14X,*RH03/RH01*,/)
    PRINT 208, U3, PRAT31, TRAT31, URAT31
    PRINT 215, P3, T3, RH03, PT3
215 FORMAT(11X,*P3 =*,E12.5,5X,*T3 =*,E12.5,5X,*RH03 =*,E12.5,5X,*PT3
1=*,E12.5,/)
    PRINT 220, T3, H3, Z3
220 FORMAT(11X,*TT3 =*,E12.5,5X,*H3 =*,E12.5,5X,*Z3 =*,E12.5,/)
    PRINT 218, DELTA3, THETA3, GAMMA3
218 FORMAT(11X,*DELTA =*,E12.5,5X,*THETA =*,E12.5,5X,*GAMMA3 =*,E12.5)
    PRINT 211
211 FORMAT(///,16X,*FLOW CONDITIONS IN REGION 6*,///)
    IF (ISHOCK.EQ.1) GO TO 701
    PRINT 214
214 FORMAT(15X,*U6*,14X,*P6/P1*,15X,*T6/T1*,14X,*RH06/RH01*,/)
    PRINT 208, U6, PRAT61, TRAT61, URAT61
    PRINT 216, P6, T6, RH06, PT6
216 FORMAT(11X,*P6 =*,E12.5,5X,*T6 =*,E12.5,5X,*RH06 =*,E12.5,5X,*PT6
1=*,E12.5,/)
    PRINT 221, T6, H6, Z6
221 FORMAT(11X,*TT6 =*,E12.5,5X,*H6 =*,E12.5,5X,*Z6 =*,E12.5,/)
    PRINT 219, DELTA6, THETA6, GAMMA6
219 FORMAT(11X,*DELTA =*,E12.5,5X,*THETA =*,E12.5,5X,*GAMMA6 =*,E12.5)
    PRINT 301
301 FORMAT(///,16X,*FLOW CONDITIONS IN THE EXPANSION FAN*,///)

```

```

    DY(1)=Y(2)
    DY(2)=Y(3)
    DY(3)=-(1./X1)*((Y(1)+X2)*Y(3))
    DY(4)=Y(5)
    DY(5)=-(1./(A3*X1))*((Y(1)+A3*X2)*Y(5)+((X1)*Y(3)**2)-Y(1)*Y(2)*Y(3
1))*A4)
    RETURN
    END

```

```

SUBROUTINE NUMIN(N,DELT,T,DV,P,TE,ER,YPR,DEP,EPS,DPSAVE,KEY,DERIV,
1 IINDEX)

```

```

C-----GENERAL NUMERICAL INTEGRATION WITH SINGLE-STEP ERROR ANALYSIS
      DOUBLE PRECISION DEP,SIX,TWO,DPSAVE
      DIMENSION A(4),B(5),DV(N),P(N),TE(N),ER(N)
      DIMENSION YPR(N,4),DEP(N),DPSAVE(N)

```

```

C-----
C-----

```

```

      EXTERNAL DERIV

```

```

C-----DATA

```

```

      GO TO (10,15,20) IINDEX

```

```

10 SIX = 24.000
   ZERO = 0.000
   A(1) = -9.000/SIX
   A(2) = 37.000/SIX
   A(3) = -59.000/SIX
   A(4) = 55.000/SIX
   B(1) = 1.000/SIX
   B(2) = -5.000/SIX
   B(3) = 19.000/SIX
   B(4) = -A(1)
   RATIO = 19.0/270.0
   SIX = 6.000
   TWO = 2.000
   M1 = 4
   M2 = 1
   M3 = 2
   M4 = 3
   RETURN

```

```

C-----SET UP FOR INTEGRATION

```

```

C-----ENTRY RESET

```

```

15 ASSIGN 2000 TO IPL5
   KOP = 0
   KOUNT = 0
   DELBY6 = DELT/SIX
   DELBY2 = DELT/TWO
   DO 16 J=1,N
     DPSAVE(J) = DEP(J)
16 DV(J) = DEP(J)
   CALL DERIV(1,DV,P,6,N)
17 CONTINUE
   DO 18 J=1,N
     YPR(J,M1) = P(J)
18 ER(J) = ZERO
19 CONTINUE
   RETURN

```

```

C-----ENTRY-POINT FOR ONE NUMERICAL INTEGRATION STEP

```

```

20 V = T
   T = V + DELT
   KOP = KOP + 1
   GO TO IPL5

```

```

C-----RUNGE-KUTTA PROCEDURE

```

```

2000 VV = V + DELBY2
   DO 250 J=1,N

```

```

250 DV(J) = DEP(J) + YPR(J,M1)*DELB2
CALL DERIV(VV,DV,P,3,N)
251 CONTINUE
DO 260 J=1,N
260 DV(J) = DEP(J) + P(J)*DELB2
CALL DERIV(VV,DV,TE,4,N)
261 CONTINUE
DO 270 J=1,N
DV(J) = DEP(J) + TE(J)*DELT
270 TE(J) = 2.0*(TE(J)+P(J))
CALL DERIV(I,DV,P,5,N)
271 CONTINUE
DO 280 J=1,N
DEP(J) = DEP(J) + DELB6*(P(J)+TE(J)+YPR(J,M1))
280 DV(J) = DEP(J)
CALL DERIV(I,DV,P,5,N)
281 CONTINUE
DO 290 J=1,N
290 YPR(J,M4) = P(J)
291 CONTINUE
KOUNT = KOUNT + 1
C----- CHECK THE NUMBER OF INTEGRATION STEPS MADE BY R-K PROCEDURE
IF(KOUNT.LT.3)GO TO 5000
292 ASSIGN 1000 TO IALS
GO TO 5000
5000 M0 = M4
M4 = M3
M3 = M2
M2 = M1
M1 = M0
IF(KEY.EQ.0)RETURN
IF(KOP.LE.3)RETURN
KINC=0
DO 500 J=1,N
IF(ER(J).GT.EPS) GO TO 515
IF(ER(J)*10000.0.LT.EPS)KINC=KINC+1
500 CONTINUE
IF(KINC.EQ.N) GO TO 550
DO 510 J=1,N
DPSAVE(J) = DEP(J)
510 CONTINUE
RETURN
515 CONTINUE
IF(KOP.EQ.4) GO TO 540
I = T - DELT
520 DELT = 0.500*DELT
DO 530 J=1,N
DEP(J) = DPSAVE(J)
530 CONTINUE
GO TO 15
540 I = T - 4.000*DELT
GO TO 520
550 DELT = 2.000*DELT
GO TO 15
C----- ADAMS PREDICTOR-CORRECTOR PROCEDURE
1000 DO 710 J=1,N
TE(J) = B(3)*YPR(J,M1) + B(2)*YPR(J,M2) + B(1)*YPR(J,M3)
DV(J) = DEP(J) + DELT*(A(4)*YPR(J,M1)+A(3)*YPR(J,M2))
DV(J) = DV(J) + DELT*(A(2)*YPR(J,M3)+A(1)*YPR(J,M4))
C----- SAVE PREDICTED VALUE
710 ER(J) = DV(J)
CALL DERIV(I,DV,P,1,N)

```

```

PRINT 302
302 FORMAT(13X,*REGION 4*,//)
PRINT 314
314 FORMAT(50X,*VELOCITIES*,/)
PRINT 315,U4(2),U4(3),U4(4),U4(5),U4(6)
315 FORMAT(11X,*UA =*,E12.5,5X,*UB =*,E12.5,5X,*UC =*,E12.5,5X,*UD =*,
1E12.5,5X,*UE =*,E12.5,5X,/)
PRINT 303
303 FORMAT(50X,*PRESSURES*,/)
PRINT 304,P4(2),P4(3),P4(4),P4(5),P4(6)
304 FORMAT(11X,*PA =*,E12.5,5X,*PB =*,E12.5,5X,*PC =*,E12.5,5X,*PD =*,
1E12.5,5X,*PE =*,E12.5,5X,/)
PRINT 305
305 FORMAT(49X,*TEMPERATURES*,/)
PRINT 306,T4(2),T4(3),T4(4),T4(5),T4(6)
306 FORMAT(11X,*TA =*,E12.5,5X,*TB =*,E12.5,5X,*TC =*,E12.5,5X,*TD =*,
1E12.5,5X,*TE =*,E12.5,5X,/)
PRINT 307
307 FORMAT(50X,*DENSITIES*,/)
PRINT 308,R4(2),R4(3),R4(4),R4(5),R4(6)
308 FORMAT(11X,*RHOA =*,E12.5,5X,*RHOB =*,E12.5,5X,*RHOC =*,E12.5,5X,
1*RHOD =*,E12.5,5X,*RHOE =*,E12.5,5X,/)
PRINT 309
309 FORMAT(50X,*ENTHALPIES*,/)
PRINT 310,H4(2),H4(3),H4(4),H4(5),H4(6)
310 FORMAT(11X,*HA =*,E12.5,5X,*HB =*,E12.5,5X,*HC =*,E12.5,5X,*HD =*,
1E12.5,5X,*HE =*,E12.5,5X,/)
PRINT 311
311 FORMAT(47X,*EFFECTIVE GAMMAS*,/)
PRINT 312,G4(2),G4(3),G4(4),G4(5),G4(6)
312 FORMAT(11X,*GA =*,E12.5,5X,*GB =*,E12.5,5X,*GC =*,E12.5,5X,*GD =*,
1E12.5,5X,*GE =*,E12.5,5X,/)
PRINT 313
313 FORMAT(13X,*REGION 5*,//)
PRINT 314
PRINT 315,U4(7),U4(8),U4(9),U4(10),U4(11)
PRINT 303
PRINT 304,P4(7),P4(8),P4(9),P4(10),P6
PRINT 305
PRINT 306,T4(7),T4(8),T4(9),T4(10),T5E
PRINT 307
PRINT 308,R4(7),R4(8),R4(9),R4(10),RHO5E
PRINT 309
PRINT 310,H4(7),H4(8),H4(9),H4(10),H5E
PRINT 311
PRINT 312,G4(7),G4(8),G4(9),G4(10),G5E
PRINT 401,DNUDIF
401 FORMAT(11X,*DNUDIF =*,E12.5,5X,/)
PRINT 316
316 FORMAT(16X,*POINTS OF INTEREST IN THE FLOW FIELD AND ON THE BODY (
1IN INCHES)*,///)
PRINT 317
317 FORMAT(13X,*INITIAL POINTS ON BOW SHOCK WAVE*)
PRINT 318,X0,Y0
318 FORMAT(11X,*X =*,E12.5,5X,*Y =*,E12.5)
PRINT 319
319 FORMAT(/,13X,*WING INTERSECTION POINT*)
PRINT 318,X30,Y30
PRINT 320
320 FORMAT(/,13X,*BOW SHOCK-WING SHOCK INTERSECTION POINT*)
PRINT 318,X1,Y1
PRINT 321

```

```

321 FORMAT(/,13X,*EXPANSION FAN INTERSECTION POINTS*)
    DO 80 IL=2,N
  88 PRINT 318,X4(1L),Y4(1L)
    PRINT 400
  400 FORMAT(1H1,16X,*FLOW ALONG THE WING IN THE EXPANSION REGION*,///)
    PRINT 405
  405 FORMAT(13X,*VELOCITIES*,/)
    PRINT 402,U4(3),U4(5),U4(7),U4(9)
  402 FORMAT(11X,*U4AW =*,E12.5,3X,*U4BW =*,E12.5,3X,*U4CW =*,E12.5,3X,
    1*U4DW =*,E12.5,/)
    PRINT 403
  403 FORMAT(13X,*PRESSURES*,/)
    PRINT 404,P4(3),P4(5),P4(7),P4(9)
  404 FORMAT(11X,*P4AW =*,E12.5,3X,*P4BW =*,E12.5,3X,*P4CW =*,E12.5,3X,
    1*P4DW =*,E12.5)
    PRINT 500
  500 FORMAT(///,16X,*FLOW CONDITIONS IN SHOCKED REGION OF EXPANSION FAN
    1*,///)
    IF(JSHOCK.EW.1)GO TO 702
    PRINT 501
  501 FORMAT(26X,*REGION 4ES*,///)
    PRINT 502,INTS4(4),XS4(7),YS4(7)
  502 FORMAT(13X,*THETA =*,E12.5,5X,*X =*,E12.5,5X,*Y =*,E12.5,/)
    PRINT 503,US4(6),PS4(6),TS4(6),RS4(6),HS4(6),GS4(6)
  503 FORMAT(13X,*U =*,E12.5,3X,*P =*,E12.5,3X,*T =*,E12.5,3X,*R =*,E12.
    15,3X,*H =*,E12.5,3X,*G =*,E12.5,/)
    PRINT 504
  504 FORMAT(26X,*REGION 5AS*,///)
    PRINT 502,INTS4(7),XS4(8),YS4(8)
    PRINT 503,US4(7),PS4(7),TS4(7),RS4(7),HS4(7),GS4(7)
    PRINT 505
  505 FORMAT(26X,*REGION 5BS*,///)
    PRINT 502,INTS4(9),XS4(9),YS4(9)
    PRINT 503,US4(8),PS4(8),TS4(8),RS4(8),HS4(8),GS4(8)
    PRINT 506
  506 FORMAT(26X,*REGION 5CS*,///)
    PRINT 502,INTS4(9),XS4(10),YS4(10)
    PRINT 503,US4(9),PS4(9),TS4(9),RS4(9),HS4(9),GS4(9)
    PRINT 507
  507 FORMAT(26X,*REGION 5DS*,///)
    PRINT 502,INTS4(10),XS4(11),YS4(11)
    PRINT 503,US4(10),PS4(10),TS4(10),RS4(10),HS4(10),GS4(10)
    IF(JSHOCK.NE.1)GO TO 704
  702 PRINT 602
  602 FORMAT(26X,*CURVED SHOCK NOT MODELED*)
  704 CONTINUE

```

C

```

    NCASE=11
    CALL PIGYBAR(HSTAG)
    GO TO 99
  701 PRINT 601
  601 FORMAT(26X,*NOT A TYPE VI PATTERN*)
  99 CONTINUE
    END

```

```

SUBROUTINE RELGAS(U1,P1,RHO1,H1,DELTA,NOPT,U2,P2,RHO2,H2,T2,Z2,
1 GAMMA2,THETA,S2)
COMMON/SHOCK/NFLUB,ISHOCK,JSHOCK

```

C

```

    DELTA=DELTA/57.296
    THETA=DELTA
    THETA=1.571
  5 THETA=(THETA + THETA)/2.0

```

```

      IF (THETA.LT.1.57079) GO TO 7
      IF (NFLUB.GT.1) GO TO 8
      LSHOCK=1
      RETURN
8     JSHOCK=1
      RETURN
7     CONTINUE
      TANT=TAN(THETA)
      TANTMD=TAN(THETA-DELTA)
      SINT=SIN(THETA)
      SINTMD=SIN(THETA-DELTA)
      COST=COS(THETA)

```

```

C     EPS=TANTMD/TANT

```

```

C     RH02G=RH01/EPS
      U1N=U1*SINT
      U1T=U1*COST
      U2N=EPS*U1N
      U2T=U1T
      P2=P1+RH01*U1N*U1N-RH02G*U2N*U2N
      H2=H1+0.5*U1N*U1N-0.5*U2N*U2N
      U2=U2N/SINTMD

```

```

C     H2=H2/(32.176*778.0)
      CALL MOLIER(H2,P2,NOPT,T2,Z2,S2,RH02,GAMMA2)
      RDIFF=RH02G-RH02
      CONV=ABS(RDIFF/RH02G)
      IF (CONV<0.001) 2,2,6
6     IF (RDIFF) 3,2,4
3     THETA=THETA
      GO TO 5
4     THETA=THETA
      GO TO 5
2     CONTINUE

```

```

C     H2=H2*32.176*778.0
      DELTA=DELTA*57.296
      THETA=THETA*57.296

```

```

C     RETURN
      END

```

```

      SUBROUTINE INTRST(X1,Y1,A1,A2,X2,Y2,XI,YI)

```

```

C     *****SUBROUTINE TO FIND THE INTERSECTION POINT OF THE SHOCKWAVES
C     AND THE INTERSECTION POINTS IN THE EXPANSION FAN*****

```

```

C     XI=(Y2-Y1+X1*TAN(A1)-X2*TAN(A2))/(TAN(A1)-TAN(A2))
C     YI=Y1+(XI-X1)*TAN(A1)
      RETURN
      END

```

```

      SUBROUTINE PIGYB-K(HS)

```

```

      DIMENSION F(200),G(200),FN(200),GN(200),YN(200),ETAD(200),ETA(200)
1     ,HTTA(200)
      DIMENSION Y(5),FDA(3),GA(3)
      DOUBLE PRECISION Y,AA,BB,CC,DD,EE
      DIMENSION DV(5),P(5),TE(5),YPR(5,4),DEP(5)
      DIMENSION ER(5),DPSAVE(5)
      DIMENSION X4(50),Y4(50),P4(50),T4(50),U4(50)
      DOUBLE PRECISION DPSAVE,DEP
      EXTERNAL DERIV
      COMMON/CONST/A1,A2,A3,A4,E,EPS

```

```

COMMON/KONST/TWALL,RADIUS,PR
COMMON/WING/PT3,TT3,U3,T3,P3,X30,Y30,X4,Y4,P4,P6,T4,U4,T5E
COMMON/CASE/NCASE
IF(NCASE.GT.1) GO TO 1100
READ 1, E, DELT, EPS
1 FORMAT(3E12.5)
1100 CONTINUE
A1=U3*U3/(2.0*HS)
A2=1.0-A1
A3=1.0/PR
A4=U3*U3*(PR-1.0)/(HS*PR)
IF(A3)999,777,20
20 CONTINUE
AA=0.
BB=0.0
CC=0.47
DD=TWALL/TT3
EE=(1-DD)*0.0
IF(NCASE.GT.1) GO TO 1200
READ 13,KEY
13 FORMAT (115)
READ 14,IN,ALF
14 FORMAT(112,E12.5)
1200 CONTINUE
Y(1)=AA
Y(2)=BB
Y(3)=CC
Y(4)=DD
Y(5)=EE
3 GPSAVE = Y(2)
FPPSAV = Y(3)
FPP01 = Y(3)
GP01 = Y(5)
FPP05 = Y(3)
GP05 = Y(5)
II = 1
30 CALL NUMIN(N,DELT,T,DV,P,TE,ER,YPR,Y,EPS,DPSAVE,KEY,DERIV,1)
I=0.
N=5
I=1
CALL NUMIN(N,DELT,T,DV,P,TE,ER,YPR,Y,EPS,DPSAVE,KEY,DERIV,2)
5 CALL NUMIN(N,DELT,T,DV,P,TE,ER,YPR,Y,EPS,DPSAVE,KEY,DERIV,3)
IF (ABS(Y(3)).LT.E) GO TO 33
I = I + 1
GO TO 5
33 IF (ABS(1.0000-Y(2)).GT.E) GO TO 34
IF (ABS(1.0000-Y(4)).LT.E) GO TO 99
34 FPA(II) = Y(2)
GA(II) = Y(4)
II = II + 1
IF (II.EQ.2) GO TO 35
IF (II.NE.3) GO TO 36
Y(1) = AA
Y(2) = BB
Y(3) = FPPSAV
Y(4) = DD
Y(5) = 1.05*GPSAVE
FPP03 = Y(3)
GP03 = Y(5)
FPP05 = Y(3)
GP05 = Y(5)
GO TO 30

```

```

35 Y(1) = AA
   Y(2) = BB
   Y(3) = 1.05*FPP01
   Y(4) = UD
   Y(5) = GPSAVE
   FPP02 = Y(3)
   GP02 = Y(5)
   FPP03 = Y(3)
   GP03 = Y(5)
   GO TO 30
36 DFPA = FPA(1)-FPA(2)
   UGA = GA(1)-GA(2)
   DFPA1 = FPA(1)-FPA(3)
   UGA1 = GA(1)-GA(3)
   DFPP0 = FPP01-FPP02
   UGP0 = GP01-GP03
   A6 = DFPA/DFPP0
   B1 = DFPA1/UGP0
   C1 = 1.0000-FPA(1)
   D1 = UGA/DFPP0
   E1 = UGA1/UGP0
   F1 = 1.0000-GA(1)
   DEFPF = (C1*E1-F1*B1)/(A6*E1-D1*B1)
   DEGP = (A6*F1-D1*C1)/(A6*E1-D1*B1)
   FPP = FPP01+DEFPF
   GP = GP01+DEGP
   Y(1) = AA
   Y(2) = BB
   Y(3) = FPP
   Y(4) = UD
   Y(5) = GP
   GO TO 3
99 CONTINUE
   Y(1)=AA
   Y(2)=BB
   Y(3) = FPP03
   Y(4) = UD
   Y(5) = GP03
   CALL NUMIN(N,DELT,T,DV,P,TE,ER,YPR,Y,EPS,DPSAVE,KEY,DERIV,1)
   I = 0.
   N = 5.
   I = 1
   ULST1 = (Y(4)-A1*(Y(2)**2))/A2 - Y(2)
   THTA1 = (Y(2))*(1.0-Y(2))
   THTE1 = (Y(2))*(1.0-(Y(2)**2))
   I11 = 1
   F(I11) = Y(2)
   G(I11) = Y(4)
   ETAD(I11) = T
   CALL NUMIN(N,DELT,T,DV,P,TE,ER,YPR,Y,EPS,DPSAVE,KEY,DERIV,2)
   ULST2 = (Y(4)-A1*(Y(2)**2))/A2 - Y(2)
   THTA2 = (Y(2))*(1.0-Y(2))
   THTE2 = (Y(2))*(1.0-(Y(2)**2))
   ADELST = (0.5*ULST1 + ULST2)*DELT
   ATHETA = (0.5*THTA1 + THTA2)*DELT
   ATHETE = (0.5*THTE1 + THTE2)*DELT
55 CALL NUMIN(N,DELT,T,DV,P,TE,ER,YPR,Y,EPS,DPSAVE,KEY,DERIV,3)
   DDELST = ((Y(4)-A1*(Y(2)**2))/A2 - Y(2))*DELT
   DTHETA = ((Y(2))*(1.0-Y(2)))*DELT
   DTHETE = ((Y(2))*(1.0-(Y(2)**2)))*DELT
   ADELST = ADELST + DDELST
   ATHE1A = ATHETA + DTHETA

```



```

    ATHETE = ATHETE + DTHETE
    I11 = I11 + 1
    ETAD(I11) = T
    F(I11) = Y(2)
    G(I11) = Y(4)
    IF (ABS(Y(3)).LT.E) GO TO 990
    I = I + 1
    GO TO 55
990 CONTINUE
    N1 = I11
    AA1 = A1
    DUM = 0.0
C    CROSS STREAM STATION TRANSFORM WITH -IN- NO. OF STATIONS
    DO 751 I = 1,N1
    YN(I) = DUM
    IF(ALF)92,92,91
92 IF(F(I)-.99)91,90,90
90 ALF=3.0/ETAD(I)
91 CONTINUE
    DUM = DUM + .05
751 CONTINUE
    J = 1
    DO 752 I = 1,IN
    ETA(I) = ALOG(1.0/(1.0-YN(I)))/ALF
    DO 753 JJ = 1,N1
    IF(ETA(I)-ETAD(J)) 760,761,762
762 CONTINUE
    J = J+1
    GO TO 752
761 CONTINUE
    GN(I) = G(J)
    FN(I) = F(J)
    GO TO 752
760 J = J-1
    IF(ETA(I)-ETAD(J))770,761,772
770 PRINT 780
780 FORMAT (2X* FUNNY *)
    GO TO 799
772 CONTINUE
    AF = (ETA(I)-ETAD(J))/(ETAD(J+1)-ETAD(J))
    FN(I) = AF*(F(J+1)-F(J)) + F(J)
    GN(I) = AF*(G(J+1)-G(J)) + G(J)
753 CONTINUE
752 CONTINUE
    DO 781 I = 1,IN
    THTTA(I) = GN(I)-AA1*FN(I)*FN(I)
781 CONTINUE
    FN(IN + 1) = 1.0
    GN(IN + 1) = 1.0
    THTTA(IN + 1) = 1.0 - AA1
799 CONTINUE
    CALL EJOYCE(FN,THTTA,ALF)
999 CONTINUE
    RETURN
    END

```

SUBROUTINE DERIV(T,Y,DY,LOC,N)

```

    DIMENSION Y(5),DY(5)
    DOUBLE PRECISION X,X1,X2
    COMMON/CONST/A1,A2,A3,A4,E
    A=((Y(4)-(A1*Y(2)**2))/A2)
    X1=(X**(-0.25))
    X2=(-0.25)*(X**(-1.25))*((Y(5)/A2)-2.*(A1/A2)*Y(2)*Y(3))

```

```

720 CONTINUE
C-----
C----- DOUBLE PRECISION ADAMS MOULTON PECEC
      DO 730 J=1,N
730  DV(J) = DEP(J) + DELT*(R(4)*P(J)+TE(J))
      CALL DERTV(1,DV,N,2,N)
731 CONTINUE
      DO 740 J=1,N
      YPR(J,M4) = P(J)
      DEP(J) = DEP(J) + DELT*(R(4)*P(J)+TE(J))
      DV(J) = DEP(J)
C----- SINGLE STEP ERROR ESTIMATE
740 ER(J) = RATIO*ABS(ER(J)-DV(J))
741 CONTINUE
      DO 10 5000
      END

```

```

SUBROUTINE EJOYCE(FN,THETA,ALF)
  DIMENSION FN(50),THETA(50)
  DIMENSION PE(50),ROVIN(50),THETAW(50),RAD(50),PRG(50),EMACH(50),
  JTE(50),VISE(50),GHOE(50),THETA_E(50),DE(50),URENOE(50),REXINT(50),
  2S(50),DS(50),BETA(50),X(50),FLCW(50),FINJ(50),EA(50)
  DIMENSION F(50),THETA(50),CS(50),F1(50),THETA1(50),CS1(50),F2(50),
  1DFLCOS(50),DFLCOS1(50),T(50),FF(50),FLC(50),FLC1(50),THETA2(50),
  2CS2(50),FLC2(50),YN(50)
  DIMENSION CP1(50),CPS(50),VISC(50),VISS(50),TCUN1(50),TCONS(50),
  1DIFFC(50),CPH(50),G12(50),G21(50),XS(50),XJ(50),VISM(50),TCUNM(50)
  2,RHOM(50),CKF(50),SCNO(50),PRNO(50)
  DIMENSION ETA(50),DETA(50),Y(50),DELST(50),THMOM(50)
  DIMENSION DSTAR(50),DDSTR(50)
  DIMENSION A(50,3,3),E(50,3,3),C(50,3,3),AH(50,3,3),H(50,3,3),BAH(5
  10,3,3),BAHINV(50,3,3),ADJBAH(50,3,3),AG(50,3,1),G(50,3,1),DAG(50,3
  2,1),D(50,3,1),FW(50,3,1),W(50,3,1)
  DIMENSION TAW(50),QDOTI(50),STNOT(50),SPECHT(50),XTC(50),QDOTM(50)
  DIMENSION TONO(50),DMDT(50)
  DIMENSION PCOFF(50),ROVINR(50),TW(50)
  DIMENSION TEMP(15),VISC(15),TC(15),CP(15),V1(15),V2(15),V3(15),
  1TC1(15),TC2(15),TC3(15),CP1(15),CP2(15),CP3(15)
  DIMENSION X1(50),Y1(50),X4(50),Y4(50),S1(50),DELX(50),P4(50),
  114(50),U4(50)
  COMMON/KONST/TWAIL,RADIUS,PR
  COMMON/WING/PT3,TT3,U3,T3,P3,X30,Y30,X4,Y4,P4,P6,T4,U4,T5E
  COMMON/CASE/NCASE
  IF(NCASE.GT.1) GO TO 1100
  READ 15,PIGYBK
15  FORMAT (E12.5)
  READ 1,MM,N,KK,NOPRNT
1  FORMAT (4I10)
  READ 2,WMI,WMS
2  FORMAT(2E12.5)
  READ 10,TEMP,VISC,TC,CP
10  FORMAT(5F15.5)
1100 CONTINUE
  CALL SPLNTRP(14,TEMP,VISC,V1,V2,V3)
  CALL SPLNTRP(14,TEMP,TC,TC1,TC2,TC3)
  CALL SPLNTRP(14,TEMP,CP,CP1,CP2,CP3)

```

```

C
C  ISENTROPIC FLOW OF A PERFECT GAS TO COMPUTE EDGE PROPERTIES
  RTE=PT3
  ITE=TT3
  DO 11 I=1,5
  X1(I)=X30-X4(I+1)
  Y1(I)=Y30-Y4(I+1)

```

```

      S1(I)=SQRT(X1(I)*X1(I)+Y1(I)*Y1(I))/12.0
11  CONTINUE
      XINT= .1*S1(I)
      X(1)=XINT
      DEL=0.2*S1(I)
      P4(1)=P3
      T4(1)=T3
      U4(1)=U3
      I=1
      L=1
      DO 14 M=1,MM
      IF (PIGYBK.EQ.1.0) GO TO 63
      READ 12,PE(M),TE(M),UE(M),TW(M),RAD(M)
12  FORMAT(5E12.5)
      GO TO 13
63  IF (KK.EQ.0) GO TO 64
      READ 3, RAD(M)
      3  FORMAT(6E12.5)
      GO TO 13
64  RAD(M)=RADIOS
13  CONTINUE
      PE(M)=P4(L)
      TE(M)=T4(L)
      UE(M)=U4(L)
      CALL MOLIER(H,PE(M),2,TE(M),Z,ENT,RHO,G)
      RHOE(M)=RHO
      VISE(M)=SPLENVAL(14,TEMP,VISC,V1,V2,V3,TE(M))
      TW(M)=FWALL
      THETAPE(M) = TE(M)/TTE
      THETAW(M)=TW(M)/TTE
      URENOE(M) = RHOE(M)*UE(M)/VISE(M)
      DELX(M)=DEL
      X(M+1)=X(M)+DELX(M)
      IF (X(M+1).GE.S1(I)) GO TO 61
      GO TO 14
61  IF (L.EQ.9) GO TO 62
      I=I+1
      L=L+2
      DEL=0.2*(S1(I)-S1(I-1))
      X(M+1)=S1(I-1) + 0.5*DEL
      GO TO 14
62  L=11
      I=11
      S1(I)=S1(5)+X(M+1)
      DEL=DELX(1)
14  CONTINUE
      PRINT 9
      9  FORMAT (1H1,2X,*OUTPUT DATA*///)
      DELT = 1.0/(N-1)
      NN = N-1
      MMAX = MM-1
      REXINT(1)=URENOE(1)*XINT
      DO 16 M=2,MM
      REXINT(M)=REXINT(M-1) + (URENOE(M-1)+URENOE(M))*DELX(M)/2.0
16  CONTINUE
      PRINT 17
17  FORMAT (2X,*M*,6X,*PE(M)*,4X,*THETAPE(M)*,6X,*UE(M)*,
      14X,*URENOE(M)*,3X,*REXINT(M)*/)
      DO 19 M=1,MM
      PRINT 18,M,PE(M),THETAPE(M),UE(M),URENOE(M),REXINT(M)

```

```

18 FORMAT (115,5E12.5)
19 CONTINUE

```

C
C
C

EVALUATION OF S

```

S(1) = RHUE(1)*VISE(1)*UE(1)*((RAD(1)**KK)**2.)*AINT/(3.0**KK)
DO 30 M=2,MMAX
S(M) = S(M-1) + (RHUE(M)*VISE(M)*UE(M)*((RAD(M)**KK)**2.))
+ RHUE(M+1)*VISE(M+1)*UE(M+1)*((RAD(M+1)**KK)**2.))*DELX(M)/2.0
30 CONTINUE
S(MM)=S(MMAX) + (RHUE(MMAX)*VISE(MMAX)*UE(MMAX)*((RAD(MMAX)**K)
**2) + RHUE(MM)*VISE(MM)*UE(MM)*((RAD(MM)**KK)**2.))*DELX(MM)/2.0
US(1) = S(2)-S(1)
BETA(1) = (2.0*(S(2) + S(1))/(UE(2) + UE(1)))*((UE(2)-UE(1))/(S(2)
1-S(1)))
DO 41 M = 2,MMAX
US(M) = (S(M+1)-S(M-1))/2.0
BETA(M) = (2.0*S(M)*(UE(M+1)-UE(M-1)))/(UE(M)*(S(M+1)-S(M-1)))
41 CONTINUE

```

C

```

PRINT 43
43 FORMAT (/2X,*,6X,*,X(M)*,8X,*,S(M)*,7X,*,US(M)*,6X,*,BETA(M)*,5X,
1*FLOW(M)*/)
DO 45 M=1,MMAX
PRINT 44,M,X(M),S(M),US(M),BETA(M),FLOW(M)
44 FORMAT (115,5E12.5)
45 CONTINUE
PRINT 451,P1E,TTF,ALF
451 FORMAT (///10X,*,E12.5,10X,*,TTF=*,E12.5,10X,*,ALF=*,E12.5//)
M = 1
DO 33 I = 1,N
YN(I) = 0.0 + (1-1)*DELT
IF (PIGYRGEQ.0.0) GO TO 35
F(1) = FN(I)
THETA(I) = INTIA(I)
CS(I) = 1.0
GO TO 36
35 CONTINUE
READ 22,F(1),THETA(1),CS(1)
32 FORMAT (3E12.5)
36 CONTINUE
F1(I) = F(I)
THETA1(I) = THETA(I)
CS1(I) = CS(I)
33 CONTINUE
F2(1) = F1(1)
F2(2) = F1(2)
DO 34 I = 1,N
DFLCDS(I) = 0.0
DFLCS1(I) = DFLCDS(I)
1(I) = TTE*THETA(1)
34 CONTINUE
DO 51 I = 1,NN
FF(I) = F(I)/(ALF*(1.0-(I-1)*DELT))
50 CONTINUE

```

C
C

EVALUATION OF THE STREAM FUNCTION,FLC1

```

FLC(1)=FLCW(M)
FLC(2) = FLC(1) + (F(1)/ALF + F(2)/(ALF*(1.0-DELT)))*DELT/2.0
DO 51 I = 3,NN,2
FLC(I) = FLC(I-2) + (FF(I-2) + 4.0*FF(I-1) + FF(I))*DELT/3.0
IF ((I+1).GT.NN) GO TO 51

```

```

51 FLC(I+1) = FLC(I-1) + (FF(I-1) + 4.0*FF(I) + FF(I+1))*DELT/3.0
   CONTINUE
   DO 52 I = 1,N
      FLC1(I) = FLC(I)
52 CONTINUE
   PRINT 53
53 FORMAT (1H1,2X,*I*,6X,*F(I)*,6X,*THETA(I)*,6X,*CS(I)*/)
   DO 55 I=1,N
      PRINT 54,I,F(I),THETA(I),CS(I)
54 FORMAT (1I5,3F12.5)
55 CONTINUE
   I = 1
   CPS(1)=SPLNVAL(14,TEMP,CP,CP1,CP2,CP3,T(I))
   ICONS(1)=SPLNVAL(14,TEMP,TC,TC1,TC2,TC3,I(I))
   VISS(1)=SPLNVAL(14,TEMP,VISC,V1,V2,V3,T(I))
   CPI(1)=CPS(1)
   TCONI(1)=TCONS(1)
   VISI(1)=VISS(1)
   CALL MOLIER(H,PE(M),2,I(1),Z,ENT,DHO,G)
   RHOM(1)=RHO
   CPM(1) = CPI(1) + CS(1)*(CPS(1)-CPI(1))
   IF (CS(1)-1.0) 550,551,551
550 AS(1) = (CS(1) * WMI)/(WMS + CS(1)*(WMI - WMS))
   XI(1) = 1.0 - XS(1)
   IF (XI(1).EQ.0.0) GO TO 551
   G12(1) = ((1.0 + ((VISS(1)/VISI(1))**0.5)*((WMI/WMS)**0.25))**2.)/
1(2.8284*((1.0 + WMS/WMI)**0.5))
   G21(1) = ((1.0 + ((VISI(1)/VISS(1))**0.5)*((WMS/WMI)**0.25))**2.)/
1(2.8284*((1.0 + WMI/WMS)**0.5))
   VISM(1) = VISS(1)/(1.0 + G12(1)*XI(1)/XS(1)) + VISI(1)/(1.0 + G21(
1)*XS(1)/XI(1))
   TCONM(1) = TCONS(1)/(1.0 + 1.065*G12(1)*XI(1)/XS(1)) + TCONI(1)/
1(1.0 + 1.065*G21(1)*XS(1)/XI(1))
   GO TO 552
551 VISM(1) = VISS(1)
   TCONM(1) = TCONS(1)
552 CONTINUE
   TAU = RHOM(1)*VISM(1)*UE(M)*UE(M)*(RAD(M)**KK)*ALF*(F(2)-F(1))/
1(DELT*((2.0*S(M))**0.5))
   CF = TAU/(0.5*RHOE(M)*UE(M)*UE(M))
   HEAT = - TCONM(1)*ITE*UE(M)*RHOM(1)*(RAD(M)**KK)*ALF*(THEIA(2)-
1THETA(1))/(DELT*((2.0*S(M))**0.5))
   QDOT = -HEAT
   I = N
   CPS(I)=SPLNVAL(14,TEMP,CP,CP1,CP2,CP3,T(I))
   ICONS(I)=SPLNVAL(14,TEMP,TC,TC1,TC2,TC3,I(I))
   VISS(I)=SPLNVAL(14,TEMP,VISC,V1,V2,V3,T(I))
   TCONM(I) = TCONS(I)
   VISM(I) = VISS(I)
   CPM(I) = CPS(I)
   PRNO(I) = VISM(I)*CPM(I)/TCONM(I)
   REC = SQRT(PRNO(I))
   TREC = REC*(ITE-TE(M)) + TE(M)
   STNO = QDOT/(RHOE(M)*UE(M)*CPM(N)*(TREC-THETA(M)*ITE))
   PRINT 556,TAU,CF
556 FORMAT (//9X,*TAU=*,E12.5,10X,*CF=*,E12.5)
   PRINT 557 , TREC,QDOT,STNO
557 FORMAT (//9X,*TREC=*,E12.5,9X,*QDOT=*,E12.5,9X,*STNO=*,E12.5//)
56 CONTINUE
59 CONTINUE
   DO 57 I = 1,N

```

```

CPS(I)=SPLNVAL(14,TEMP,CP,CP1,CP2,CP3,T(I))
ICONS(I)=SPLNVAL(14,TEMP,TC,TC1,TC2,TC3,T(I))
VISS(I)=SPLNVAL(14,TEMP,VISC,V1,V2,V3,T(I))
CPI(I)=CPS(I)
ICONI(I)=ICONS(I)
VISI(I)=VISS(I)
C-----EVALUATION OF THE THERMO PROPERTIES OF THE MIXTURE
FI=(WMI/26.0)**.461
FS=(WMS/26.0)**.461
DIFFC(I)=2.640/(10.**8)*(T(I)**1.5)/(PE(M)*FI*FS)
57 CONTINUE
DO 58 I=1,NN
  IF (CS(I)-1.0) 72,71,71
71 CONTINUE
  CPM(I)=CPS(I)
  VISM(I)=VISS(I)
  ICONM(I)=ICONS(I)
  GO TO 73
72 CONTINUE
  CPM(I)=CPI(I)+CS(I)*(CPS(I)-CPI(I))
  G12(I)=((1.0+((VISS(I)/VISI(I))**.5)*((WMI/WMS)**.25))**.2)/
  1(2.8284*((1.0+WMS/WMI)**.5))
  G21(I)=((1.0+((VISI(I)/VISS(I))**.5)*((WMS/WMI)**.25))**.2)/
  1(2.8284*((1.0+WMI/WMS)**.5))
  XS(I)=(CS(I)*W(I)/(WMS+CS(I)*(WMI-WMS))
  XI(I)=1.-XS(I)
  IF (XI(I).EQ.0.0) GO TO 71
  VISM(I)=VISM(I)/(1.0+G12(I)*XI(I)/XS(I)) +
  1VISI(I)/(1.0+G21(I)*(XS(I)/XI(I)))
  ICONM(I)=ICONS(I)/(1.0+1.065*G12(I)*(XI(I)/XS(I)))
  1 + ICONI(I)/(1.0+1.065*G21(I)*(XS(I)/XI(I)))
73 CONTINUE
  CALL MOLIER(H,PE(M),2,T(I),Z,ENT,RHO,G)
  RHOM(I)=RHO
58 CONTINUE
C-----COMPUTATION OF FLOW PROPERTIES AT THE D. L. EDGE
I=0
  ICONM(I)=ICONS(I)
  VISM(I)=VISS(I)
  CPM(I)=CPS(I)
  CALL MOLIER(H,PE(M),2,T(I),Z,ENT,RHO,G)
  RHOM(I)=RHO
  ROMUE=RHOE(M)*VISE(M)
  DO 60 I=1,NN
    CRF(I)=RHOM(I)*VISM(I)/ROMUE
    SCNO(I)=VISM(I)/(RHOM(I)*DIFFC(I))
    PRNO(I)=VISM(I)*CPM(I)/ICONM(I)
60 CONTINUE
C COMPUTATION OF THE MATRIX ELEMENTS
DO 99 I=2,NN
  ALFT=ALF*(1.0-(I-1)*DELT)
  A(I,1,1)=-(CRF(I)*(ALFT**2.)/(2.0*(DELT**2.))+(ALFT/(4.0*DELT))
  1*(ALF*CRF(I)-FLC(I)-ALFT*(CRF(I+1)-CRF(I-1)))/(2.0*DELT)-2.0*S(M)*
  2DFLCDS(I))
  A(I,1,2)=0.0
  A(I,1,3)=0.0
  A(I,2,1)=CRF(I)*(UE(M)**2.)*(ALFT**2.)*(F(I+1)-F(I-1))/(CPM(I)*T
  1E*4.0*(DELT**2.))*777.9)
  A(I,2,2)=-(CRF(I)*(ALFT**2.)/(2.0*(DELT**2.))*PRNO(I)+
  1(ALFT/(4.0*DELT))*(ALF*CRF(I)/PRNO(I)-(ALFT/CPM(I))*
  2((CRF(I+1)*CPM(I+1)/PRNO(I+1)-CRF(I-1)*CPM(I-1)/PRNO(I-1))/(2.0
  3*DELT))-F(I)-2.0*S(M)*DFLCDS(I)-CRF(I)*(CPS(I)-CPI(I))*ALFT*(CS(

```

```

41+1)-CS(I-1))/(CPM(I)*SCNO(I)*2.0*DELT)))
A(I,2,3)=(ALFT**2.)*CRF(I)*(CPS(I)-CPI(I))*(THETA(I+1)-THETA(I-1))
1/(CPM(I)*SCNO(I)*(8.0)*(DELT**2.))
A(I,3,1)=0.0
A(I,3,2)=0.0
A(I,3,3)=-((ALFT**2.)*CRF(I)/(2.0*(DELT**2.)*SCNO(I))
1*(ALFT/(4.0*DELT))*(ALF*CRF(I)/SCNO(I)-FLC(I)-2.0*S(M)*DFLCDS(I)
2-ALFT*(CRF(I+1)/SCNO(I+1)-CRF(I-1)/SCNO(I-1))/(2.0*DELT)))
B(I,1,1)=(ALFT**2.)*CRF(I)/(DELT**2.)+BETA(M)*F(I)+2.0*S(M)*F(I)/DS(M)
1S(M)
B(I,1,2)=0.0
B(I,1,3)=0.0
B(I,2,1)=BETA(M)*(UE(M)**2.)*RHOE(M)/(CPM(I)*11E*RHOH(M)/77.9)
B(I,2,2)=(ALFT**2.)*CRF(I)/(PRNO(I)*(DELT**2.))+2.0*S(M)*F(I)/DS(M)
1)
B(I,2,3)=0.0
B(I,3,1)=0.0
B(I,3,2)=0.0
B(I,3,3)=(ALFT**2.)*CRF(I)/(SCNO(I)*(DELT**2.))+2.0*S(M)*F(I)/DS(M)
1)
C(I,1,1)=-A(I,1,1)-(ALFT**2.)*CRF(I)/(DELT**2.)
C(I,1,2)=0.0
C(I,1,3)=0.0
C(I,2,1)=-A(I,2,1)
C(I,2,2)=-A(I,2,2)-(ALFT**2.)*CRF(I)/(PRNO(I)*(DELT**2.))
C(I,2,3)=-A(I,2,3)
C(I,3,1)=0.0
C(I,3,2)=0.0
C(I,3,3)=-A(I,3,3)-(ALFT**2.)*CRF(I)/(SCNO(I)*(DELT**2.))
D(I,1,1)=(ALFT**2.)*CRF(I)*(F(I+1)-2.*F(I)+F(I-1))/
1(2.0*(DELT**2.))+ALFT*(F(I+1)-F(I-1))/(4.0*DELT))*(FLC(I)+
2ALFT*(CRF(I+1)-CRF(I-1))/(2.0*DELT)-ALF*CRF(I)+2.0*S(M)*DFLCDS(I))
3+BETA(M)*RHOE(M)/RHOH(M)+2.0*S(M)*(F(I)**2.)/DS(M)
D(I,2,1)=(ALFT**2.)*CRF(I)*(THETA(I+1)-2.0*THETA(I)+THETA(I-1))/
1(2.0*(DELT**2.)*PRNO(I))+ALFT*(THETA(I+1)-THETA(I-1))/(4.0*DELT))
2*(2.0*S(M)*DFLCDS(I)+FLC(I)-ALF*CRF(I)/PRNO(I)+ALFT*((CRF(I+1)*CPM
3(I+1)/PRNO(I+1)-CRF(I-1)*CPM(I-1)/PRNO(I-1))/(2.0*DELT))/CPM(I))
4+2.0*S(M)*F(I)*THETA(I)/DS(M)
D(I,3,1)=(ALFT**2.)*CRF(I)*(CS(I+1)-2.0*CS(I)+CS(I-1))/
1(2.0*(DELT**2.)*SCNO(I))+ALFT*(CS(I+1)-CS(I-1))/(4.0*DELT))*
2(FLC(I)+2.0*S(M)*DFLCDS(I)-ALF*CRF(I)/SCNO(I)+ALFT*(CRF(I+1)/
3SCNO(I+1)-CRF(I-1)/SCNO(I-1))/(2.0*DELT))+2.0*S(M)*F(I)*CS(I)/DS(M)
4)

```

99 CONTINUE

```

ENS = (ROVIN(M)*SCNO(I)*((2.0*S(M))**0.5)/(ALF*RHOH(M)*VISM(M)*
1UE(M)*(RAD(M)**KK)))*(DELT + .5*DELT*DELT*(1. - (SCNO(I)/CRF(I))*
2(CRF(2)/SCNO(2)-CRF(1)/SCNO(1))/DELT + ROVIN(M)*((2.0*S(M))**0.5)*
3SCNO(I)/(ALF*RHOH(M)*VISM(M)*UE(M)*(RAD(M)**KK)))

```

C
C
C

EVALUATION OF THE COEFFICIENTS

```

H(1,1,1)=0.0
H(1,1,2)=0.0
H(1,1,3)=0.0
H(1,2,1)=0.0
H(1,2,2)=0.0
H(1,2,3)=0.0
H(1,3,1)=0.0
H(1,3,2)=0.0
H(1,3,3)=-1.0/(1.0+ENS)
G(1,1,1)=0.0
G(1,2,1)=THETA(M)

```

```

      G(1,3,1)=0.0
      DO 124      I = 2,NN
      DO 111 J=1,3
      DO 111 K=1,3
      AH(I,J,K)=0.
      DO 111 L=1,3
      AH(I,J,K)=AH(I,J,K)+A(I,J,L)*H(I-1,L,K)
111  CONTINUE
      DO 112 J=1,3
      DO 112 K=1,3
      BAH(I,J,K)=B(I,J,K)-AH(I,J,K)
112  CONTINUE
      ADJBAH(I,1,1)=BAH(I,2,2)*BAH(I,3,3)-BAH(I,3,2)*BAH(I,2,3)
      ADJBAH(I,2,1)=-BAH(I,2,1)*BAH(I,3,3)+BAH(I,2,3)*BAH(I,3,1)
      ADJBAH(I,3,1)=BAH(I,2,1)*BAH(I,3,2)-BAH(I,2,2)*BAH(I,3,1)
      ADJBAH(I,1,2)=-BAH(I,1,2)*BAH(I,3,3)+BAH(I,1,3)*BAH(I,3,2)
      ADJBAH(I,2,2)=BAH(I,1,1)*BAH(I,3,3)-BAH(I,1,3)*BAH(I,3,1)
      ADJBAH(I,3,2)=-BAH(I,1,1)*BAH(I,3,2)+BAH(I,1,2)*BAH(I,3,1)
      ADJBAH(I,1,3)=BAH(I,1,2)*BAH(I,2,3)-BAH(I,1,3)*BAH(I,2,2)
      ADJBAH(I,2,3)=-BAH(I,1,1)*BAH(I,2,3)+BAH(I,1,3)*BAH(I,2,1)
      ADJBAH(I,3,3)=BAH(I,1,1)*BAH(I,2,2)-BAH(I,2,1)*BAH(I,1,2)
      DETBAH=BAH(I,1,1)*BAH(I,2,2)*BAH(I,3,3)+BAH(I,1,2)*BAH(I,2,3)*BAH(I,3,1)
      +BAH(I,1,3)*BAH(I,3,2)*BAH(I,2,1)-BAH(I,1,3)*BAH(I,3,1)*BAH(I,2,2)
      -BAH(I,2,3)*BAH(I,3,2)*BAH(I,1,1)-BAH(I,1,2)*BAH(I,2,1)*BAH(I,3,3)
      DO 113 J=1,3
      DO 113 K=1,3
      BAHINV(I,J,K)=ADJBAH(I,J,K)/DETBAH
113  CONTINUE
      DO 114 J=1,3
      DO 114 K=1,3
      H(I,J,K)=0.
      DO 114 L=1,3
      H(I,J,K)=H(I,J,K)+BAHINV(I,J,L)*C(I,L,K)
114  CONTINUE
      DO 121 J=1,3
      AG(I,J,1)=0.
      DO 121 L=1,3
      AG(I,J,1)=AG(I,J,1)+A(I,J,L)*G(I-1,L,1)
121  CONTINUE
      DO 122 J=1,3
      DAG(I,J,1)=D(I,J,1)-AG(I,J,1)
122  CONTINUE
      DO 123 J=1,3
      G(I,J,1) = 0.0
      DO 123 L=1,3
      G(I,J,1) = G(I,J,1) + BAHINV(I,J,L)*DAG(I,L,1)
123  CONTINUE
124  CONTINUE
C  SOLUTION FOR THE W VECTOR
      W(N,1,1) = 1.0
      W(N,2,1) = THETA(N)
      W(N,3,1) = 1.0
      F(N) = W(N,1,1)
      THETA(N) = W(N,2,1)
      CS(N) = W(N,3,1)
      DO 134 II=1,NN
      I = N - II
      DO 132 J=1,3
      HW(I,J,1) = 0.
      DO 132 L=1,3
      HW(I,J,1) = HW(I,J,1) + H(I,J,L)*W(I+1,L,1)

```



```

132 CONTINUE
DO 133 J=1,3
W(I,J,1) = U(I,J,1) - HW(I,J,1)
133 CONTINUE
F(1) = W(1,1,1)
THETA(1) = A(I,2,1)
CS(1) = W(1,3,1)
134 CONTINUE
CONVG = (F(2)-F(1)-F2(2)+F2(1))/(F(2)-F(1))
IF (NOPRNT.GT.0) GO TO 98
PRINT 998,CONVG
998 FORMAT (10X,*CONVG=*,E12.5)
98 CONTINUE
IF (ABS((F(2)-F(1)-F2(2)+F2(1))/(F(2)-F(1))).LE.0.0005) GO TO 150
DO 136 I = 1,N
F2(I) = F(I)
THETA2(1)=THETA(I)
CS2(1) = CS(I)
136 CONTINUE
DO 137 I = 1,N
F(I) = 0.5*(F2(I)+F1(I))
THETA(I) = .5*(THETA2(1) + THETA1(I))
I(I) = ITE*THETA(I)
CS(I) = 0.5*(CS2(1) + CS1(I))
137 CONTINUE
C
C EVALUATION OF THE STREAM FUNCTION, FCL2
C
DO 140 I = 1,NN
FF(I) = F(I)/(ALF*(1.0-(I-1)*DELT))
140 CONTINUE
FLC(1) = 0.5*(FLCW(M) + FLCW(M+1))
FLC(2) = FLC(1) + (F(1)/ALF + F(2)/(ALF*(1.0-DELT)))*DELT/2.0
DO 141 I = 3,NN,2
FLC(I) = FLC(I-2) + (FF(I-2) + 4.0*FF(I-1) + FF(I))*DELT/3.0
IF ((I-1).GT.NN) GO TO 141
FLC(I+1) = FLC(I-1) + (FF(I-1) + 4.0*FF(I) + FF(I+1))*DELT/3.0
141 CONTINUE
DO 142 I = 1,NN
FLC2(1) = FLC(1)
DFLCDS(I) = (FLC2(1)-FLC1(I))/DS(M)
142 CONTINUE
IF (NOPRNT.GT.0) GO TO 90
PRINT 999
999 FORMAT (5X,*REJOYCE,SALVATION IS NEAR*)
90 CONTINUE
GO TO 56
150 CONTINUE
M = M+1
DO 160 I=1,NN
ETA(I) = ALUG(1.0/(1.0 - YN(I)))/ALF
I(I) = THETA(I)*ITE
CALL MOLIER(H,PE(M),2,I(I),Z,ENT,RHO,G)
RHOM(I)=RHO
160 CONTINUE
FACTOR = ((2.0*S(M))**0.5)/(RHOE(M)*UE(M)*((RAD(M))**KK))
Y(1) = 0.0
DO 161 I = 2,NN
DETA(I) = ETA(I) - ETA(I-1)
Y(I) = FACTOR*RHOE(M)*(1.0/RHOM(I-1) + 1.0/RHOM(I))*DETA(I)/2.0 +
1Y(I-1)
161 CONTINUE

```

```

1 = N
DETA(I-1)=DELT/(ALF*(1.0-YN(I-1)))
ETA(I)=ETA(I-1)+DETA(I-1)
Y(I)=RHOE(M)*FACTOR*(1.0/RHOM(I-1)+1.0/RHOM(I))*DETA(I-1)/2.0+Y(I-1)
DELST(1) = 0.0
DELST(2) = FACTOR*((RHOE(M)/RHOM(1)-F(1)) + (RHOE(M)/RHOM(2)-F(2)))/(1.0-DELT))*DELT/(2.0*ALF)
DO 162 I=3,NN,2
DELST(I) = DELST(I-2) + FACTOR*((RHOE(M)/RHOM(I-2)-F(I-2))/(1.0-YN(I-2)) + 4.0*(RHOE(M)/RHOM(I-1)-F(I-1))/(1.0-YN(I-1)) + 2*(RHOE(M)/RHOM(I)-F(I))/(1.0-YN(I)))*DELT/(3.0*ALF)
IF((I+1).GT.NN) GO TO 162
DELST(I+1) = DELST(I-1) + FACTOR*((RHOE(M)/RHOM(I-1)-F(I-1))/(1.0-YN(I-1)) + 4.0*(RHOE(M)/RHOM(I)-F(I))/(1.0-YN(I)) + (RHOE(M)/RHOM(I+1)-F(I+1))/(1.0-YN(I+1)))*DELT/(3.0*ALF)
162 CONTINUE
USTAR(M) = USTAR(M) + DELST(NN)
THMOM(1) = 0.0
THMOM(2) = FACTOR*((F(1)-F(1)*F(1))+(F(2)-F(2)*F(2))/(1.0-DELT))*DELT/(2.0*ALF)
DO 163 I=3,NN,2
THMOM(I) = THMOM(I-2) + FACTOR*((F(I-2)-F(I-2)*F(I-2))/(1.0-YN(I-2)) + 4.0*(F(I-1)-F(I-1)*F(I-1))/(1.0-YN(I-1)) + (F(I)-F(I)*F(I))/(1.0-YN(I)))*DELT/(3.0*ALF)
IF((I+1).GT.NN) GO TO 163
THMOM(I+1) = THMOM(I-1) + FACTOR*((F(I-1)-F(I-1)*F(I-1))/(1.0-YN(I-1)) + 4.0*(F(I)-F(I)*F(I))/(1.0-YN(I)) + (F(I+1)-F(I+1)*F(I+1))/(1.0-YN(I+1)))*DELT/(3.0*ALF)
163 CONTINUE
IF (NOPRINT.GT.0) GO TO 179
PRINT 175,M,X(M)
175 FORMAT (1H1,10X,*,M=*,15,5X,*,X(M)=*,F10.5/)
PRINT 176
176 FORMAT (7X,*,1*,2*,*Y(I)*,2X,*Y(I)*,3X,*ETA(I)*,5X,*F(I)*,6X,*THETA(I)*,5X,*CS(I)*,
DO 180 I=1,N
PRINT 177,I,YN(I),Y(I),ETA(I),F(I),THETA(I),CS(I)
177 FORMAT (5X,115,F5.3,2F8.5,3E12.5)
180 CONTINUE
179 CONTINUE
CALL MOLIER(M,PE/M),2,1(1),Z,ENT,RHO,G)
RHOM(1)=RHO
CPM(1) = CPI(1) + CS(1)*(CPS(1)-CPI(1))
IF (CS(1)-1.0) 300,301,301
300 XS(1) = (CS(1) * WMI)/(WMS + CS(1)*(WMI - WMS))
XI(1) = 1.0 - XS(1)
IF (XI(1).EQ.0.0) GO TO 301
ICONS(1)=SPLNVAL(14,TEMP,TC,TC1,TC2,TC3,I(1))
VISS(1)=SPLNVAL(14,TEMP,VISC,V1,V2,V3,I(1))
ICONI(1)=ICONS(1)
VISI(1)=VISS(1)
G12(1) = ((1.0 + ((VISS(1)/VISI(1))**0.5)*((WMI/WMS)**0.25))**2.)/1(2.8284*((1.0 + WMS/WMI)**0.5))
G21(1) = ((1.0 + ((VISI(1)/VISS(1))**0.5)*((WMS/WMI)**0.25))**2.)/1(2.8284*((1.0 + WMI/WMS)**0.5))
VISM(1) = VISS(1)/(1.0 + G12(1)*XI(1)/XS(1)) + VISI(1)/(1.0 + G21(1)*XS(1)/XI(1))
ICONM(1) = ICONS(1)/(1.0 + 1.065*G12(1)*XI(1)/XS(1)) + ICONI(1)/(1.0 + 1.065*G21(1)*XS(1)/XI(1))
GO TO 302
301 VISM(1) = VISS(1)

```

```

      ICONM(1) = ICONS(1)
302 CONTINUE
      TAU = RHOM(1)*VISM(1)*UE(M)*UE(M)*(RAD(M)**KK)*ALF*(F(2)-F(1))/
      1(DELTA*((2.0*S(M))**0.5))
      CF = TAU/(0.5*RHOF(M)*UE(M)*UE(M))
      HEAT = - ICONM(1)*ITE*UE(M)*RHOM(1)*(RAD(M)**KK)*ALF*(THETA(2)-
      1THETA(1))/(DELTA*((2.0*S(M))**0.5))
      QDOT = -HEAT
      CPE=SPLNVAL(14,TEMP,CP,CP1,CP2,CP3,TE(M))
      ICONE=SPLNVAL(14,TEMP,IC,IC1,IC2,IC3,TE(M))
      PRNO(N) = VISE(M)*CPE/ICONE
      REC = SQRT(PRNO(N))
      TREC = REC*(ITE-TE(M)) + TE(M)
      STNO = QDOT/(RHOF(M)*UE(M)*CPM(N)*(TREC-THETA(M)*ITE))
      TAW(M)=TREC
      QDOTT(M)=QDOT
      STNOT(M)=STNO
      SPECHI(M)=CPE
      IF (NOPRNT.GT.0) GO TO 309
      PRINT 306,TAU,CF
306 FORMAT(/9X,*TAU=*,E12.5,10X,*CF=*,E12.5)
      PRINT 307 , TREC,QDOT,STNO
307 FORMAT(/9X,*TREC=*,E12.5,9X,*QDOT=*,E12.5,9X,*STNO=*,E12.5//)
      PRINT 308,DELST(MN),THMOM(MN),DSTAR(M)
308 FORMAT(9X,*DELST=*,E12.5,8X,*THMOM=*,E12.5,8X,*DSTAR=*,E12.5//)
309 CONTINUE
      DO 280 I=1,NN
      FF(I) = F(I)/(ALF*(1.0-(I-1)*DELTA))
280 CONTINUE
      FLC(1) = 0.5*(FLCW(M) + FLCW(M+1))
      FLC(2) = FLC(1) + (F(1)/ALF + F(2)/(ALF*(1.0-DELTA)))*DELTA/2.0
      DO 281 I=3,NN,2
      FLC(I) = FLC(I-2) + (FF(I-2) + 4.0*FF(I-1) + FF(I))*DELTA/3.0
      IF ((I+1).GT.NN)GO TO 281
      FLC(I+1) = FLC(I-1) + (FF(I-1) + 4.0*FF(I) + FF(I+1))*DELTA/3.0
281 CONTINUE
      DO 282 I = 1,NN
      DFLEDS(I) = (FLC(I)-FLC1(I))/DS(M)
282 CONTINUE
      DO 290 I=1,NN
      F1(I) = F(I)
      THETA1(I) = THETA(I)
      CS1(I) = CS(I)
      FLC1(I) = FLC(I)
      T1(I) = ITE*THETA(I)
290 CONTINUE
      F2(1)=F1(1)
      F2(2) = F1(2)
      IF (M-MM) 57,900.900
900 CONTINUE
      RETURN
      END

```

SUBROUTINE SPLNTRP(N,X,F,R,Z,T)

```

C*****
C* ACCEPTS AND LEAVES UNALTERED...
C*      N = NUMBER OF POINTS-1 (CURRENTLY DIMENSIONED FOR 30 PTS)
C*      X = INDEPENDENT VARIABLE ARRAY
C*      F = DEPENDENT VARIABLE ARRAY
C*      BOTH X AND F MUST BE DIMENSIONED AS THEY ARE IN THIS ROUTINE*
C* PRODUCES AND RETURNS THE PARAMETERS R,Z,T
C* PARAMETERS OF SPLNTRP CHARACTERIZE THE INTERPOLATING NATURAL SPLINE*
C* FUNCTION S(X)

```

C*****

C
 DIMENSION X(30),F(30),R(31),Z(30),T(30),BB(29),AA(29),GG(29),
 DD(29)

C
 NU=N-1
 DO 1 I=1,NU
 1 R(I)=(F(I+1)-F(I))/(X(I+1)-X(I))
 DO 2 J=1,NU
 DD(J)=6.0*((F(J)-F(J+2))/(X(J)-X(J+2))-R(J))/(X(J+2)-X(J+1))
 DUM=X(J+2)-X(J)
 AA(J)=(X(J+1)-X(J))/DUM
 BR(J)=2.0
 2 GG(J)=(X(J+2)-X(J+1))/DUM
 CALL TRISOLV(I,AA,BB,GG,DD,Z)
 NP=N+1
 Z(NP)=0.0
 Z(1)=0.0
 DO 3 K=1,N
 3 T(K)=(Z(K+1)-Z(K))/(X(K+1)-X(K))*6.0
 R(N+2)=R(1)-T(1)*((X(2)-X(1))**2)
 C R(N+2)=R(-1)
 R(NP)=R(N)+(X(NP)-X(N))*(Z(N)/2.0+T(N)*2.0*(X(NP)-X(N)))
 RETURN
 END

SUBROUTINE TRISOLV(N,ALPHA,BETA,GAMMA,DELTA,Z)

C
 DIMENSION ALPHA(29),BETA(29),DELTA(29),GAMMA(29),Z(30)

C
 NU=N-1
 IF(2.GT.NU) GO TO 3
 DO 1 ID=2,NU
 QDUM=(ALPHA(ID))/(BETA(ID-1))
 BETA(ID)=BETA(ID)-QDUM*GAMMA(ID-1)
 1 DELTA(ID)=DELTA(ID)-QDUM*DELTA(ID-1)
 3 Z(N)=DELTA(NU)/BETA(NU)
 IF(2.GT.NU) GO TO 4
 DO 2 JD=2,NU
 JI = N-JD
 JI1=JI+1
 2 Z(JI1)=(DELTA(JI)-GAMMA(JI)*Z(JI1+1))/BETA(JI)
 4 CONTINUE
 RETURN
 END

FUNCTION SPLNVAL(N,X,F,R,Z,T,ARG)

C*****
 C* RETURNS THE VALUE OF S(ARG)
 C*****

C
 DIMENSION X(30),F(30),R(31),Z(30),T(30)
 C
 MUST FIRST CHECK TO SEE IN WHAT INTERVAL ARG LIES
 NN=N+1
 IF(X(1).LE.ARG) GO TO 4
 SPLNVAL=F(1)+R(N+2)*(ARG-X(1))
 GO TO 99
 4 IF(X(NN).GT.ARG) GO TO 5
 SPLNVAL=F(NN)+R(NN)*(ARG-X(NN))
 GO TO 99
 5 DO 1 I=2,NN
 ICNT=I
 IF(X(1).GT.ARG) GO TO 2

```

1  CONTINUE
2  IVAL = ICNT
   IVAL1=IVAL -1
   VAL=Z(IVAL1)/2.0+T(IVAL1)*(ARG+X(IVAL)-2.0*X(IVAL1))
   VAL=VAL*(ARG-X(IVAL))+K(IVAL1)
   VAL=VAL*(ARG-X(IVAL1))+F(IVAL1)
   SPLNVAL=VAL
99  CONTINUE
   RETURN
   END
----- SUBROUTINE MOLIER(H,P,NOPT,T,Z,S,RHO,GAMMA) -----
C  NOPT=0  LOOK UP PROPS BASED ON P AND H
C  NOPT=1  LOOK UP PROPS BASED ON P AND S
C  NOPT=2  LOOK UP PROPS BASED ON P AND T
C  NOPT=3  LOOK UP PROPS BASED ON H AND S
   DIMENSION  FLP(33,20),HZ(33,20),TT(33,20),ZT(33,20),GAME(33,20),
1  ENTRO(33,20),FLPV(660),HZO(660),TTC(660),ZTO(660),GAMEO(660),
2  ENTROO(660),FLPZ(20),HTBL(33),ENTROV(20,33),FLPV(20,33)
   EQUIVALENCE(FLPV,FLP),(HZO,HZ),(TTC,TT),(ZTO,ZT),(GAMEO,GAME),
1  (ENTROO,ENTRO)
   DATA PO,CPOR,HC,SOR,G,R,ALE,RT0,CP/2116.,3.48158,117.346,23.6,
132.2,53.35,2.302585,33.705.,.23866/
   COMMON/FLAG/ IDEAL,IFP
   COMMON/CHECK/I2
   IDEAL=0
   Z=1.0
   GAMMA=1.4
   IF(I2.EQ.33) GO TO 5
   DO 2 K=1,20
   LL=33*(K-1)
   DO 2 L=1,33
   FLP(LL+L)=FLPZ(K)
   IF(K.EQ.1) GO TO 2
   HZO(LL+L)=HZO(L)
2  CONTINUE
   IZ=33
   JZ=20
   DO 1 I=1,IZ
   HTBL(I)=HZ(1,1)
   DO 1 J=1,JZ
   ENTROV(J,I)=ENTRO(I,JZ-J+1)
1  FLPV(J,I)=FLP(I,IZ-J+1)
5  IF(NOPT.EQ.3) GO TO 40
   PL=ALOG10(P/2116.) + 10.
   IF(NOPT-1) 10,20,30
10  IF(H.LT.100.) GO TO 100
   CALL DINT(H,HZ,Z,ZT,PL,FLPZ,IZ,JZ,T,TT,S,ENTROO,GAMMA,GAME)
   IF(Z-.2222E+30)11,12,12
11  RHO= P/(32.2*53.35*Z*T)
   GO TO 50
100  IF(H.LT.0.) GO TO 12
   I=H/CP
   RHO=P/(G*R*I)
101  S=(CPOR*ALOG10(H/HO)-ALOG10(P/PO))*ALE+SOR
   GO TO 50
12  IFP=1
   IDEAL=1
   GO TO 50
20  IF(PL.LT.FLPZ(1)) GO TO 22
   DO 21 J=2,JZ
   IF(PL-FLPV(J)) 203,202,21
21  CONTINUE

```

```

202 IF(S-ENTRO(2,J)) 205,204,204
203 IF(S-ENTRO(2,J-1)) 205,204,204
204 CALL DINT(S,ENTRO,H,HZ,PL,FLPZ,IZ,JZ,T,IT,Z,ZT,1,GAMMA,GAME)
    IF(H-.222E+30)11,22,22
205 H=RT0*CPOR*EXP((S-SOR+ALE*ALOG10(P/P0))/(CPOR*ALE))
    I=H/CP
    RH0=P/(G*R*I)
    GO TO 50
22 IFP=1
    IDEAL=1
    GO TO 50
30 IF(I.LT.419.) GO TO 301
    CALL DINT(T,IT,H,HZ,PL,FLPV,IZ,JZ,Z,ZT,S,ENTRO,1,GAMMA,GAME)
    IF(H-.222E+30)11,31,31
301 IF(T.LT.0.) GO TO 31
    H=CP*T
    RH0=P/(G*R*I)
    GO TO 101
31 IFP=1
    IDEAL=1
    GO TO 50
40 IF(H.LT.100.) GO TO 401
    CALL DINT1(S,ENTROV,PL,FLPV,H,HTBL,JZ,IZ)
    IF(PL-.222E+30)*1,42,42
41 IF(PL.GT.12.69897) GO TO 44
    P=10.**(PL-10.)*2116.
    GO TO 10
401 IF(H.LT.0.) GO TO 42
    ALP=(SOR-S)/ALE+CPOR*ALOG10(H/RH0)
    P=P0*10.**2LP
    I=H/CP
    RH0=P/(G*R*I)
    GO TO 50
42 IFP=1
49 IDEAL=1
    GO TO 50
44 IDEAL=2
50 RETURN
    DATA (FLPZ(J),J=1,20) /6.30103, 6.69897, 7.0, 7.30103, 7.69897, 8.
10, 8.30103, 8.69897, 9.0, 9.30103, 9.69897, 10.0, 10.30103, 10.698
297, 11.0, 11.30103, 11.69897, 12.0, 12.30103, 12.69897/
    DATA T10(L),L=1,204) / 0., 419., 834., 1616., 2339., 3032., 3478.,
13848., 4025., 4175., 4320., 4468., 4600., 4880., 5148., 5730., 6238., 6565.,
26836., 7005., 7155., 7270., 7380., 7693., 7911., 8100., 8262., 8410., 8568.,
38723., 8900., 9140., 9450., 0., 419., 834., 1616., 2339., 3032., 3517.,
43907., 4130., 4300., 4460., 4600., 4750., 4940., 5260., 5760., 6300., 6705.,
56984., 7195., 7350., 7490., 7596., 7927., 8172., 8374., 8550., 8712., 8878.,
69054., 9250., 9490., 9780., 0., 419., 834., 1616., 2339., 3032., 3546.,
73964., 4224., 4390., 4563., 4708., 4865., 5060., 5346., 5775., 6350., 6795.,
87092., 7305., 7495., 7648., 7772., 8125., 8388., 8595., 8784., 8950., 9135.,
99324., 9520., 9750., 10030., 0., 419., 834., 1616., 2339., 3032., 3571.,
14035., 4295., 4500., 4669., 4830., 4990., 5180., 5450., 5890., 6450., 6870.,
27218., 7450., 7640., 7790., 7920., 8323., 8604., 8827., 9018., 9216., 9405.,
39594., 9780., 10030., 10350., 0., 419., 834., 1616., 2339., 3032., 3586.,
44100., 4410., 4630., 4815., 4985., 5150., 5340., 5594., 5990., 6498., 6995.,
57353., 7620., 7840., 8015., 8172., 8597., 8901., 9150., 9378., 9576., 9765.,
69963., 10180., 10420., 10730., 0., 419., 834., 1616., 2339., 3032., 3596.,
74150., 4485., 4735., 4930., 5100., 5270., 5480., 5724., 6050., 6580., 7050.,
87470., 7760., 8000., 8190., 8334., 8811., 9144., 9410., 9648., 9846.,
910060., 10220., 10500., 10740., 11040., 0., 419., 834., 1616., 2339., 3032./
    DATA T10(L),L=205,400) /3619., 4208., 4555., 4829., 5040., 5240., 5410.,
15610., 5672., 6195., 6650., 7165., 7596., 7908., 8150., 8355., 8532., 9036.,

```

29414.,9657.,9927.,10160.,10380.,10590.,10820.,11100.,11400., 0.,
 3 419., 834.,1616.,2339.,3032.,3630.,4259.,4655.,4960.,5202.,5408.,
 45640.,5840.,6066.,6350.,6790.,7250.,7722.,8095.,8360.,8600.,8725.,
 59378.,9756.,10060.,10350.,10580.,10800.,11040.,11300.,11580.,
 611880., 0., 419., 834.,1616.,2339.,3032.,3640.,4300.,4750.,5060.,
 75323.,5550.,5758.,5990.,6228.,6505.,6900.,7310.,7830.,8215.,8520.,
 88760.,9000.,9630.,10040.,10320.,10660.,10920.,11180.,11420.,
 911680.,11970.,12290.,0., 419., 834.,1616.,2339.,3032.,3654.,4314.,
 14800.,5150.,5445.,5683.,5910.,6150.,6394.,6650.,7045.,7485.,7956.,
 28350.,8680.,8955.,9198.,9864.,10350.,10690.,11000.,11290.,11550.,
 311810.,12100.,12380.,12700.,0.,419., 834.,1616.,2339.,3032.,3654.,
 44328.,4880.,5295.,5598.,5880.,6110.,6355.,6628.,6900.,7250.,7660.,
 58118.,8550.,8910.,9210.,9468.,10230.,10740.,11150.,11480.,11790.,
 612080.,12370.,12450.,12980.,13300.,0.,419.,834.,1616.,2339.,3032.,
 73654.,4416.,4945.,5395.,5724.,6015.,6285.,6540.,6808.,7100.,7450.,
 87810.,8270.,8695.,9085.,9415.,9702.,10510.,11070.,11500.,11870.,
 912200.,12510.,12820.,13110.,13450.,13800., 0., 419., 834.,1616./
 DATA (T10(L),L=4,1,590)/2339.,3032.,3654.,4455.,4980.,5475.,5839.,
 10150.,6450.,6735.,7002.,7300.,7640.,8000.,8433.,8848.,9245.,9600.,
 29900.,10800.,11400.,11880.,12280.,12630.,12970.,13280.,13610.,
 313960.,14310., 0., 419., 834.,1616.,2339.,3032.,3654.,4469.,5010.,
 45548.,5976.,6348.,6655.,6950.,7281.,7575.,7910.,8275.,8658.,9100.,
 57496.,9865.,10180.,11200.,11860.,12420.,12820.,13270.,13600.,
 613960.,14310.,14490.,15080.,0.,419., 834.,1616.,2339.,3032.,3654.,
 74483.,5025.,5580.,6080.,6474.,6830.,7150.,7488.,7800.,8140.,8500.,
 88892.,9300.,9700.,10070.,10400.,11500.,12260.,12840.,13300.,
 913770.,14140.,14500.,14880.,15270.,15660., 0., 419., 834.,1616.,
 12339.,3032.,3654.,4497.,5038.,5675.,6169.,6580.,6975.,7340.,7686.,
 28008.,8350.,8740.,9108.,9525.,9930.,10310.,10683.,11440.,12650.,
 313280.,13810.,14270.,14700.,15100.,15490.,15890.,16290., 0., 419.,
 4 834.,1616.,2339.,3032.,3654.,4505.,5050.,5725.,6260.,6750.,7188.,
 57566.,7950.,8300.,8670.,9050.,9450.,9850.,10260.,10660.,11052.,
 612290.,13120.,13410.,14500.,15010.,15480.,15930.,16350.,16800.,
 717220., 0., 419., 834.,1616.,2339.,3032.,3654.,4515.,5075.,5750.,
 86336.,6848.,7220.,7755.,8154.,8540.,8945.,9310.,9720.,10110.,
 915540.,10920.,11340.,12630.,13630.,14400.,1505 15010.,15110./
 DATA (T10(L),L=5,1,660)/16600.,17070.,17520.,17980.,0.,419.,834.,
 11616.,2339.,3032.,3654.,4425.,5110.,5774.,6386.,6935.,7440.,7905.,
 28352.,8755.,9155.,9570.,9990.,10400.,10846.,11230.,11630.,13010.,
 314090.,14940.,15840.,16240.,16830.,17320.,17800.,18300.,18820.,0.,
 4 419., 834.,1616.,2339.,3032.,3654.,4425.,5110.,5790.,6440.,7030.,
 57580.,8090.,8590.,9040.,9490.,9905.,10370.,10800.,11210.,11640.,
 612060.,13540.,14710.,15680.,16480.,17140.,17770.,18300.,18910.,
 719450.,19980./

DATA (ZT0(L),L=1,249)/0*1.0,1.007,1.024,1.049,1.076,1.103,1.130,
 11.156,1.180,1.201,1.210,1.216,1.226,1.238,1.251,1.265,1.280,1.296,
 21.358,1.422,1.486,1.551,1.617,1.681,1.746,1.810,1.874,1.934,6*1.0,
 31.004,1.020,1.044,1.071,1.098,1.124,1.152,1.176,1.197,1.208,1.214,
 41.224,1.235,1.248,1.260,1.275,1.290,1.352,1.416,1.480,1.545,1.609,
 51.674,1.738,1.802,1.865,1.925,6*1.0,1.003,1.018,1.040,1.067,1.094,
 61.119,1.147,1.171,1.193,1.206,1.213,1.221,1.232,1.244,1.258,1.272,
 71.287,1.348,1.411,1.475,1.539,1.604,1.667,1.732,1.795,1.858,1.918,
 86*1.0,1.001,1.016,1.037,1.060,1.088,1.115,1.140,1.165,1.188,1.204,
 91.212,1.219,1.229,1.241,1.255,1.268,1.283,1.343,1.406,1.470,1.534,
 11.597,1.661,1.725,1.788,1.851,1.909,7*1.0,1.013,1.032,1.056,1.081,
 21.108,1.132,1.156,1.181,1.197,1.208,1.216,1.226,1.237,1.249,1.264,
 31.277,1.337,1.398,1.461,1.526,1.589,1.652,1.715,1.778,1.840,1.899,
 47*1.0,1.012,1.028,1.052,1.076,1.100,1.128,1.152,1.175,1.193,1.205,
 51.214,1.223,1.234,1.246,1.259,1.273,1.332,1.393,1.455,1.518,1.582,
 61.644,1.707,1.770,1.831,1.891,7*1.0,1.011,1.024,1.047,1.070,1.096,
 71.120,1.144,1.160,1.188,1.201,1.211,1.220,1.231,1.242,1.256,1.269,
 81.326,1.387,1.449,1.511,1.574,1.636,1.699,1.761,1.822,1.880,7*1.0,

91.010,1.022,1.042,1.063,1.088,1.112,1.136,1.160,1.183,1.196,1.206/
 DATA (Z10(L),L=240,502)/1.215,1.226,1.237,1.249,1.263,1.318,1.378,
 11.439,1.500,1.563,1.625,1.687,1.748,1.808,1.867,7*1.0,1.009,1.017,
 21.037,1.058,1.080,1.104,1.128,1.152,1.172,1.190,1.201,1.211,1.220,
 31.232,1.244,1.258,1.312,1.372,1.431,1.492,1.554,1.616,1.677,1.738,
 41.798,1.855,7*1.0,1.008,1.015,1.032,1.052,1.076,1.098,1.121,1.144,
 51.164,1.184,1.197,1.207,1.216,1.228,1.240,1.252,1.306,1.304,1.424,
 61.484,1.545,1.606,1.667,1.727,1.787,1.844,7*1.0,1.007,1.012,1.026,
 71.046,1.066,1.088,1.110,1.133,1.154,1.173,1.188,1.200,1.210,1.220,
 81.232,1.245,1.297,1.353,1.412,1.472,1.531,1.592,1.653,1.711,1.770,
 91.826,7*1.0,1.005,1.009,1.022,1.040,1.058,1.080,1.101,1.124,1.144,
 11.164,1.180,1.193,1.204,1.215,1.227,1.238,1.289,1.345,1.403,1.462,
 21.522,1.581,1.640,1.699,1.757,1.812,7*1.0,1.004,1.007,1.018,1.034,
 31.052,1.072,1.092,1.115,1.135,1.154,1.172,1.186,1.197,1.208,1.219,
 41.231,1.281,1.337,1.394,1.452,1.510,1.569,1.627,1.685,1.742,1.798,
 57*1.0,1.003,1.005,1.013,1.027,1.044,1.063,1.081,1.102,1.122,1.140,
 61.159,1.174,1.188,1.199,1.210,1.221,1.270,1.324,1.379,1.437,1.494,
 71.552,1.609,1.666,1.721,1.777,7*1.0,1.002,1.004,1.012,1.023,1.037,
 81.055,1.072,1.092,1.112,1.129,1.148,1.164,1.177,1.189,1.200,1.213,
 91.261,1.314,1.360,1.424,1.480,1.537,1.594,1.650,1.705,1.759,7*1.0/
 DATA (Z10(L),L=543,660)/1.001,1.003,1.008,1.019,1.030,1.040,1.064,
 11.082,1.098,1.117,1.130,1.152,1.165,1.179,1.191,1.203,1.251,1.302,
 21.355,1.410,1.464,1.522,1.577,1.632,1.687,1.739,8*1.0,1.002,1.005,
 31.014,1.024,1.037,1.052,1.069,1.085,1.103,1.119,1.136,1.150,1.164,
 41.176,1.189,1.235,1.285,1.338,1.390,1.445,1.500,1.553,1.607,1.660,
 51.712,8*1.0,1.001,1.003,1.010,1.019,1.030,1.044,1.059,1.075,1.091,
 61.107,1.122,1.136,1.150,1.163,1.175,1.223,1.272,1.322,1.375,1.428,
 71.480,1.534,1.586,1.639,1.692,9*1.0,1.001,1.007,1.015,1.024,1.037,
 81.050,1.064,1.079,1.093,1.108,1.122,1.136,1.148,1.161,1.208,1.256,
 91.300,1.357,1.416,1.460,1.512,1.564,1.615,1.665,10*1.0,1.003,1.010,
 11.019,1.028,1.039,1.050,1.063,1.076,1.090,1.104,1.116,1.128,1.141,
 21.187,1.234,1.282,1.332,1.382,1.431,1.480,1.531,1.581,1.630/
 DATA (GAMEO(L),L=1,212)/2*1.4,1.390,1.344,1.317,1.295,1.206,1.143,
 11.114,1.109,1.103,1.114,1.131,1.169,1.226,1.264,1.238,1.180,1.143,
 21.121,1.110,1.103,1.099,1.094,1.092,1.093,1.094,1.096,1.099,1.104,
 31.111,1.122,1.138,2*1.4,1.390,1.344,1.317,1.295,1.214,1.149,1.119,
 41.113,1.113,1.118,1.131,1.162,1.212,1.262,1.248,1.190,1.152,1.128,
 51.116,1.109,1.105,1.098,1.096,1.097,1.098,1.100,1.102,1.107,1.114,
 61.124,1.138,2*1.4,1.390,1.344,1.317,1.295,1.220,1.154,1.124,1.117,
 71.116,1.121,1.132,1.159,1.203,1.258,1.255,1.198,1.158,1.133,1.121,
 81.114,1.109,1.101,1.099,1.100,1.101,1.103,1.105,1.110,1.116,1.126,
 91.139,2*1.4,1.390,1.344,1.317,1.295,1.227,1.160,1.130,1.121,1.120,
 11.124,1.134,1.156,1.195,1.250,1.261,1.206,1.165,1.140,1.120,1.118,
 21.114,1.105,1.102,1.103,1.104,1.106,1.108,1.112,1.118,1.128,1.140,
 32*1.4,1.390,1.344,1.317,1.295,1.236,1.169,1.138,1.128,1.125,1.129,
 41.137,1.154,1.186,1.237,1.261,1.218,1.174,1.148,1.134,1.125,1.120,
 51.110,1.107,1.107,1.108,1.110,1.112,1.116,1.122,1.130,1.142,2*1.4,
 61.390,1.344,1.317,1.295,1.244,1.176,1.144,1.133,1.130,1.133,1.140,
 71.154,1.181,1.225,1.258,1.227,1.182,1.156,1.140,1.131,1.120,1.114,
 81.111,1.111,1.112,1.113,1.116,1.120,1.125,1.135,1.145,2*1.4,1.390,
 91.344,1.317,1.295,1.250,1.183,1.151,1.138,1.134,1.137,1.143,1.155/
 DATA (GAMEO(L),L=213,276)/1.179,1.218,1.252,1.236,1.191,1.163,
 11.147,1.139,1.131,1.118,1.114,1.114,1.115,1.117,1.120,1.123,1.128,
 21.136,1.147,2*1.4,1.390,1.344,1.317,1.295,1.258,1.193,1.101,1.146,
 31.140,1.142,1.148,1.157,1.177,1.209,1.244,1.244,1.207,1.177,1.159,
 31.148,
 41.139,1.124,1.124,1.119,1.120,1.122,1.124,1.128,1.133,1.141,1.150,
 52*1.4,1.390,1.344,1.317,1.295,1.263,1.201,1.199,1.152,1.146,1.147/
 DATA (GAMEO(L),L=277,424)/1.152,
 61.160,1.177,1.204,1.237,1.245,1.219,1.189,1.169,1.156,1.145,1.128,
 71.124,1.123,1.124,1.126,1.128,1.132,1.137,1.143,1.154,2*1.4,1.390,
 81.344,1.317,1.295,1.267,1.210,1.177,1.159,1.152,1.152,1.156,1.163,

91.178,1.200,1.230,1.242,1.226,1.201,1.179,1.164,1.152,1.134,1.128,
11.127,1.128,1.130,1.132,1.136,1.140,1.147,1.150,2*1.4,1.390,1.344,
21.317,1.295,1.271,1.223,1.188,1.168,1.160,1.159,1.161,1.169,1.180,
31.197,1.221,1.230,1.231,1.214,1.192,1.174,1.162,1.141,1.135,1.133,
41.133,1.136,1.130,1.142,1.146,1.152,1.161,2*1.4,1.390,1.344,1.317,
51.295,1.273,1.232,1.190,1.175,1.167,1.164,1.160,1.173,1.182,1.196,
61.217,1.231,1.232,1.222,1.202,1.183,1.170,1.147,1.146,1.138,1.138,
71.140,1.142,1.146,1.150,1.156,1.164,2*1.4,1.390,1.344,1.317,1.295,
81.274,1.238,1.200,1.183,1.172,1.170,1.171,1.178,1.186,1.197,1.214,
91.228,1.232,1.220,1.210,1.192,1.179,1.153,1.145,1.143,1.143,1.145/
DATA (GAMEU(L),L=425,630)/1.147,1.15,1.154,1.160,1.168,2*1.4,1.390,
11.344,1.317,1.295,1.275,1.244,1.218,1.195,1.182,1.178,1.178,1.183,
21.190,1.200,1.213,1.225,1.231,1.228,1.218,1.204,1.191,1.162,1.153,
31.150,1.150,1.150,1.153,1.156,1.160,1.160,1.173,2*1.4,1.390,1.344,
41.317,1.295,1.275,1.247,1.226,1.204,1.189,1.184,1.184,1.188,1.194,
51.202,1.213,1.224,1.230,1.230,1.224,1.212,1.200,1.169,1.159,1.155,
61.155,1.156,1.154,1.161,1.165,1.171,1.177,2*1.4,1.390,1.344,1.317,
71.295,1.275,1.250,1.232,1.211,1.196,1.190,1.190,1.192,1.198,1.205,
81.214,1.224,1.23,1.231,1.227,1.219,1.208,1.176,1.165,1.161,1.160,
91.161,1.163,1.166,1.169,1.175,1.182,2*1.4,1.390,1.344,1.317,1.295,
11.276,1.253,1.237,1.219,1.205,1.199,1.198,1.199,1.204,1.210,1.216,
21.224,1.230,1.232,1.231,1.226,1.216,1.186,1.174,1.169,1.167,1.168,
31.170,1.173,1.177,1.181,1.187,2*1.4,1.390,1.344,1.317,1.295,1.276,
41.254,1.240,1.223,1.212,1.205,1.203,1.204,1.208,1.214,1.220,1.225,
51.230,1.233,1.232,1.228,1.221,1.194,1.181,1.170,1.173,1.174,1.176,
61.179,1.182,1.186,1.192,2*1.4,1.390,1.344,1.317,1.295,1.270,1.255,
71.241,1.226,1.217,1.211,1.208,1.209,1.212,1.218,1.223,1.226,1.229,
81.233,1.232,1.220,1.224,1.203,1.188,1.182,1.179,1.180,1.182,1.184,
91.187,1.191,1.196,2*1.4,1.390,1.344,1.317,1.295,1.276,1.255,1.242/
DATA (GAMEU(L),L=637,660)/1.228,1.223,1.22,1.214,1.218,1.219,1.223,
11.228,1.228,1.23,1.233,1.233,1.229,1.227,1.214,1.198,1.191,1.187,
21.188,1.189,1.192,1.195,1.198,1.202/
DATA (ENTROU(L),I=1,204)/ 23.08,31.56,33.97,36.43,37.92,39.01,
139.88,40.87,41.78,42.65,43.50,44.33,45.16,45.94,46.67,47.33,47.94,
248.50,49.04,49.58,50.10,50.59,51.08,53.05,54.88,56.70,58.46,60.16,
361.93,63.61,65.22,66.85,68.40,72.76,30.64,33.05,35.51,37.00,38.09,
438.96,39.93,40.84,41.70,42.54,43.32,44.08,44.84,45.56,46.22,46.81,
547.39,48.01,48.41,48.95,49.43,49.93,51.84,53.58,55.32,57.08,58.72,
600.36,62.00,63.50,65.10,66.66,72.07,29.95,32.36,34.82,36.31,37.40,
738.25,39.21,40.11,40.99,41.79,42.57,43.30,44.01,44.75,45.40,45.99,
846.53,47.16,47.56,48.02,48.51,49.02,50.85,52.61,54.37,55.99,57.64,
959.24,60.80,62.33,63.84,65.34,71.37,29.26,31.66,34.12,35.61,36.70,
137.50,38.50,39.40,40.24,41.01,41.75,42.52,43.22,43.92,44.56,45.15,
245.70,46.20,46.70,47.17,47.65,48.12,49.94,51.65,53.31,54.96,56.52,
358.06,59.61,61.10,62.57,63.99,70.46,28.34,30.75,33.21,34.70,35.79,
436.63,37.57,38.43,39.23,40.01,40.77,41.45,42.14,42.82,43.44,44.02,
544.57,45.09,45.55,46.03,46.49,46.93,48.73,50.35,51.98,53.54,55.06,
656.56,58.04,59.46,60.86,62.28,77.19,27.65,30.06,32.52,34.01,35.10,
735.96,36.89,37.72,38.53,39.27,40.00,40.72,41.36,42.00,42.62,43.20,
843.74,44.23,44.70,45.18,45.63,46.04,47.77,49.38,50.94,52.49,53.97,
955.42,56.87,58.23,59.60,60.98,79.07,26.96,29.36,31.82,33.31,34.40/
DATA (ENTROU(L),I=205,408)/ 35.27,36.17,37.01,37.80,38.51,39.22,
139.90,40.57,41.17,41.80,42.37,42.90,43.39,43.86,44.32,44.76,45.17,
246.80,48.42,49.93,51.40,52.87,54.31,55.66,57.00,58.36,59.68,61.16,
326.04,28.45,30.91,32.40,33.49,34.35,35.25,36.08,36.85,37.56,38.25,
438.88,39.53,40.12,40.64,41.25,41.80,42.30,42.74,43.16,43.61,44.00,
545.61,47.11,48.62,50.00,51.40,52.80,54.13,55.40,56.68,57.90,59.17,46,
625.34,27.75,30.21,31.70,32.79,33.64,34.55,35.38,36.12,36.81,37.50,
738.13,38.75,39.33,39.90,40.43,40.95,41.42,41.89,42.32,42.72,43.13,
844.70,46.19,47.62,49.00,50.33,51.64,52.97,54.24,55.42,56.60,57.77,
924.65,27.06,29.52,31.01,32.10,32.96,33.88,34.66,35.40,36.08,36.72,
137.37,37.97,38.54,39.11,39.63,40.12,40.60,41.02,41.48,41.88,42.27,

243.79,45.25,46.64,47.96,49.28,50.52,51.80,53.00,54.20,55.32,15.85,
 323.74,26.14,28.60,30.09,31.18,32.03,32.97,33.75,34.45,35.11,35.76,
 436.35,36.93,37.48,38.04,38.54,39.02,39.48,39.94,40.35,40.75,41.13,
 542.60,43.99,45.33,46.65,47.87,49.06,50.26,51.45,52.58,53.67,15.16,
 623.04,25.45,27.91,29.40,30.49,31.34,32.26,33.04,33.74,34.41,35.00,
 735.61,36.16,36.68,37.23,37.73,38.19,38.66,39.10,39.50,39.89,40.28,
 841.70,43.04,44.35,45.60,46.80,47.98,49.10,50.27,51.35,52.40,14.47,
 922.35,24.76,27.22,28.71,29.80,30.67,31.57,32.35,33.02,33.68,34.28/
 DATA (ENTROU(L),I=409,612)/ 34.45,35.40,35.92,36.45,36.92,37.40,
 137.84,38.27,38.68,39.03,39.40,40.81,42.13,43.38,44.56,45.73,46.88,
 247.98,49.07,50.15,51.15,13.55,21.43,23.84,26.30,27.75,28.88,29.75,
 330.64,31.42,32.10,32.72,33.30,33.87,34.39,34.90,35.40,35.86,36.32,
 436.75,37.17,37.57,37.95,38.30,39.65,40.93,42.10,43.27,44.34,45.45,
 546.51,47.53,48.53,49.50,12.86,20.74,23.15,25.91,27.10,28.19,29.01,
 629.97,30.71,31.39,32.00,32.60,33.15,33.68,34.14,34.62,35.10,35.54,
 735.95,36.35,36.77,37.11,37.44,38.77,40.02,41.16,42.27,43.32,44.37,
 845.42,46.38,47.36,48.28,12.16,20.05,22.45,24.91,26.40,27.49,28.36,
 929.25,30.03,30.68,31.30,31.86,32.41,32.93,33.40,33.88,34.31,34.73,
 135.14,35.53,35.91,36.27,36.62,37.90,39.10,40.22,41.31,42.34,43.31,
 244.28,45.27,46.18,47.09,11.25,19.13,21.54,24.00,25.49,26.58,27.44,
 328.34,29.11,29.77,30.37,30.95,31.46,31.96,32.41,32.88,33.30,33.72,
 434.11,34.50,34.84,35.19,35.53,36.77,37.90,38.99,40.00,41.00,41.95,
 542.87,43.79,44.63,45.49,10.55,18.44,20.84,23.30,24.79,25.88,26.75,
 627.64,28.42,29.04,29.69,30.22,30.76,31.22,31.68,32.12,32.54,32.95,
 733.31,33.68,34.05,34.38,34.71,35.93,37.06,38.05,39.08,40.00,40.92,
 841.80,42.64,43.51,44.30, 9.86,17.76,20.15,22.61,24.16,25.19,26.08,
 926.95,27.72,28.37,28.98,29.53,30.04,30.50,30.95,31.46,31.80,32.20/
 DATA (ENTROU(L),I=613,660)/ 32.55,32.91,33.24,33.59,33.90,35.09,
 136.16,37.10,38.12,39.04,39.90,40.76,41.57,42.37,43.15, 8.95,16.83,
 219.24,21.70,23.19,24.28,25.15,26.03,26.79,27.44,28.83,28.59,29.10,
 329.50,30.00,30.41,30.80,31.18,31.54,31.89,32.23,32.54,32.84,33.94,
 435.01,35.96,36.90,37.77,38.57,39.33,40.14,40.92,41.68/
 DATA (H2O(L),L=1,33)/0.,100.,200.,400.,600.,800.,1000.,1250.,
 11500.,1750.,2000.,2250.,2500.,2750.,3000.,3250.,3500.,3750.,4000.,
 24250.,4500.,4750.,5000.,6000.,7000.,8000.,9000.,10000.,11000.,
 312000.,13000.,14000.,15000./
 END

SUBROUTINE DINT(X,XI,Y1,YT1,Z,ZT,ML,NL,Y2,YT2,Y3,YT3,IL,YE,YT4)
 DOUBLE INTERPOLATION SUBROUTINE. IF IL=1, THE SECOND INDEPENDENT
 VARIABLE IS NOT CONSTANT WITH THE FIRST. (THE RANGE OF THE SECOND)
 IS NOT THE SAME AT EACH VALUE OF THE FIRST.)
 DIMENSION ZI(NL),XI(ML,NL),YT1(ML,NL),YT2(ML,NL),YT3(ML,NL)
 DIMENSION YI4(ML,NL)
 IF(ZZ-ZT(1))802,801,801
 801 IF(IL.FQ.1) GO TO 803
 IF(XI.LI.XT(1,1))GO TO 802
 803 DO 800 I=1,NL
 L=I
 LL=I-1
 IF(ZZ-ZT(I))902,804,800
 800 CONTINUE
 802 YI=.2252E+30
 RETURN
 902 RATIO=(ZZ-ZI(LL))/(ZT(L)-ZT(LL))
 IF(IL)1111,1111,1113
 804 DO 904 J=1,ML
 LM=J
 LLM=J-1
 IF(XI-XI(LLM,L))905,906,904
 904 CONTINUE
 GO TO 802
 905 RATIO=(XI-XI(LLM,L))/(XT(LM,L)-XT(LLM,L))

```

Y1=YT1(LLM,L)+RATIO*(YT1(LM,L)-YT1(LLM,L))
Y2=YT2(LLM,L)+RATIO*(YT2(LM,L)-YT2(LLM,L))
Y3=YT3(LLM,L)+RATIO*(YT3(LM,L)-YT3(LLM,L))
YE=YT4(LLM,L)+RATIO*(YT4(LM,L)-YT4(LLM,L))
RETURN
906 Y1=YT1(LM,L)
Y2=YT2(LM,L)
Y3=YT3(LM,L)
YE=YT4(LM,L)
RETURN
1111 DO 913 J=1,ML
LM=J
LLM=J-1
IF (XX-X1(J,L)) 911,912,913
913 CONTINUE
GO TO 802
912 Y1=YT1(LM,LL)-RATIP*(YT1(LM,LL)-YT1(LM,L))
Y2=YT2(LM,LL)-RATIP*(YT2(LM,LL)-YT2(LM,L))
Y3=YT3(LM,LL)-RATIP*(YT3(LM,LL)-YT3(LM,L))
YE=YT4(LM,LL)-RATIP*(YT4(LM,LL)-YT4(LM,L))
RETURN
911 RATIO=(XX-X1(LLM,L))/(X1(LM,L)-X1(LLM,L))
Y4=Y11(LLM,LL)+RATIO*(YT1(LM,LL)-YT1(LLM,LL))
Y5=Y11(LLM,L)+RATIO*(Y11(LM,L)-YT1(LLM,L))
Y1=Y4-RATIP*(Y4-Y5)
Y4=YT2(LLM,LL)+RATIO*(YT2(LM,LL)-YT2(LLM,LL))
Y5=YT2(LLM,L)+RATIO*(YT2(LM,L)-YT2(LLM,L))
Y2=Y4-RATIP*(Y4-Y5)
Y4=YT3(LLM,LL)+RATIO*(YT3(LM,LL)-YT3(LLM,LL))
Y5=YT3(LLM,L)+RATIO*(YT3(LM,L)-YT3(LLM,L))
Y3=Y4-RATIP*(Y4-Y5)
Y4=YT4(LLM,LL)+RATIO*(YT4(LM,LL)-YT4(LLM,LL))
Y5=Y14(LLM,L)+RATIO*(YT4(LM,L)-YT4(LLM,L))
YE=Y4-RATIP*(Y4-Y5)
RETURN
1113 DO 918 J=1,ML
IF (XX-LT.X1(1,L)) GO TO 802
LM=J
LLM=J-1
IF (XX-X1(J,L)) 914,917,918
918 CONTINUE
GO TO 802
917 Y5=YT1(LM,L)
Y7=YT2(LM,L)
Y9=YT3(LM,L)
Y0=YT4(LM,L)
GO TO 1114
916 RATIO=(XX-X1(LLM,L))/(X1(LM,L)-X1(LLM,L))
Y5=YT1(LLM,L)+RATIO*(Y11(LM,L)-YT1(LLM,L))
Y7=YT2(LLM,L)+RATIO*(YT2(LM,L)-YT2(LLM,L))
Y9=YT3(LLM,L)+RATIO*(YT3(LM,L)-YT3(LLM,L))
Y0=YT4(LLM,L)+RATIO*(YT4(LM,L)-YT4(LLM,L))
1114 DO 921 J=1,ML
LM=J
LLM=J-1
IF (XX-X1(J,LL)) 919,920,921
921 CONTINUE
GO TO 802
920 Y4=YT1(LM,LL)
Y6=YT2(LM,LL)
Y8=YT3(LM,LL)
YA=YT4(LM,LL)

```

```

      GO TO 925
919  RATIO=(XX-X1(LLM,LL))/(XT(LM,LL)-XT(LLM,LL))
      Y4=Y11(LLM,LL)+RATIO*(YT1(LM,LL)-YT1(LLM,LL))
      Y6=Y12(LLM,LL)+RATIO*(YT2(LM,LL)-YT2(LLM,LL))
      Y8=Y13(LLM,LL)+RATIO*(YT3(LM,LL)-YT3(LLM,LL))
      YA=Y14(LLM,LL)+RATIO*(YT4(LM,LL)-YT4(LLM,LL))
925  Y1=Y4-RATIP*(Y4-Y5)
      Y2=Y6-RATIP*(Y6-Y7)
      Y3=Y8-RATIP*(Y8-Y9)
      YE=YA-RATIP*(YA-Y0)
      RETURN
      END

```

```

C  SUBROUTINE DINT1(XX,XT,Y1,YT1,ZZ,ZT,ML,NL)
  DOUBLE INTERPOLATION SUBROUTINE.
  DIMENSION Z1(NL),XT(ML,NL),YT1(ML,NL)
  IF(ZZ-ZT(1))802,801,801
801  IF(XX-X1(1,1))802,803,803
802  Y1=.2222E+30
      RETURN
803  DO 80  I=1,NL
      L=I
      LL=I-1
      IF(ZZ-ZT(I))902,904,800
800  CONTINUE
      GO TO 802
902  RATIP=(ZZ-Z1(LL))/(ZT(L)-ZT(LL))
      GO TO 1113
804  DO 904 J=1,ML
      LM=J
      LLM=J-1
      IF(XX-XT(J,L))905,906,904
904  CONTINUE
      GO TO 802
905  RATIO=(XX-X1(LLM,L))/(XT(LM,L)-XT(LLM,L))
      Y1=Y11(LLM,L)+RATIO*(YT1(LM,L)-YT1(LLM,L))
      RETURN
906  Y1=Y11(LM,L)
      RETURN
1113 DO 918 J=1,ML
      LM=J
      LLM=J-1
      IF(XX-XT(J,L))916,917,918
918  CONTINUE
      GO TO 802
917  Y5=Y11(LM,L)
      GO TO 1114
916  RATIO=(XX-X1(LLM,L))/(XT(LM,L)-XT(LLM,L))
      Y5=Y11(LLM,L)+RATIO*(YT1(LM,L)-YT1(LLM,L))
1114 DO 921 J=1,ML
      LM=J
      LLM=J-1
      IF(XX-XT(J,LL))919,920,921
921  CONTINUE
      GO TO 802
920  Y4=Y11(LM,LL)
      GO TO 925
919  RATIO=(XX-X1(LLM,LL))/(XT(LM,LL)-XT(LLM,LL))
      Y4=Y11(LLM,LL)+RATIO*(YT1(LM,LL)-YT1(LLM,LL))
925  Y1=Y4-RATIP*(Y4-Y5)
      RETURN
      END

```

DESCRIPTION OF OUTPUT

The output for the real-gas code includes the flow condition from each region of the flow-field model, the geometry of the shock waves and the expansion waves, the heat-transfer distribution along the second wedge (i.e., the wing leading-edge), the boundary-layer velocity profile and temperature distribution profile, and boundary-layer parameters. The units for a particular parameter in any region will be the same as the free-stream parameter, unless otherwise noted. The output for the free-stream flow includes:

- U1 - free-stream velocity (ft/sec)
- P1 - free-stream static pressure (lbf/ft²)
- T1 - free-stream temperature (°R)
- RH01 - free-stream density (slugs/ft³)
- PT1 - free-stream stagnation pressure (lbf/ft²)
- TT1 - free-stream stagnation temperature (°R)
- GAMMA1 - free-stream γ
- H1 - free-stream enthalpy (Btu/lbm)
- Z1 - free-stream molecular weight ratio

Output for the flow condition in region "I", where I = 2,3, or 6 includes:

- U1 - the velocity
- PI/P1 - the static pressure ratio
- TI/T1 - the temperature ratio
- RH0I/RH01 - the density ratio
- PI - the static pressure
- TI - the temperature
- RH0I - the density
- PTI - the stagnation pressure
- TTI - the stagnation temperature

HI - the enthalpy
ZI - the molecular weight ratio
GAMMAI - the γ for the particular region
DELTA - the change in flow direction from one region to the next
THETA - the shock wave angle

The output for the flow conditions in the expansion from regions 4 and 5, where I = A, B, C, D, or E (i.e., the five subregions) includes:

UI - the velocity
PI - the static pressure
TI - the temperature
RHOI - the density
HI - the enthalpy
GI - the effective γ for the particular region
NUDIF - the difference between the total change of the Prandtl-Meyer angle in region 4 and the total change of the Prandtl-Meyer angle in region 5 (should be zero so that flow in region 5e is parallel to the wing)

Output of intersection points include:

INITIAL POINTS ON BOW SHOCK WAVE, i.e., the origin of the coordinate system, or the nose.

WING INTERSECTION POINT, i.e., intersection of the two wedges.

BOW SHOCK: WING SHOCK INTERSECTION POINT, i.e., the intersection of the shock of the first wedge with the shock of the second wedge.

Next Five Points - the intersection of the centered expansion fan with the wing leading edge.

Last Five Points - the intersections of the reflected waves with the inboard shear layer.

Output listed for the interaction region between the left running and right running expansion fan waves includes:

U4IW - the velocity

P4IW = - the static pressure

where "I" = A, B, C, and D.

The output for the subregions between the inboard shear layer and the shock waves between the shock layer and the free stream include:

THETA - shock wave angle

x - x-coordinate point of the intersection of the shock waves
of two adjacent regions (in.)

y - y-coordinate point of the shock waves intersection (in.)

v - the velocity

P - the static pressure

T - the temperature

R - the density

H - the enthalpy (ft^2/sec^2)

G - the effective γ for the region

The output for the viscous-region subroutines is tabulated under the title "OUTPUT DATA" includes:

M - station number in x-direction

PE(M) - Static pressure at the edge of the boundary layer

THETA E(M) - temperature ratio (T_e/T_{te}) at the edge of the boundary layer

UE(M) - velocity at the edge of the boundary layer

URENOE(M) - unit Reynolds number at the edge of the boundary layer

REXINT(M) - Reynolds number at the edge of the boundary layer integrated over the distance from the origin

X(M) - distance along wing leading edge (ft)

S(M) - transformed x-coordinate

DS(M) - step-size of S(M)
 BETA(M) - velocity gradient at the edge of the boundary layer
 FLOW(M) - stream function at the wall used to indicate mass injection
 PTE - stagnation pressure at the edge of the boundary layer
 TTE - stagnation temperature at the edge of the boundary layer
 ALF - coordinate transformation parameter

The next page of output is the initial boundary-layer profile for the first x-station. The output that follows is at each of the next (M-1) x-stations and includes:

M - station number in x-direction
 X(M) - distance along wing leading edge (ft)
 I - station number in y-direction
 YN(I) - transformed η -coordinate (see Ref. 11), n
 Y(I) - physical y-coordinate (ft)
 ETA(I) - transformed y-coordinate, η
 F(I) - velocity profile in the boundary layer
 THETA(I) - temperature distribution profile in the boundary layer
 CS(I) - mass fraction of the stream species
 TAU - skin friction (lbf/ft^2)
 CF - skin friction coefficient
 TREC - recovery temperature, $^{\circ}\text{R}$
 QDOT - heat transfer rate ($\text{Btu / ft}^2\text{-sec}$)
 STNO - Stanton number
 DELST - displacement thickness (ft)
 THMOM - momentum thickness (ft)
 DSTAR - displacement thickness with mass injection (see Ref. 11) (ft)

CASE = 1

FREE-STREAM FLOW CONDITIONS

U1	P1 (LBF/IN ²)	T1 (RANKINE)	RHO1 (SLUGS/IN ³)	PT1	TT1
1.42000E+04	9.29874E+01	4.89740E+02	1.10527E-06	0.	0.

GAMMA1 = 1.39830E+00 M1 = 1.17046E+02 Z1 = 1.00000E+00

FLOW CONDITIONS IN REGION 2

U2	P2/P1	T2/T1	RHO2/RHO1
1.40739E+04	4.03179E+00	1.60331E+00	2.51467E+00

P2 = 3.74986E+00 T2 = 7.85204E+02 RHO2 = 2.77939E-06 PT2 = 0.
TT2 = 0. M2 = 1.88242E+02 Z2 = 1.00000E+00 GAMMA2 = 1.39118E+00
DELTA = 5.00000E+00 THETA = 8.33116E+00

FLOW CONDITIONS IN REGION 3

U3	P3/P1	T3/T1	RHO3/RHO1
1.21951E+04	1.31133E+02	8.31941E+00	1.56555E+01

P3 = 1.21937E+02 T3 = 4.07435E+03 RHO3 = 1.73035E-05 PT3 = 6.79894E+04
TT3 = 9.52090E+03 M3 = 1.17404E+03 Z3 = 1.00682E+00
DELTA = 2.50000E+01 THETA = 3.03806E+01 GAMMA3 = 1.21420E+00

FLOW CONDITIONS IN REGION 4

U6	P6/P1	T6/T1	RHO6/RHO1
1.16256E+04	7.07399E+01	9.23262E+00	7.50963E+00

P6 = 6.57792E+01 T6 = 4.52159E+03 RHO6 = 8.30016E-06 PT6 = 1.78411E+04

$IT6 = 9.07513E+03$ $MG = 1.44499E+03$ $Z6 = 1.02028E+00$
 $DELTA = 3.00000E+01$ $THETA = 3.54064E+01$ $GAMMA6 = 1.16285E+00$

FLOW CONDITIONS IN THE EXPANSION FAN

REGION 4

VELOCITIES

$UA = 1.22283E+04$ $UH = 1.22613E+04$ $UC = 1.22943E+04$ $UD = 1.23271E+04$ $UE = 1.23599E+04$

PRESSURES

$PA = 1.15001E+02$ $PH = 1.08534E+02$ $PC = 1.02330E+02$ $PD = 0.64658E+01$ $PE = 9.09521E+01$

TEMPERATURES

$TA = 4.03078E+03$ $TH = 3.94754E+03$ $TC = 3.94470E+03$ $TU = 3.90224E+03$ $TE = 3.86011E+03$

DENSITIES

$RHOA = 1.65138E-05$ $RHUB = 1.57553E-05$ $RHOC = 1.50250E-05$ $RHOD = 1.43270E-05$ $RHOE = 1.36641E-05$

ENTHALPIES

$HA = 1.15787E+03$ $HH = 1.14170E+03$ $HC = 1.12554E+03$ $HD = 1.10937E+03$ $HE = 1.09320E+03$

EFFECTIVE GAMMAS

$GA = 1.21779E+00$ $GH = 1.22140E+00$ $GC = 1.22503E+00$ $GD = 1.22867E+00$ $GE = 1.23232E+00$

REGION 5

VELOCITIES

$UA = 1.23926E+04$ $UH = 1.24253E+04$ $UC = 1.24578E+04$ $UD = 1.24902E+04$ $UE = 1.25226E+04$

PRESSURES

$PA = 8.57668E+01$ $PH = 8.08897E+01$ $PC = 7.63010E+01$ $PD = 7.19849E+01$ $PE = 6.57792E+01$

TEMPERATURES

$TA = 3.81831E+03$ $TH = 3.77684E+03$ $TC = 3.73569E+03$ $TD = 3.69487E+03$ $TE = 3.63329E+03$

DENSITIES

RHOA = 1.30344E-05 RHOB = 1.24362E-05 RHOC = 1.18678E-05 RHOD = 1.13275E-05 RHOE = 1.05118E-05

ENTHALPIES

HA = 1.07703E+03 HB = 1.06087E+03 HC = 1.04470E+03 HD = 1.02853E+03 HE = 1.01236E+03

EFFECTIVE GAMMAS

GA = 1.23600E+00 GB = 1.23969E+00 GC = 1.24340E+00 GD = 1.24712E+00 GE = 1.24881E+00

UNUUIF = -5.68940E-04

POINTS OF INTEREST IN THE FLOW FIELD AND ON THE BODY (IN INCHES)

INITIAL POINTS ON BOW SHOCK WAVE
X = 0. Y = 0.

WING INTERSECTION POINT
X = 0.00000E+00 Y = 8.10000E-01

BOW SHOCK-WING SHOCK INTERSECTION POINT
X = 9.99108E+00 Y = 1.44991E+00

EXPANSION FAN INTERSECTION POINTS
X = 1.93102E+01 Y = 1.58988E+00
X = 1.93371E+01 Y = 1.58196E+00
X = 1.93604E+01 Y = 1.57545E+00
X = 1.93867E+01 Y = 1.61060E+00
X = 1.94164E+01 Y = 1.62775E+00
X = 1.94420E+01 Y = 1.96687E+00
X = 1.94717E+01 Y = 1.99861E+00
X = 1.94954E+01 Y = 2.03202E+00
X = 1.95355E+01 Y = 2.06724E+00
X = 1.95163E+01 Y = 2.10442E+00

FLOW ALONG THE WING IN THE EXPANSION REGION

VELOCITIES

U4AW = 1.22613E+04 U4BW = 1.23271E+04 U4CW = 1.23926E+04 U4DW = 1.24578E+04

PRESSURES

P4AW = 1.08534E+02 P4BW = 9.64658E+01 P4CW = 8.57688E+01 P4DW = 7.63016E+01

FLOW CONDITIONS IN SHOCKED REGION OF EXPANSION FAN

REGION 4ES

THEIA = 3.05272E+01 X = 1.11255E+01 Y = 2.42477E+00
U = 1.11578E+04 P = 7.72159E+01 T = 4.66883E+03 R = 9.34221E-06 H = 3.85743E+07 G = 1.15922E+00

REGION 5AS

THEIA = 3.78372E+01 X = 1.12482E+01 Y = 2.52012E+00
U = 1.12628E+04 P = 7.47660E+01 T = 4.50774E+03 R = 9.27802E-06 H = 3.73947E+07 G = 1.15700E+00

REGION 5BS

THEIA = 3.71435E+01 X = 1.13849E+01 Y = 2.62366E+00
U = 1.13669E+04 P = 7.23278E+01 T = 4.53351E+03 R = 9.10333E-06 H = 3.62170E+07 G = 1.16366E+00

REGION 5CS

THEIA = 3.64604E+01 X = 1.15374E+01 Y = 2.73634E+00
U = 1.14679E+04 P = 6.99277E+01 T = 4.46129E+03 R = 8.94333E-06 H = 3.50632E+07 G = 1.16919E+00

REGION 5DS

THEIA = 3.57740E+01 X = 1.17077E+01 Y = 2.85903E+00
U = 1.15678E+04 P = 6.75422E+01 T = 4.38485E+03 R = 8.81779E-06 H = 3.39124E+07 G = 1.17470E+00

OUTPUT DATA

1	PE (M)	METAL (M)	UE (M)	URENUE (M)	REXINT (M)
1	1.21937E+02	4.27934E-01	1.21951E+04	1.52511E+05	1.93151E+03
2	1.21937E+02	4.27934E-01	1.21951E+04	1.52511E+05	5.79452E+03
3	1.21937E+02	4.27934E-01	1.21951E+04	1.52511E+05	9.65744E+03
4	1.21937E+02	4.27934E-01	1.21951E+04	1.52511E+05	1.35216E+04
5	1.21937E+02	4.27934E-01	1.21951E+04	1.52511E+05	1.73836E+04
6	1.08534E+02	4.18817E-01	1.22613E+04	1.41355E+05	1.74427E+04
7	1.08534E+02	4.18817E-01	1.22613E+04	1.41355E+05	1.74947E+04
8	1.08534E+02	4.18817E-01	1.22613E+04	1.41355E+05	1.75566E+04
9	1.08534E+02	4.18817E-01	1.22613E+04	1.41355E+05	1.76135E+04
10	1.08534E+02	4.18817E-01	1.22613E+04	1.41355E+05	1.76705E+04
11	9.64658E+01	4.09858E-01	1.23271E+04	1.30835E+05	1.77316E+04
12	9.64658E+01	4.09858E-01	1.23271E+04	1.30835E+05	1.77905E+04
13	9.64658E+01	4.09858E-01	1.23271E+04	1.30835E+05	1.78493E+04
14	9.64658E+01	4.09858E-01	1.23271E+04	1.30835E+05	1.79081E+04
15	9.64658E+01	4.09858E-01	1.23271E+04	1.30835E+05	1.79669E+04
16	8.57668E+01	4.01043E-01	1.23920E+04	1.21150E+05	1.80305E+04
17	8.57668E+01	4.01043E-01	1.23920E+04	1.21150E+05	1.80917E+04
18	8.57668E+01	4.01043E-01	1.23920E+04	1.21150E+05	1.81529E+04
19	8.57668E+01	4.01043E-01	1.23920E+04	1.21150E+05	1.82141E+04
20	8.57668E+01	4.01043E-01	1.23920E+04	1.21150E+05	1.82753E+04
21	7.63016E+01	3.92365E-01	1.24578E+04	1.12264E+05	1.83420E+04
22	7.63016E+01	3.92365E-01	1.24578E+04	1.12264E+05	1.84062E+04
23	7.63016E+01	3.92365E-01	1.24578E+04	1.12264E+05	1.84704E+04
24	7.63016E+01	3.92365E-01	1.24578E+04	1.12264E+05	1.85346E+04
25	7.63016E+01	3.92365E-01	1.24578E+04	1.12264E+05	1.85988E+04
26	6.57792E+01	3.81609E-01	1.25220E+04	1.01767E+05	2.13046E+04
27	6.57792E+01	3.81609E-01	1.25220E+04	1.01767E+05	2.38871E+04
28	6.57792E+01	3.81609E-01	1.25220E+04	1.01767E+05	2.64648E+04
29	6.57792E+01	3.81609E-01	1.25220E+04	1.01767E+05	2.90425E+04
30	6.57792E+01	3.81609E-01	1.25220E+04	1.01767E+05	3.16202E+04
1	X (M)	S (M)	US (M)	HETA (M)	FLOW (M)
1	1.26647E-02	3.69764E-09	7.39528E-09	0.	0.
2	3.79941E-02	1.10949E-08	7.39528E-09	0.	0.
3	6.33235E-02	1.84882E-08	7.39528E-09	0.	0.
4	8.88529E-02	2.58835E-08	7.21823E-09	0.	0.
5	1.13962E-01	3.29247E-08	3.57370E-09	5.00072E-02	0.
6	1.26848E-01	3.30310E-08	1.06330E-10	1.67707E+00	0.
7	1.27251E-01	3.31373E-08	1.06330E-10	0.	0.
8	1.27654E-01	3.32437E-08	1.06330E-10	0.	0.
9	1.28057E-01	3.33500E-08	1.03752E-10	0.	0.
10	1.28459E-01	3.34512E-08	1.04160E-10	1.72438E+00	0.
11	1.28866E-01	3.35503E-08	1.07158E-10	1.67261E+00	0.
12	1.29335E-01	3.36655E-08	1.07158E-10	0.	0.
13	1.29784E-01	3.37726E-08	1.07158E-10	0.	0.
14	1.30244E-01	3.38798E-08	1.04570E-10	0.	0.
15	1.30683E-01	3.39818E-08	1.05370E-10	1.71322E+00	0.
16	1.31161E-01	3.40905E-08	1.08770E-10	1.65627E+00	0.
17	1.31666E-01	3.41993E-08	1.08770E-10	0.	0.
18	1.32171E-01	3.43001E-08	1.08770E-10	0.	0.
19	1.32676E-01	3.44169E-08	1.06161E-10	0.	0.
20	1.33181E-01	3.45204E-08	1.07445E-10	1.64892E+00	0.
21	1.33719E-01	3.46317E-08	1.11337E-10	1.62058E+00	0.
22	1.34291E-01	3.47431E-08	1.11337E-10	0.	0.
23	1.34863E-01	3.48544E-08	1.11337E-10	0.	0.

24	1.35435E-01	3.49608E-08	1.07962E-10	0.	0.
25	1.3607E-01	3.50703E-08	2.21911E-09	8.22124E-02	0.
26	1.36579E-01	3.94040E-08	4.33363E-09	4.70555E-02	0.
27	1.61908E-01	4.37370E-08	4.33363E-09	0.	0.
28	1.87237E-01	4.80712E-08	4.33363E-09	0.	0.
29	2.12567E-01	5.24049E-08	4.33363E-09	0.	0.

PTE= 6.74894E+04

TTE= 9.52096E+03

ALF= 8.45070E-01

I	F(I)	THEIA(I)	CS(I)
1	0.	1.45723E-02	1.00000E+00
2	2.10499E-02	5.93270E-02	1.00000E+00
3	4.41654E-02	1.05012E-01	1.00000E+00
4	6.95029E-02	1.21573E-01	1.00000E+00
5	9.73751E-02	1.39066E-01	1.00000E+00
6	1.27970E-01	1.57362E-01	1.00000E+00
7	1.61636E-01	1.76433E-01	1.00000E+00
8	1.98685E-01	1.96102E-01	1.00000E+00
9	2.39571E-01	2.16236E-01	1.00000E+00
10	2.84789E-01	2.36606E-01	1.00000E+00
11	3.34886E-01	2.56849E-01	1.00000E+00
12	3.90444E-01	2.76432E-01	1.00000E+00
13	4.52239E-01	2.94770E-01	1.00000E+00
14	5.20774E-01	3.10706E-01	1.00000E+00
15	5.96521E-01	3.23147E-01	1.00000E+00
16	6.79338E-01	3.30401E-01	1.00000E+00
17	7.67725E-01	3.30702E-01	1.00000E+00
18	8.57307E-01	3.22673E-01	1.00000E+00
19	9.37963E-01	3.07022E-01	1.00000E+00
20	9.90375E-01	2.89473E-01	1.00000E+00
21	1.00000E+00	2.83273E-01	1.00000E+00

TAU= 2.85860E+01

CF= 2.22168E-02

TREC= 6.87268E+03

QUOT= 1.58773E+02

STNU= 9.94272E-03

CONVG=-3.67487E-01
 REJOICE,SALVATION IS NEAR
 CONVG=-4.10836E-02
 REJOICE,SALVATION IS NEAR
 CONVG= 3.49228E-02
 REJOICE,SALVATION IS NEAR
 CONVG=-4.72607E-02
 REJOICE,SALVATION IS NEAR
 CONVG= 2.85767E-02
 REJOICE,SALVATION IS NEAR
 CONVG=-1.87575E-02
 REJOICE,SALVATION IS NEAR
 CONVG= 1.06889E-02
 REJOICE,SALVATION IS NEAR
 CONVG=-6.23458E-03
 REJOICE,SALVATION IS NEAR
 CONVG= 3.43850E-03
 REJOICE,SALVATION IS NEAR
 CONVG=-1.90844E-03
 REJOICE,SALVATION IS NEAR
 CONVG= 1.03039E-03
 REJOICE,SALVATION IS NEAR
 CONVG=-5.56364E-04
 REJOICE,SALVATION IS NEAR
 CONVG= 2.95724E-04

```

M=      Z      A(M)=      .03799
1  YN(I)  Y(I)  ETA(I)  F(I)  THETA(I)  CS(I)
10.000  0.00000  0.00000  0.  7.45723E-02  1.00000E+00
2 .050  .00001  .06070  1.48839E-02  9.64407E-02  1.00000E+00
3 .100  .00002  .12468  3.17431E-02  1.20383E-01  1.00000E+00
4 .150  .00003  .19231  5.08626E-02  1.45632E-01  1.00000E+00
5 .200  .00005  .26405  7.25324E-02  1.71697E-01  1.00000E+00
6 .250  .00008  .34042  9.71162E-02  1.98492E-01  1.00000E+00
7 .300  .00010  .42207  1.24452E-01  2.26168E-01  1.00000E+00
8 .350  .00014  .50976  1.56446E-01  2.55014E-01  1.00000E+00
9 .400  .00018  .60448  1.92072E-01  2.85120E-01  1.00000E+00
10 .450  .00023  .70744  2.32461E-01  3.16203E-01  1.00000E+00
11 .500  .00029  .82022  2.78408E-01  3.47542E-01  1.00000E+00
12 .550  .00037  .94490  3.30823E-01  3.77987E-01  1.00000E+00
13 .600  .00046  1.08428  3.90853E-01  4.06015E-01  1.00000E+00
14 .650  .00057  1.24229  4.58779E-01  4.29847E-01  1.00000E+00
15 .700  .00070  1.42470  5.35932E-01  4.47375E-01  1.00000E+00
16 .750  .00086  1.64045  6.22361E-01  4.56183E-01  1.00000E+00
17 .800  .00106  1.90450  7.17104E-01  4.53745E-01  1.00000E+00
18 .850  .00131  2.24493  8.16549E-01  4.38339E-01  1.00000E+00
19 .900  .00165  2.72473  9.12176E-01  4.12447E-01  1.00000E+00
20 .950  .00219  3.54495  9.85372E-01  3.91944E-01  1.00000E+00
211.000  .00291  4.72828  1.00000E+00  4.27934E-01  1.00000E+00

```

TAU= 1.16097E+01

CF= 9.06457E-03

TREC= 8.70123E+03

QUOT= 1.35863E+02

STNU= 8.25691E-03

DELST= 6.72703E-04

THMUM= 3.43955E-04

DSTAR= 6.92703E-04

```

CONVG=-6.07831E-02
REJOICE,SALVATION IS NEAR
CONVG= 6.77040E-02
REJOICE,SALVATION IS NEAR
CONVG=-4.04731E-03
REJOICE,SALVATION IS NEAR
CONVG= 2.01940E-02
REJOICE,SALVATION IS NEAR
CONVG=-1.60793E-03
REJOICE,SALVATION IS NEAR
CONVG= 6.90395E-03
REJOICE,SALVATION IS NEAR
CONVG=-5.09363E-04
REJOICE,SALVATION IS NEAR
CONVG= 2.28959E-03

```


M= 19 A(M)= .13268

I	YN(I)	Y(I)	ETA(I)	F(I)	THETA(I)	CS(I)
10.000	0.00000	0.00000	0.	7.45723E-02	1.00000E+00	
2.050	.00002	.06070	2.26324E-02	9.79708E-02	1.00000E+00	
3.100	.00005	.12468	4.83174E-02	1.23079E-01	1.00000E+00	
4.150	.00009	.19231	7.73831E-02	1.48821E-01	1.00000E+00	
5.200	.00013	.26405	1.10129E-01	1.74711E-01	1.00000E+00	
6.250	.00019	.34042	1.46729E-01	2.00647E-01	1.00000E+00	
7.300	.00026	.42207	1.87198E-01	2.26911E-01	1.00000E+00	
8.350	.00035	.50976	2.31428E-01	2.53417E-01	1.00000E+00	
9.400	.00045	.60448	2.79294E-01	2.80090E-01	1.00000E+00	
10.450	.00057	.70744	3.30772E-01	3.06561E-01	1.00000E+00	
11.500	.00072	.82022	3.85931E-01	3.32201E-01	1.00000E+00	
12.550	.00089	.94490	4.44965E-01	3.56140E-01	1.00000E+00	
13.600	.00110	1.08428	5.08128E-01	3.77302E-01	1.00000E+00	
14.650	.00134	1.24229	5.75724E-01	3.94428E-01	1.00000E+00	
15.700	.00164	1.42470	6.47892E-01	4.06170E-01	1.00000E+00	
16.750	.00200	1.64045	7.24153E-01	4.11408E-01	1.00000E+00	
17.800	.00244	1.90450	8.02945E-01	4.09335E-01	1.00000E+00	
18.850	.00299	2.24493	8.80462E-01	3.99601E-01	1.00000E+00	
19.900	.00375	2.72473	9.48885E-01	3.83732E-01	1.00000E+00	
20.950	.00500	3.54495	9.94377E-01	3.69144E-01	1.00000E+00	
211.000	.00684	4.72828	1.00000E+00	4.01043E-01	1.00000E+00	

TAU= 7.31746E+00

CF= 7.31100E-03

TREC= 8.77682E+03

QUOT= 5.89893E+01

STN0= 4.49780E-03

DELST= 1.18442E-03

THMOM= 7.35693E-04

DSTAR= 1.18462E-03

CONVG=-3.90920E-02
 REJOICE, SALVATION IS NEAR
 CONVG= 8.86402E-05

APPENDIX C. - SOLUTIONS FOR A SINGLE WEDGE CONFIGURATION

It has been noted that the local heat-transfer rates along the "wing leading-edge" (which were nondimensionalized using a current shuttle design parameter) increased significantly with velocity. The velocity dependence which has been found in the present study of the Type VI shock-interference pattern had been found in previous studies of cones (work done at the Johnson Space Center) and of wedges (work done at the University). Using procedures similar to those described previously, theoretical solutions have been obtained for a single wedge configuration with a 30° deflection angle. The solutions for the three flow conditions of the main text:

Condition 1. - $U_\infty = 1167$ m/sec, $P_\infty = 2.98$ mmHg, $T_\infty = 53^\circ\text{K}$

Condition 2. - $U_\infty = 4330$ m/sec, $P_\infty = 0.333$ mmHg, $T_\infty = 273^\circ\text{K}$

Condition 3. - $U_\infty = 7610$ m/sec, $P_\infty = 0.0268$ mmHg, $T_\infty = 195^\circ\text{K}$

are reviewed briefly in this appendix.

The heat-transfer rate at a point 0.30m (1.0 ft) from the apex is presented in Fig. C.1 as a function of the free-stream velocity. The local heating has been divided by the theoretical heat-transfer to the stagnation point of a sphere whose radius is 0.30m. The nondimensionalized heat-transfer rates increased by approximately 40% over the velocity range considered. The increase in heating with velocity for the single wedge is not as great as that observed for the double-wedge configuration which produces the Type VI shock-interference pattern. For a given velocity, the difference between the perfect-gas and the real-gas solutions is relatively small.

Other flow parameters are presented in Table C1. The pressure ratio across the oblique shock wave, the temperature ratio, the density ratio, the entropy increase, the shock-wave angle, and the effective gamma of the

shock-layer flow. The relatively high density ratio which occurs when the real-gas effects are accounted for results in a thinner shock-layer for the real-gas solution. Thus, the effective gamma and the shock-wave angle are smaller for the real-gas solution. However, for a given flow condition, the pressure ratio for the perfect-gas solution is approximately equal to that for the real-gas solution.

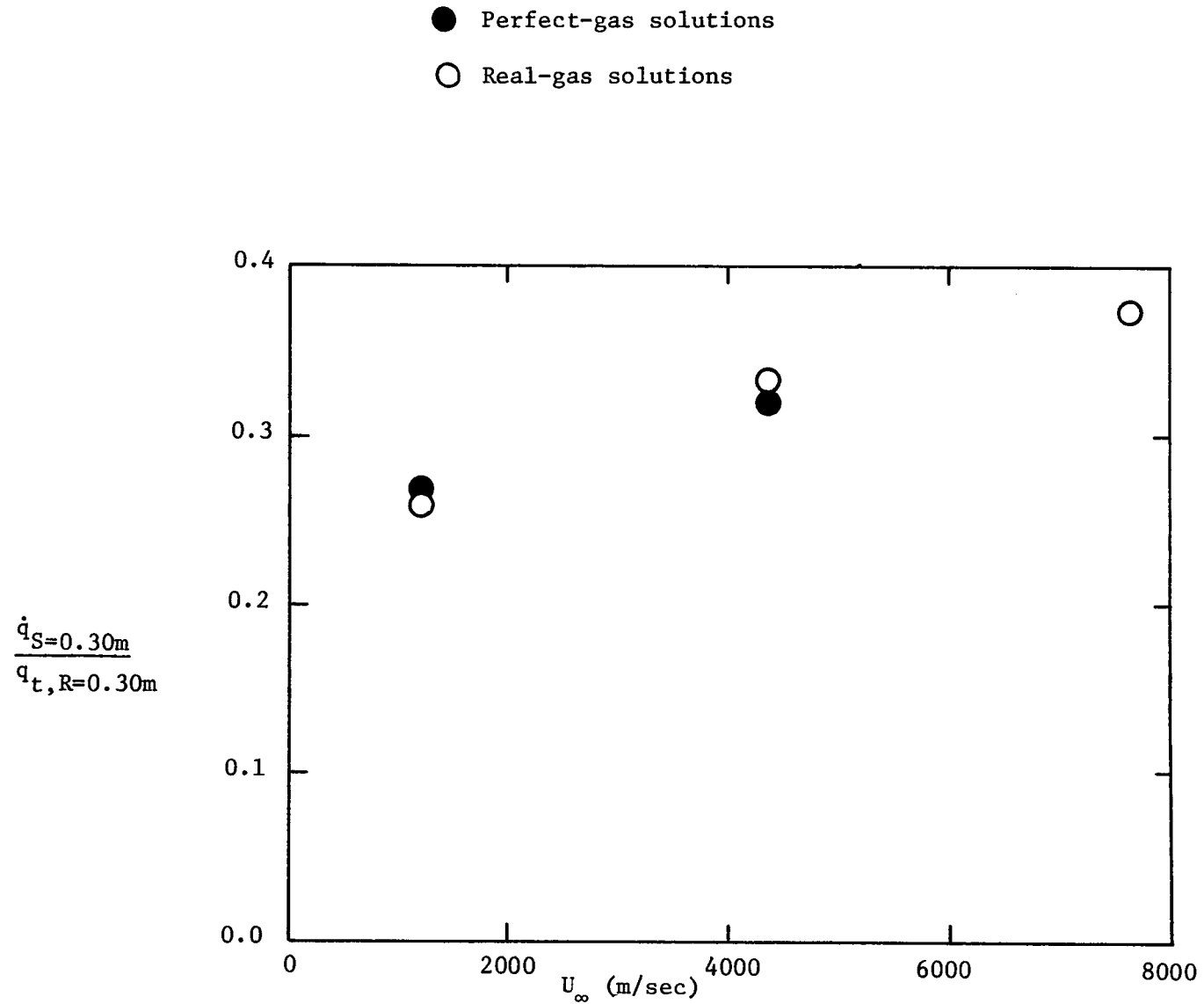
Also presented are the theoretical value of the heat-transfer rate to the stagnation point of a sphere whose radius is 0.30m and the entropy increase across the normal shock for the assumed stagnation point. Note that the ratio

$$\left(\frac{s_2 - s_1}{s_1} \right) / \left(\frac{s_{t,ns} - s_1}{s_1} \right)$$

i.e., the increase of entropy across the oblique shock-wave divided by the increase of entropy across a normal shock-wave, is approximately 0.5 for all three velocities. The constancy of this ratio suggests that the mechanism which produces the velocity dependence of the nondimensionalized heat-transfer rate is not related to the shock-induced entropy change (which relates to the shock-wave strength). This question is relevant because the heat transfer for the wedge flow (which passes through an oblique shock) is divided by the stagnation-point heat-transfer for the sphere flow-field (which passes through a normal shock wave).

Table C 1. - Flow parameters for a 30° single-wedge configuration

<u>Flow Condition</u>	<u>Gas</u>	<u>P₂/P₁</u>	<u>T₂/T₁</u>	<u>ρ₂/ρ₁</u>	<u>(S₂ - S₁)/ S₁</u>	<u>θ_s</u>	<u>γ</u>	<u>$\dot{q}_{t,R=0.3m}^*$ (watts/m²)</u>	<u>(S_{t,ns} - S₁)/ S₁</u>
1	Perf	29.75	5.925	5.021	—	39.27	1.400	3.47x10 ⁴	—
1	Real	29.58	5.915	5.000	0.1111	39.29	1.397	3.47x10 ⁴	0.216
2	Perf	75.51	13.556	5.571	—	38.01	1.400	6.35x10 ⁵	—
2	Real	70.65	9.221	7.510	0.1666	35.41	1.163	5.96x10 ⁵	0.338
3	Real	284.21	20.269	11.530	0.3420	33.25	1.216	1.12x10 ⁶	0.696



Appendix C : Figure 1. - Effect of free-stream velocity on the dimensionless heat-transfer for a wedge
 whose deflection angle is 30° . $T_w = 394^{\circ}\text{K}$